

Vorschlag für den Bau einer Synchrotron-Lichtquelle in der Schweiz

Teil II — SLS-KONZEPT

Conceptual Design of the Swiss Synchrotron Light Source

7. September 1993 Paul Scherrer Institut CH - 5232 Villigen PSI Schweiz

CONTENTS

| | List | of Authors | 3 |
|-----|-------|--|----|
| | Ack | nowledgements | 4 |
| 1. | Intro | oduction | 5 |
| 2. | Desi | ign Philosophy | 7 |
| | 2.1 | Choice of energy | 7 |
| | 2.2 | Layout | 8 |
| | 2.3 | Main features offered by SLS | 9 |
| 3. | Latti | ce Description | 17 |
| | 3.1 | Linear lattice and storage ring layout | |
| | 3.2 | Nonlinear dynamics of the lattice | 19 |
| | 3.3 | Analysis of lattice errors | 22 |
| 4. | RF S | System | 26 |
| 5. | Inter | nsity Limitations and Beam Instabilities | 27 |
| | 5.1 | Impedance model | |
| | 5.2 | Bunch lengthening | 28 |
| | 5.3 | Transverse mode-coupling instability | 28 |
| | 5.4 | Beam lifetime | |
| | 5.5 | Multibunch limitations | |
| | 5.6 | Control of bunch length | 29 |
| | 5.7 | Coherent radiation | 29 |
| 6. | Injec | | 30 |
| | 6.1 | Injection into the Storage Ring | 30 |
| | 6.2 | The injection chain | 30 |
| 7. | | uum System | 33 |
| | | Introduction | |
| | 7.2 | Vacuum chamber constraints | 34 |
| | 7.3 | Design implications | 34 |
| | 7.4 | Photon absorbers | 34 |
| | 7.5 | Pumping system | 35 |
| 8. | The | Superconducting Dipole | 36 |
| | 8.1 | General magnet design considerations | 36 |
| | 8.2 | Cryogenic design | 38 |
| 9. | Repr | resentative Photon Sources | 41 |
| 10. | Aligr | nment and Stability | 47 |
| | 10.1 | Introduction | 47 |
| | | Survey and alignment | |
| | | Measurements of Ground Tremor at PSI | |

| 11. | Infrastructure | 50 |
|-----|---|-----|
| | 11.1 Site | 50 |
| | 11.2 Building layout | |
| | 11.3 Supplies | |
| | 11.4 Radioactivity and radiation protection | |
| 12. | Budget Estimate | 60 |
| | 12.1 Project costs | 60 |
| | 12.2 Operating costs | |
| | 12.3 Manpower Requirements | |
| | Figures | 65 |
| | Comments on the Swiss Light Source | |
| | by the Machine Advisory Committee (MAC) | 109 |
| | References | 111 |

LIST OF AUTHORS

Paul Scherrer Institute

R. Abela, S. Adam, R. Andres, A. Anghel, J. Gobrecht,

G. Heidenreich, W. Hirt, M. Jermann, W. Joho, K. Knop, P. Marchand,

C. Marinucci, Ch. Markovits, Ch. Perret, L. Rivkin, U. Schryber,

P. Seiler, A. Streun

EPF Lausanne

G. Margaritondo

University of Neuchâtel

Y. Baer

ETH Zürich

G. Kostorz, H. R. Ott, R. Prins, T. Richmond, B. Rossi, B. Schönfeld

University of Zürich

B. Larsson

EAWAG Dübendorf

A. J. B. Zehnder

IBM Rüschlikon

B. Reihl

SLS Project Management:

W. Hirt PSI
R. Abela PSI
W. Joho PSI
L. Rivkin PSI
G. Margaritondo EPFL

3

ACKNOWLEDGEMENTS

At this point we would like to thank a number of people for their contributions during the preparation of this report. The following list is by no means complete.

A. Baldereschi (EPFL), K. Kern (EPFL), W. Kündig (Uni Zürich), A. Müller (IBM Zürich), P. Pattison (Uni Lausanne), D. Pescia (ETHZ), M. Peter (Uni Geneva), M. Quack (ETHZ), H. Rohrer (IBM Zürich), L. Schlapbach (Uni Fribourg), W. D. Schneider (Uni Lausanne), H. C. Siegmann (ETHZ), C. von Planta (Hoffmann-LaRoche), H. P. Weber (Uni Lausanne), K. Yvon (Uni Geneva) were involved in many stimulating discussions of the scientific case for the SLS project.

Considerable help in formulating the concept was received from the following industrial companies: Ciba-Geigy (Basel), Hoffmann-LaRoche (Basel), Sandoz (Basel), SMH (Biel).

The members of the SLS Machine Advisory Committee, A. Hofmann (chairman, CERN), G. Mülhaupt (ESRF), A. Wrulich (ELETTRA) looked closely at the critical aspects of the machine design and provided valuable suggestions. Their comments on the SLS design can be found in the Appendix to Part II.

In working out the machine concept for SLS we have benefited from contacts with many experts working in the field of synchrotron light sources: J. Bengtsson (LBL), S. Chattopadhyay (LBL), R. Coisson (Parma), M. Cornacchia (SSRL), M. Eriksson (Lund), A. Jackson (LBL), K. Kim (LBL), R. Keller (LBL), N. Mezentsev (Novosibirsk), S. Milton (APS, formerly PSI), H. Padmore (Daresbury), C. Pellegrini (UCLA), V. Suller (Daresbury), G. van Dorssen (Daresbury), G. Vignola (Frascati), P. Vobly (Novosibirsk), H. Wiedemann (Stanford), H. Winick (SSRL) and K. Wille (Dortmund).

The experimental hall concept was developed by the Schindler & Schindler Architects, Zürich together with K. Daniels (ETHZ). H.J. Lang (ETHZ) and D. Mayer-Rosa (ETHZ) helped in the study of the feasibility of the prospective site.

We have enjoyed the hospitality and support of the following laboratories, while visiting their synchrotron radiation facilities: ALS (Berkeley), APS (Argonne), BESSY (Berlin), ELETTRA (Trieste), ESRF (Grenoble), ETL (Tsukuba), HASYLAB (Hamburg), INS (Tokyo), LURE (Orsay), NSLS (Brookhaven), Photon Factory (Tsukuba), SORTEC (Tsukuba), SPring-8 (Riken), SSRL (Stanford).

Last, but not least, we would like to thank K. Barth, C. Bachmann, P. Müller and M. Salzmann for their dedicated editorial help with this report.

1. Introduction

The present document "Vorschlag für den Bau einer Synchrotron Lichtquelle in der Schweiz" proposes to construct a synchrotron light source at PSI, based on a 2.1 GeV electron storage ring. It is partitioned into two parts: The first part of the report ("Teil I - Übersichtsbericht") contains the scientific and political motivation for the SLS project. As a presentation to the Swiss authorities, it is written in German, with the exception of the Annex "Scientific and Technological Case", written in English. In this second part of the report ("Teil II - SLS-Konzept") we present the design concept for the accelerator facilities of the SLS project. Below we outline briefly some of the main ideas presented in the first part (Teil I).

As a national center SLS is intended to serve as a multidisciplinary facility, providing a state-of-the-art tool not only for basic research, but also for specific needs of the Swiss industry. The highest possible quality of the source is emphasised over maximizing the number of users.

The interaction of electromagnetic radiation with matter is one of the essential tools to understand the complex world of atoms and molecules. The corresponding photon wavelength has to be comparable or smaller than the object under study, or the photon energy should be matched to the corresponding binding energies.

Synchrotron light sources provide researchers with a powerful probe, easily tunable over an extremely wide range of wavelengths and energies. Beams of electrons, ions, neutrons and muons are alternative probes, with quite complementary characteristics. Neutrons and muons are already produced and routinely used for materials research at PSI. In the near future a spallation neutron source (SINQ) will be put into operation. PSI is thus a natural choice for the location of SLS.

We believe that SLS will offer attractive research opportunities well into the next century. It will have a strong impact within the Swiss research community on a wide variety of disciplines, e.g.

- solid state physics and material science
- chemistry
- atomic and molecular physics
- biology and medicine
- industrial fabrication of micro- and nanostructures

Although conceived as a national facility, its innovative features and advanced performance level will attract high quality research on an international scale. SLS is well embedded in the European context, complementary to ESRF in many aspects.

With a projected start in 1996, construction of SLS should be finished by the end of 1999. The costs are estimated to be 190 MSFr (not including PSI personnel costs).

Part II starts with an outline of the design philosophy behind the SLS concept, followed by a description of some aspects of the accelerator facilities. The main focus is on some key issues, like the crucial lattice characteristics, which ensure that the innovative design of SLS is indeed feasible. Other important parts, not treated in this document, like control system, diagnostics and feedback, magnet layouts, power supplies etc. are not considered to endanger the feasibility of the SLS concept.

2. Design Philosophy

From discussions with potential users it became clear, that a future synchrotron light facility should offer some unique features with respect to the "third generation" machines that are coming on line within the next few years (e.g. ALS in Berkeley [1], BESSY II in Berlin [2] or ELETTRA in Trieste [3]). In the following we list the main considerations leading to the SLS concept [8].

2.1 Choice of energy

The present and potential Swiss user community can be roughly divided into two groups according to the photon energy required:

- VUV/XUV radiation (10 3000 eV)
- Hard X-rays (3 50 keV)

The first community would be best served by radiation produced in **undulators** placed in the straight sections of an electron storage ring operating at the energy E = 1.5 - 2 GeV.

To serve the X-ray community with undulator radiation, one has to raise the electron energy to 6 GeV or more (as is done in the very large facilities like ESRF [4], APS [5], SPring-8 [6]). In the lower energy rings one can still obtain significant flux of X-rays from the bending magnets. There are essentially three possibilities:

- Normal conducting bending magnets in a storage ring of about E≥3.5 GeV
- 2. Superconducting wavelength shifters, placed in straight sections of a ring of about E = 2 GeV
- Superconducting bending magnets integrated into the lattice of a 2 GeV ring

We found the first two options less attractive for the following reasons:

- the first variant with a 3.5 GeV ring, the conventional solution, is also the most expensive one. In addition, it compromises the low energy photon spectrum (below 50 eV) and leads to a larger beam emittance, lowering the brightness achievable with undulators.
- in the second variant the number of wavelength shifters will be limited, because they are in competition with the undulators for the available straight sections. The electron beam size will be higher than for the s. c. bends, with a corresponding decrease in brightness. In addition, one is forced to have a low β value in the middle of the wavelength shifter, otherwise one may have an adverse effect on very low emittance operation, reducing the achievable brightness for all users.

The proposed lattice for SLS integrates the superconducting dipoles into a low emittance lattice, leading to a very small crossection of the electron beam in the middle of these dipoles. This results in very bright X-ray beams. As an upper limit on operating energy we chose 2.1 GeV.

2.2 SLS Layout

Main parameters of SLS design are summarised in the Table 1 given below and the overall layout of the storage ring and the injector complex is shown in Figure 1

Table 1: SLS main parameters

| Circumference L Harmonic number h Straight sections Total current (multibunch) I _{tot} Bunch current (few bunches) I _b | [m] [mA] [mA/bunch] | 4(2 × 18 m 4(| 40 00 1, 4 × 7 m 00 10 |
|--|---------------------------|----------------------|------------------------------------|
| Energy Ε | [GeV] | 1.5 | 2.1 |
| Emittance ε _{x0} | [nm·rad] | 1.6 | 3.2 |
| Radiation loss per turn U_0 | [MeV] | 0.124 | 0.477 |
| Bunch length σ_S | [mm] | 3 | 4.5 |
| Bunch length σ_τ | [ps] | 10 | 15 |

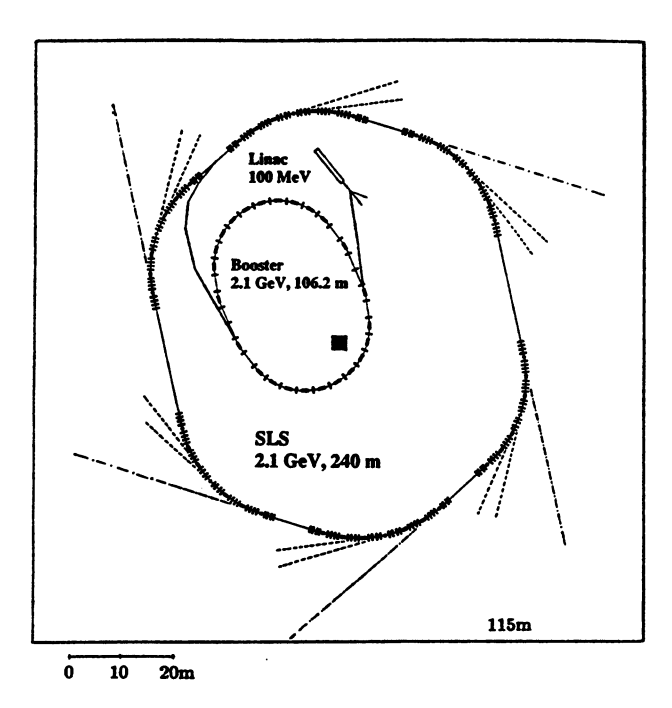


Figure 1: SLS layout with storage ring, booster synchrotron and injector linac.

2.3 Main features offered by SLS

The proposed SLS design offers several important advantages as compared to the present or proposed synchrotron light sources. They are summarised in Table 2 and are discussed in detail in the following sections.

Table 2: SLS Main Features

| High brightness VUV/XUV light (10 - 3000 eV) | E = 1.5 - 2.1 GeV low emittance |
|--|---|
| High flux, bright X-rays (3 - 50 keV) | 6 superconducting bends small source size circular polarisation possible proprietary beamlines |
| Very long straight sections | 2 × 18 meters Iong undulators 2 or 3 undulators in series circular polarisation short bunches future options |
| Flexibility | several operating modes top-up injection on-axis injection ideal matching to IDs |
| Growth potential | long straights short wavelength FEL IR FEL based on linac neutrons plus photons |

High brightness VUV/XUV light

The source brightness is one of the frontiers that are continually pushed in the development of the new synchrotron light sources. A sufficient number of photons to make single shot measurements is a goal of paramount importance for a wide variety of applications. Brightness can be increased either by decreasing the emittance or, (a slower dependence), by increasing the beam current. It should be noted also that for a conventional optical system, including collimation, the smaller the emittance is, the greater is the overall transmission. Thus, achieving smaller equilibrium emittance of the electron and photon beams is one of the most important design goals.

Figure 2 (page 14) shows a universal diagram of the photon wavelength (or energy) obtainable from undulators in an electron linear accelerator or a storage ring. Indicated is the range for some existing or soon to be commissioned facilities. The SLS machine

could cover essentially the same photon spectrum as other machines in the E 2 GeV region, of which we have given the ELETTRA machine in Trieste as an example.

Undulators placed in the short straight sections of SLS are optimised for the photon energies in the VUV region (10 - 3000 eV) and would provide record bright photon beams (above 10¹⁹ photons/sec/mm²/mrad²/0.1%BW) thanks to the very low emittance and good matching of the beam to the undulators that has been achieved with this design. The brightness curves for the SLS sources based on undulators as well as on the bending magnets are given in the Figure 3.

An order of magnitude higher brightness can be achieved with a long undulator placed in one of the two long straight sections of SLS. Thus, in the future, SLS will be able to provide a source of VUV light with the bandwidth $\Delta\lambda/\lambda < 3 \cdot 10^{-3}$ and with a brightness of well above 10^{20} photons/sec/mm²/mrad²/0.1%BW. (More details on a possible long undulator are given in the discussion of the long straight sections below).

High flux, bright X-rays

Notable is the high brightness of the soft X-ray sources based on normal conducting and superconducting bending magnets. This is due to the choice of lattice for SLS, where to minimise the emittance of the electron beam, a very sharp focus had to be achieved in the middle of the dipoles. The typical beam size in the middle of the bending magnets is $\sigma_{\rm X}=30\mu{\rm m}$ and $\sigma_{\rm V}=60\mu{\rm m}$.

Half of the synchrotron radiation power is emitted above the critical photon energy ϵ_c , which is proportional to the strength of the magnetic field and to the square of the electron energy: $\epsilon_c = 0.665 \text{ keV} \cdot \text{B[T]} \cdot \text{E}^2$ [GeV]. It was possible to integrate into the low emittance lattice six superconducting dipoles (B = 4.7 T), extending the useful coverage of the X-ray region by SLS up to a photon energy of 50 keV, as could be seen in Figure 4.

An important feature of the sources based on bending magnets is the high degree of **circular polarisation** of the light taken off the median plane.

With the six superconducting dipoles built into the lattice, each being able to provide at least two X-ray beamlines, there exists a possibility of **proprietary beamlines** for industry (e.g. chemistry, microfabrication).

Long straight sections

Two very long straight sections (each 18 meters long) are provided for in the SLS design. We have considered several possible options for the use of these straights.

• Long undulators. An undulator with several hundred periods would provide a very narrow bandwidth source of VUV radiation with exceptional brightness. For some experiments, that could use the bandwidth of the source, the need for a monochromator would be eliminated, thus avoiding typical losses in flux associated with the use of monochromators. At the same time, this would greatly simplify the beamline optics, eliminating precision components that had to take very high heat losses. As a result, the useful flux into the experimental acceptance would be greatly increased.

Such a device could be constructed in comparatively short sections, with dispersive inserts in between, for phasing the radiation from different sections. Tolerances on matching and beam orbit through this undulator will be rather tight, and need further investigation.

As an example, we give here a set of parameters for a long undulator that could be installed in the future in a long straight of SLS (cf. table below).

Table 3: A possible set of long undulator parameters

| Length L _u | 15 m |
|-----------------------------------|---|
| Period λ _u | 40 mm |
| Number of periods N _p | 375 |
| Gap | 20 mm |
| Peak magnetic field | 0.4 T |
| Strength parameter K | 1.3 |
| Photon energy (first harmonic) | ≈ 600 eV |
| Wavelength | 2 nm |
| Bandwidth Δλ/λ ≈ 1/N _p | 3 · 10 ⁻³ |
| Brightness | 2 · 10 ²⁰ photons/sec/mm ² /mrad ² /0.1%BW |

- Two or three undulators in series. These could be installed in a
 chicane configuration (with small bending in between to separate
 the radiation into different experiments), thus making the long
 straight section equivalent to three short ones. Another interesting
 possibility would be to place undulators with quite different periods
 in line to provide an experiment with a very large tunability range.
- Circular polarisation. There is a great interest in the users community in circularly polarised source of VUV light, with fast switching of polarisation. A possible scheme [11] for such a source would be to use "crossed undulators", i.e. two planar undulators, one horizontal and one vertical with a dispersive section in between. Linearly polarised light from the two undulators would be combined at the experiment, resulting in left or right circularly polarised light, depending on the relative phase of the radiation, which could be changed fast with the dispersive section.

• Short bunches Time resolved experiments require a few very short intense bunches, i.e. high peak current bunches. In this regime, the beam lifetime will become rather short (mainly limited by Touschek effect). Implementing the top-up injection scheme (cf. discussion on flexibility below) will alleviate this problem.

While the achievable peak current is limited for the *stored beam* by the collective effects, significantly shorter bunches can be obtained for short periods of time (one or two turns). For this purpose, an **RF bunch length compressor** could be installed in one of the long straight sections. Short pulses of light with repetition rates on the order of 100 Hz can be obtained this way.

• Future options The long straight sections should help SLS in the future to implement new innovative ideas in the field of Insertion Devices (IDs).

Another possibility would be to install a short wavelength FEL, either in one of the long straights, or in a special bypass constructed for this purpose.

Flexibility

The SLS lattice has been designed to be very flexible to be able to accommodate alternative operating modes (e.g. relaxed mode, with long beam lifetime). The price to pay for this flexibility is a large number of quadrupole families in the arcs and straight sections, as well as the reduced number of straights in order to avoid a very large and thus expensive ring.

Matching to various kinds of **insertion devices** is possible with the help of two sets of four quadrupoles, positioned at each end of the straights.

The very low emittance reduces the lifetime of the stored beam due to intrabeam Coulomb-scattering (Touschek effect) to a few hours. In order to compensate for this drawback we envisage to offer a so-called **top-up injection** process, where the beam intensity is kept constant by very frequent injection of new electrons to compensate for the lost ones. In this operating mode the heat load on optical elements such as mirrors and monochromators would stay constant as well, resulting in very stable conditions for experiments.

For some operating modes, the stable beam region might be reduced (e.g. with crossed undulators for the production of circularly polarised light). For such cases we leave the possibility of **on-axis injection** with a fast kicker open. This would allow us to inject full current bunches into SLS on axis, avoiding the accumulation process that requires large dynamic aperture.

Growth potential of SLS

It is very desirable to build a synchrotron light facility which could accommodate new ideas that may come up after the SLS has been constructed. Below we give just a sample of a few possible future developments at SLS, being fully aware that it is very difficult to make predictions, especially about the future.

- Coherent radiation. As already mentioned in the discussion on the uses of long straight sections, a short wavelength FEL could be implemented on the storage ring. Furthermore, new schemes of highly coherent (temporal, spatial coherence) radiation production will play a growing role in the field of synchrotron radiation, and SLS will be able to provide an excellent platform for such developments.
- IR FEL based on the injector linac. With the recent developments in the field of laser driven photocathode guns, that are capable of creating very high peak current, high charge small emittance electron bunches, it will be possible to operate a low energy (up to 100 MeV) FEL using the injector between fillings (only feasible without top-up injection). Such a device could be used in pump-probe experiments in conjunction with the VUV ring based sources.
- Neutrons plus photons. The SLS at PSI would be the only facility in the world where synchrotron light experiments and neutron experiments could be performed in the same experimental chamber. This opportunity is offered by the unique topography of the existing PSI neutron source and of the SLS. It will be possible, therefore, to combine in real time two of the most powerful (and in many respects complementary) probes in materials research, a possibility that by itself will put the SLS at the forefront of this domain.
- Future sources. SLS could serve as an injector into a future, very advanced 4th generation light source; be it a very small emittance ring or a linac based FEL.

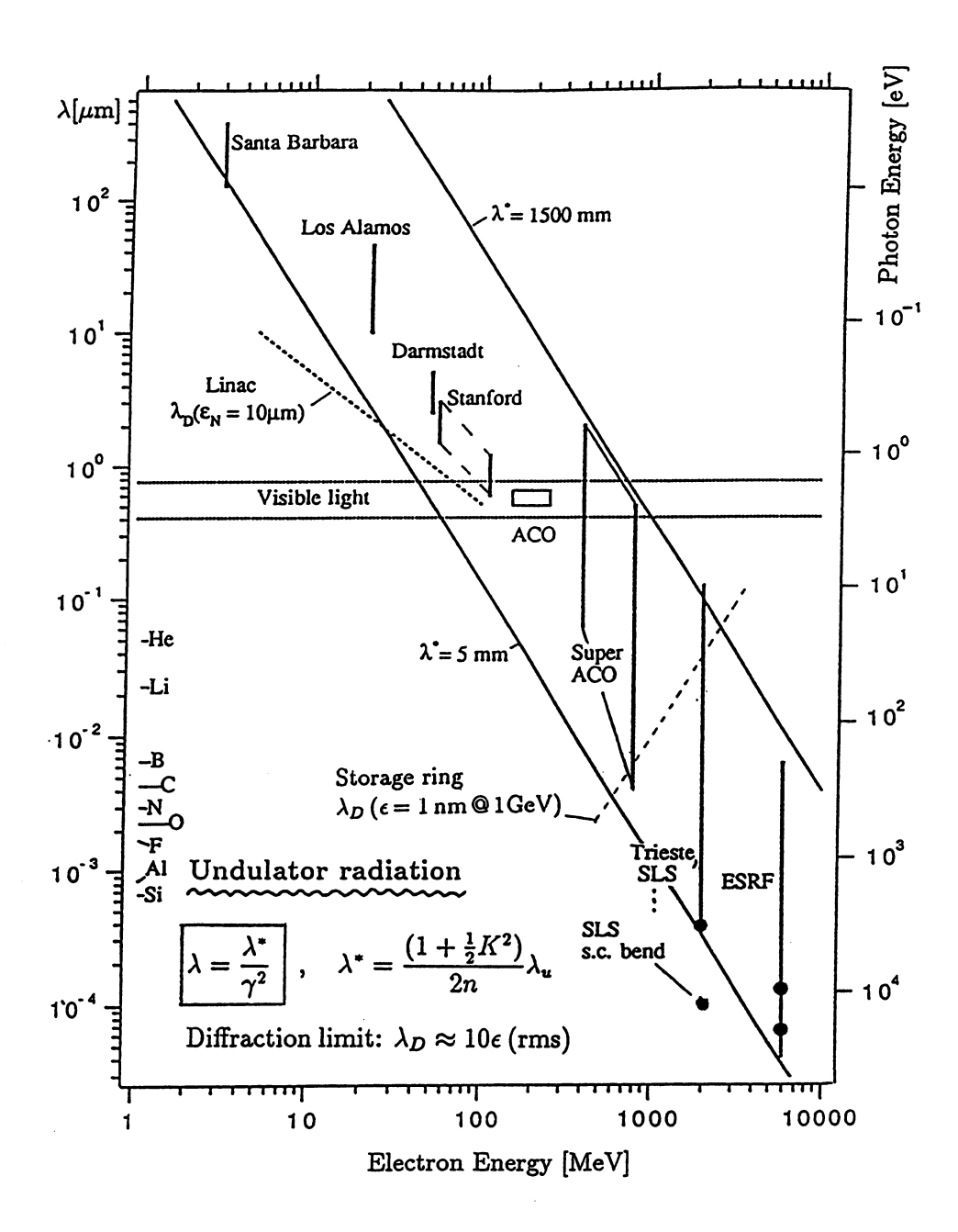


Figure 2: Universal undulator radiation diagram

Wavelength range of undulator radiation (in μ m) as a function of electron energy for a selection of linacs (infrared FEL) and storage rings (VUV and X-ray) region. The wavelength of the undulator radiation can be tuned via changing the magnetic field (undulator strength parameter K) or the electron energy. It also depends on the choice of the undulator period λ_u and of the harmonic number n. The broken lines show the diffraction limit for a Linac with a normalised emittance of 10 μ m rad and for a storage ring with an emittance of 1nm rad at 1 GeV. The solid circle indicates the critical wavelength of the radiation from the storage ring bends. The K-absorption edges of some elements are shown as well.

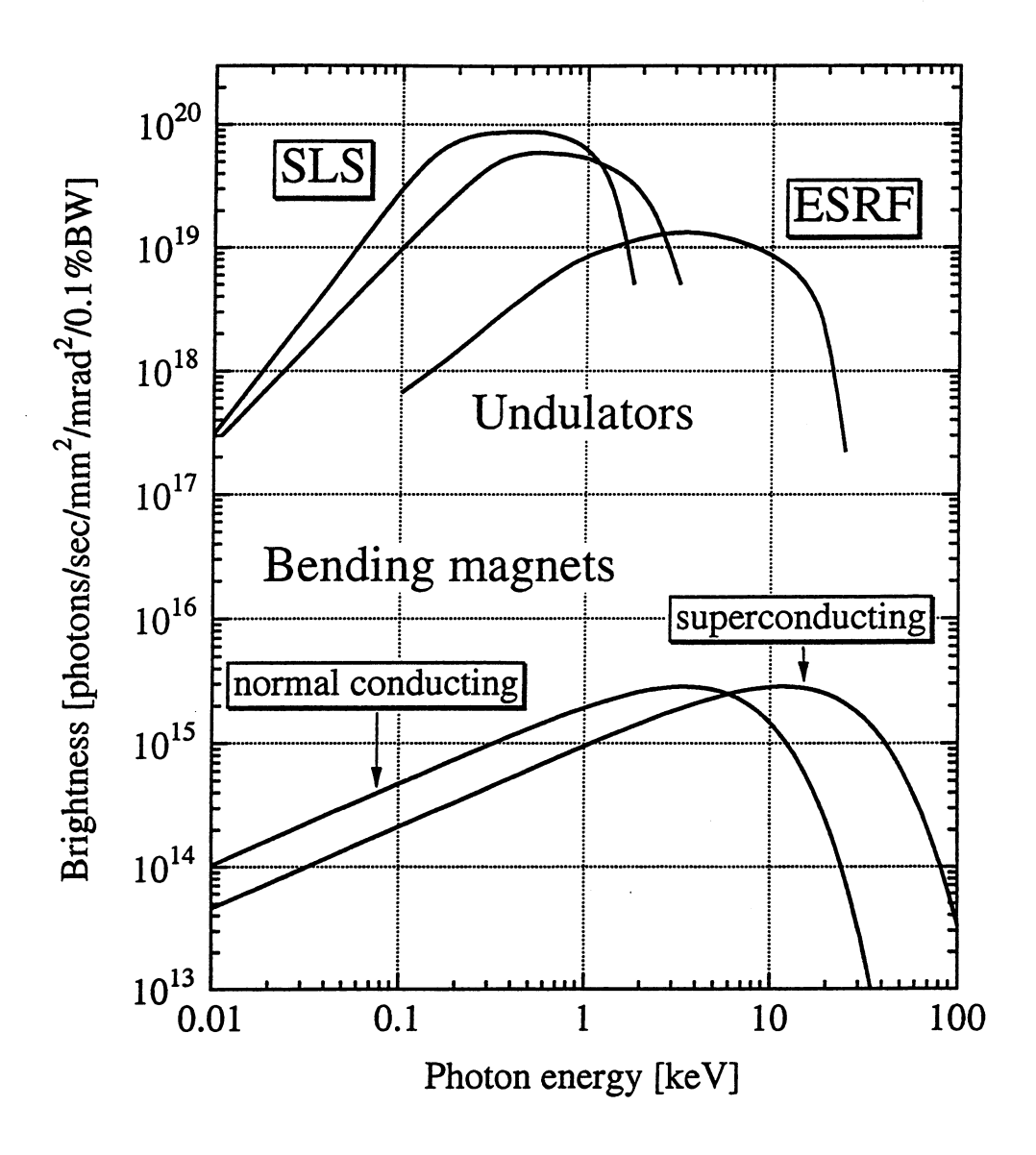


Figure 3: SLS brightness curves

The **Undulator** based sources for SLS are optimised for the VUV region (10 - 3000 eV). The corresponding two undulator curves are for undulators placed in the short straight sections (5 meters long devices) operated at two different energies: E = 1.5 GeV and E = 2.1 GeV. Each of these curves is actually an envelope of possible undulator devices with varying period, magnetic field and taking into account the possibility of taking the light at the first, third or fifth harmonic. As a comparison we also display the brightness of the undulators of ESRF (6 GeV, 200 mA), optimised for the region around 10 keV.

The SLS **bending magnets** based sources provide very bright sources of soft X-rays due to the very small electron beam size in the dipoles. Utilising both normal conducting ($B = 1.4\ T$) and superconducting dipoles ($B = 4.7\ T$) allows SLS to provide high brightness, high flux X-rays over a wide region of photon energies (3 - 50 keV).

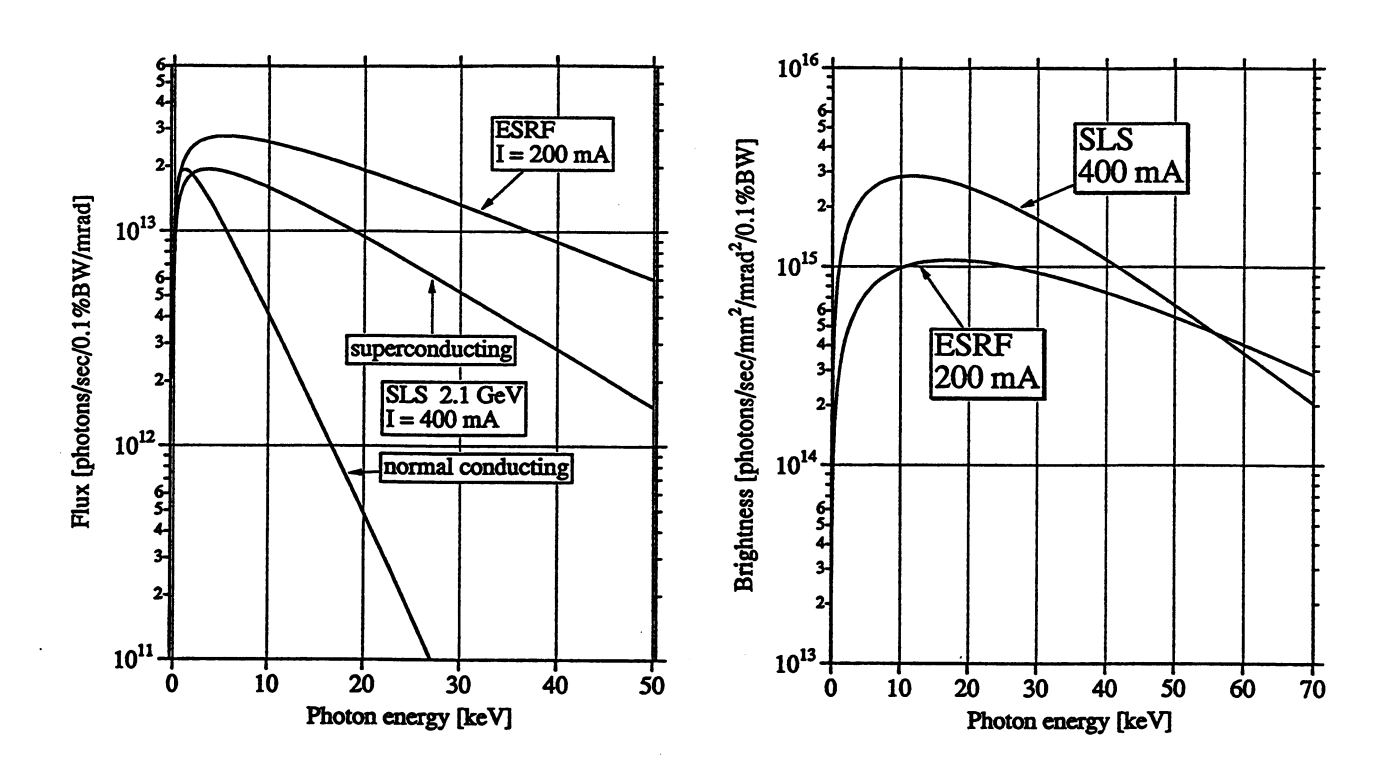


Figure 4: Flux and brightness from bending magnets

The figure at left shows the flux as a function of photon energy for normal conducting bends at SLS and ESRF and for the superconducting bend at SLS. The high magnetic field of B=4.7 Tesla allows to cover the X-ray region up to a photon energy of 50 keV. To obtain a similar spectrum of hard X-rays with a normal conducting bend, the energy of the electrons would have to be raised above 3.5 GeV.

The figure at right compares the brightness of the SLS superconducting bend with that of the normal conducting bend at ESRF.

3. Lattice Description

Developments for a Swiss synchrotron Light Source started in 1990. The lattice layout has gone through several stages [8], leading to the lattice choice presented below.

3.1 Linear lattice and storage ring layout

Storage ring layout

A hexagon shaped lattice [12] will be used for the SLS storage ring. It consists of six straight sections and six (60° bending angle) achromatic arcs.

The length of the straight sections may be freely chosen during design according to the demands from the planned insertion devices. However, too short straight sections are not useful and too long straight sections will result in large beta functions at their ends, thus restricting the geometric aperture and creating large chromaticities in the following quadrupoles, whose correction would cause restrictions of the dynamic aperture as well. In the present design, the length for the straight sections was set to 7.0 m for the short and 18.48 m for the long straight section. In combination with the achromatic arcs as described below, this results in appropriate building blocks, allowing to compose five "isomers" of the hexagon type lattice as shown in Figure 5.

These lattices with their 2-, 3- or 6-fold symmetry all have convenient harmonic numbers – assuming 500 MHz radio frequency system – allowing for many different bunch patterns. The optical functions in these lattices are only slightly different for adjusting proper tune values, and the dynamic acceptances in all cases are rather large for such small emittance machines. We have chosen the second smallest variant, which provides two long straight sections, with a total circumference of 240 m. This is the lattice of the SLS storage ring.

Figure 6 shows a possible layout of storage ring, booster synchrotron and injector linac in a 115 m x 115 m square hall, providing sufficient space for the photon beam lines. One of the four short straight sections is occupied by injection, another one will accommodate the RF system but still leaving enough space for an undulator of about 2 meters length (see Figure 23).

The 60° achromatic arc

Each of the 60° arcs consists of five cells containing 10° bending magnets and of two end cells for dispersion suppression, each containing a 5° bending magnet. The deflection angle of 10° per dipole was found sufficiently small to achieve a very low emittance of 3 nm rad at 2.1 GeV beam energy. The central one of the five 10° dipoles will be superconducting with a field strength of 4.7 Tesla in order to produce a hard X-ray spectrum with a critical wavelength of

0.9 Å at 2.1 GeV, whereas for the normal conducting dipoles a moderate field strength of 1.4 Tesla was chosen.

Initial operation may start with only two or four out of possible six superconducting dipoles. The remaining central normal conducting dipoles may be exchanged for superconducting ones at a later stage, if there is a big demand in the future to have more X-ray beamlines. Due to the difference in path length between the orbits through the two dipole types, the exchange of one dipole requires a slight detuning of the accelerating 500 MHz RF by –3.3 kHz (–4 · 10⁻⁵), which should be easily manageable.

One quarter of the SLS lattice is shown in Figure 9, it includes 1 1/2 arcs, one short and half of a long straight section. (A preliminary naming convention for the two sectors with long straight sections is 'E' and 'W' (East/West) and 'A', 'B', 'C', 'D' for the four sectors with short straight sections).

The magnet elements

Figure 9 also gives a summary of the magnet elements for SLS: Three types of quadrupoles with different lengths are to be used, so that in no magnet the poletip field strength exceeds a maximum of 0.77 T in order to avoid saturation effects. Sufficient space is left for installation of the beam steering dipole coils. To leave room for coils, flanges, etc., the distances between the elements (using their magnetic lengths) were chosen in the following manner:

- from quadrupole to quadrupole 30 cm
- from quadrupole to sextupole 16 cm
- from quadrupole to normal conducting dipole 34 cm
- from quadrupole to superconducting dipole 76 cm.

The centre cell containing the superconducting dipole was stretched in length to accommodate four fast correctors (not shown in Figure 9) to keep control of the photon beam position and angle.

Focusing properties

As can be seen from Figure 9 too, the focusing between the cells is done by quasi-triplets with the central, horizontally focusing quadrupole (QF*) split into two in order to accommodate a sextupole for horizontal chromaticity correction. Two more sextupoles per cell for (mainly) vertical chromaticity correction are located between the horizontally (QF*) and vertically (QD*) focusing quadrupoles.

The optics of the three middle cells of an achromatic arc is shown in Figure 7 with the superconducting dipole in the centre, and Figure 8 shows variation of emittance, dispersion, phase advance per cell and horizontal beta function in the 3-cell-structure with a scaling factor applied to all four quadrupole families involved: QF and QFS control the emittance by creating an appropriate beam waist and suppressing

the dispersion inside the dipoles, whereas QD and QDS work to keep the periodicity of the structure and to maintain a vertical beta function of $\beta_Z \approx 10$ m inside the dipoles through the shown range of the scaling parameter F.

Matching to insertion devices

One unique feature of SLS is to give every insertion device its special required beam parameters, or vice versa to compensate the distortion of beam optics by the insertion without affecting the global storage ring optics, i.e. the straight sections are made transparent. As might be seen from Figures 9, 10 which show magnet arrangement and optical functions of one quarter of SLS, this is achieved by four quadrupole pairs in every straight section (QSsi in short, QLli in long straights, i=1....4), which match to the required beam waist (β_x , β_z , $\alpha_x = \alpha_z = 0$ at the centre of the straights).

Changing the beam waist, however, also changes the tunes. Therefore the quadrupoles of the 1 1/2 cells before/after each straight section are grouped into four families of two or four kids (QFsi, QDsi, QFli, QDli; i=1,2). This arrangement allows to maintain (or change) the machine tunes Q_X , Q_Z and the constraint on the dispersion ($D_X = 0$, $D_X' = 0$) despite the distortion from the insertion device.

In summary, eight quadrupole families are required in every straight section to match the eight beam parameters which could be influenced by the inserted device. (However, if the emittance is affected too, it is, as a matter of principle, impossible to counteract that.)

This demand for ultimate flexibility of course requires a relatively large number of 52 independent quadrupole families and power supplies, as presented in Table 4.

3.2 Nonlinear dynamics of the lattice

Chromaticity correction with harmonic compensation

The natural chromaticities of the SLS storage ring are rather large due to the strong focusing required to achieve small emittance (see Table 5).

The correction of chromaticity with only two families of sextupoles, SF (merging into one the families SF, SFS and SFL from Figure 9) and SD, results in a dynamic aperture that is much smaller than the geometric aperture, as shown in the upper half of Figure 11. After introduction of six sextupole families by dividing the horizontally acting sextupoles into three families and adding two more families (SHS, SHL) in the dispersion free regions, the dynamic aperture was considerably increased by means of minimising sums over the harmonics of sextupole resonances as well as the linear derivatives of tune with amplitude [13]. The dynamic aperture after minimization is

Table 4: The Magnet Families of the SLS Lattice

| Family | Kids | L [cm] | |
|--------------|------|--------|-----------------|
| Bending magn | ets | | |
| BST | 6 | 26 | 10° s.c. |
| BNT | 24 | 88 | 10° <i>n.c.</i> |
| BNF | 12 | 44 | 5° п.с. |
| 3 Families | 42 | | |

| Quadrupoles | | | |
|-------------|-------|----|--------------------|
| QF | 24 | 26 | normal cells |
| QD | 24 | 18 | |
| QFS | 12 | 26 | cells with s.c. |
| QDS | 12 | 18 | bending magnets |
| QFs1 | 4 x 2 | 26 | dispersion and |
| QDs1 | 4 x 2 | 26 | tune matching |
| QFs2 | 4 x 4 | 26 | to short straights |
| QDs2 | 4 x 4 | 18 | $s = \{A,B,C,D\}$ |
| QFI1 | 2 x 2 | 26 | dispersion and |
| QDI1 | 2 x 2 | 26 | tune matching |
| QFI2 | 2 x 4 | 26 | to long straights |
| QDI2 | 2 x 4 | 18 | I = {E,W} |
| QSs1 | 4 x 2 | 26 | matching to |
| QSs2 | 4 x 2 | 26 | insertion devices |
| QSs3 | 4 x 2 | 32 | in short straights |
| QSs4 | 4 x 2 | 26 | $s = \{A,B,C,D\}$ |
| QLI1 | 2 x 2 | 18 | matching to |
| QLI2 | 2 x 2 | 32 | insertion devices |
| QL13 | 2 x 2 | 32 | in long straights |
| QLI4 | 2 x 2 | 26 | I = {E,W} |
| 52 Families | 192 | | |

| Sextupoles | | | |
|------------|-----|----|--------------|
| SF | 24 | 16 | chromaticity |
| SD | 60 | 16 | correction |
| SFS | 8 | 16 | |
| SFL | 4 | 16 | harmonic |
| SHS | 8 | 16 | compensation |
| SHL | 4 | 16 | • |
| 6 Families | 108 | | |

shown in the lower half of Figure 11. The corresponding dynamic acceptances amount to 50 μm horizontally and 39 μm vertically (onmomentum particles only). The code OPTIK [14] was used for the calculations described in this section.

A Poincaré section of phase space motion taken at the centre of the long straight is shown in Figure 12. The amplitude dependent tune shift, as shown in Figure 13, corresponds to a twist in phase space, thus creating resonance islands, which beyond a certain amplitude start to overlap, restricting the stable region. This is clearly seen in the horizontal plane, where the stable region is limited at $Q_{\chi}=20\,$ 1/6 (six small islands in Figure 12, left), whereas vertically, the region of stability completely covers the available geometric aperture. However, the harmonic compensation method is only valid to first order in perturbations and thus, as a matter of principle, may only serve to minimise the first order derivatives of tune shift with amplitude. The advantageous bending of $Q_{\chi}(\varepsilon_{\chi})$, seen in Figure 13, is not predictable by this method and is a result of trial and error procedure.

Higher order chromaticity

The price to be paid for dynamic aperture is a rather large variation of beta function with momentum as observed in Figure 14 at the centre of the long straight section (most sensitive location). This causes a serious mismatch of the off-energy particles' eigenfigures, thus restricting their dynamic and even the geometric acceptances as to be shown later in Figure 20. This effect corresponds to a large second order chromaticity $\Delta Q \sim (\Delta p/p)^2$. Other sextupole arrangements have been studied and gave a more moderate variation of beta function with momentum – but with it also a poor dynamic aperture. Further investigation of possibilities to get both small second order chromaticity and large dynamic aperture are in progress.

Figure 15 shows the location of the linear lattice working point in the resonance diagram. It is important to keep the working point as far away as possible from the sextupole resonances. Tune values $Q_x = 20.2$ and $Q_z = 5.4$ were found to correspond to the largest dynamic acceptance. The boxes in Figure 15 enclose the area of momentum- and amplitude dependent tune spread (beam footprint) for different values of momentum deviation (neglecting synchrotron oscillations). All particles with momentum deviation $|\Delta p/p| \le 2\%$ and any transverse amplitude stay confined in an area which is not intersected by any regular resonances of lower than 5^{th} order.

The influence of synchrotron motion

Still in progress are calculations of dynamic apertures including synchrotron oscillations. On one hand, synchrotron oscillations average the momentum dependent tuneshift and thus lead to a decreased tune spread, on the other hand they excite synchrobetatron resonances as further gateways to instability.

Table 5: SLS lattice parameters

| Geometric properties | | | |
|---------------------------|-----------------------|--|--|
| Circumference | 240 m | | |
| Harmonic number (500 MHz) | $400 = 24 \cdot 5^2$ | | |
| Straight sections | 2 x 18.5 m, 4 x 7.0 m | | |
| Size of machine | 82 m x 67 m | | |

| Energy independent lattice parameters (low emittance) | | | |
|---|--------------|--|--|
| Momentum compaction factor 6 · 10 ⁻⁴ | | | |
| Horizontal tune | 20.2 | | |
| Vertical tune | 5.4 | | |
| Horizontal chromaticity - (corrected) | -55.0 (+1.0) | | |
| Vertical chromaticity - (corrected) | -16.8 (+1.0) | | |

| Energy dependent lattice parameters (low emittance) | | | | |
|---|-------------------------|-------------------------|--|--|
| Energy [GeV] | 1.5 | 2.1 | | |
| Natural emittance [nm · rad] | 1.6 | 3.2 | | |
| Energy loss per turn [keV] | 124 | 477 | | |
| Relative energy spread | 0.80 · 10 ⁻³ | 1.12 · 10 ⁻³ | | |
| Transverse damping times [ms] | 19.2 | 7.0 | | |
| Longitudinal damping time [ms] | 9.6 | 3.5 | | |

| Ideal acceptances (no errors) | horizontal [μm] | vertical [μm] |
|-----------------------------------|-----------------|---------------|
| on-momentum | 50 | 39 |
| dp/p= -2% (no sync. osc.) | 36 | 33 |
| dp/p= +2% (no sync. osc.) | 31 | 36 |
| Energy acceptance (no sync. osc.) | ± 4 ° | % |

A first calculation was done by Max Cornacchia using the code KRAKPOT [15]. The dynamic aperture for particles with a synchrotron oscillation amplitude of $|\Delta p/p\>|=2.8\%$ is rather restricted compared to on-momentum particles and was found to amount to 10 μm horizontally and 3.5 μm vertically. The particles were tracked for one longitudinal damping time (3.5 ms at 2.1 GeV). Radiation damping and quantum noise were not included. The code MAD8 [16] was used to cross-check some of the particles near the calculated limits of stability and gave fair confirmation of the results. Taking into account synchrotron oscillations the energy acceptance may be limited to about \pm 3% in relative energy deviation.

3.3 Analysis of lattice errors

Various kinds of errors affect the acceptance of the storage ring. Simulations with the code TRACY [17], were done to determine the quality requirements for magnet elements, girders etc. to obtain the desired performance of SLS.

Closed orbit distortion and correction

Figure 16 shows a histogram of closed orbit distortions (standard deviations) accumulated over 100 sets of Gaussian distributed random transverse displacement errors in quadrupoles, bending magnets and sextupoles. In all error settings, the Gaussian distribution was cut at two standard deviations, assuming that it would be guaranteed to stay within this limit. The amplification factors characterize the machine sensitivity to displacement errors: They are defined as the ratio of the average (from several runs) standard deviations (from all monitors) of the closed orbit distortion to the standard deviation (from all magnet elements) of the transverse displacement errors. They were found to be 40.3 horizontally and 11.4 vertically, i.e. a 100 μm r.m.s. displacement error in all magnet elements creates in average closed orbit distortions of 4 mm r.m.s., which need to be corrected.

For observation of the closed orbit distortion each of the 108 sextupoles was equipped with horizontal and vertical beam position monitors. For closed orbit correction all the horizontally (vertically) focusing quadrupoles were assumed to have horizontal (vertical) dipole coils for beam steering. Furthermore, all the bending magnets are natural horizontal correctors by slightly trimming their field strength. Summing up, the lattice prepared for error analysis contained 126 horizontal and 84 vertical correctors. The average betatron phase advances between successive correctors of the same kind are 58° horizontally and 23° vertically, resulting in some redundancy.

The influence of statistical errors on the acceptance

Figure 17 shows the decay of the on-momentum dynamic acceptance with increasing standard deviation of the Gaussian distributed transverse positioning errors. A closed orbit correction was performed before every run. Each element was shifted independently from the others, which is a simplified model, because usually groups of elements are mounted on the same girder. The relative alignment within these groups can be much better than between the separated girders. Further investigations of misalignment errors are in progress. Interpretation and summary of the results are presented at the end of this section.

Figure 18 shows the decay of dynamic acceptance with increasing standard deviation of tilt errors. (Tilt means rotation around the beam orbit (s-axis)). A closed orbit correction was performed before every run to compensate the beam displacement produced by vertical dipole field components in the tilted bending magnets.

Figure 19 shows the decay of dynamic acceptance with increasing standard deviation of errors in quadrupole strength. Closed orbit correction would have been inappropriate in this case, because quadrupole strength errors only affect the focusing but not the beam orbit. Strength errors in sextupoles have much weaker influence, and

strength errors in bending magnets would be easily compensated by the horizontal beam steering magnets.

The influence of combined errors on the acceptance as a function of momentum is shown in Figure 20: The dashed line represents the geometric acceptance due to the mismatch of particles with momentum deviation as shown in Figure 14. The solid line represents the dynamic aperture, calculated by binary search for the outermost stable particle and ellipse fit to the points of its eigenfigure's Poincaré section taken at the centre of the long straight section. The crosses depict results for the lattice with errors, calculated by the same procedure, and the dotted line connects averages of the columns of results for each value of the momentum deviation. The magnitudes of errors were thought to represent a realistic lattice: All magnet elements and the beam position monitors were displaced transversely by 100 µm r.m.s. and tilted by 1 mrad r.m.s., quadrupole and sextupole field strengths were changed relatively by 0.1 % r.m.s. For the runs within ± 2 % momentum deviation an average decrease of dynamic acceptance about roughly 15 % is observed, which appears to be tolerable. The energy acceptance shrinks from \pm 4 % to \pm 3 % and meets the estimated stability limit from the runs including synchrotron oscillation.

Systematic higher multipole errors

For extraction of the synchrotron radiation fans from the bending magnets SLS will use quadrupoles with two separate yokes, fixed by C-shaped plates (Figure 32). This breaking of the quadrupoles' 4-fold symmetry may give rise to systematic octupole components; so does the quadrupole fringe field. Figure 21 shows the dynamic acceptances as a function of a systematic octupole component, measured as the ratio of octupole and quadrupole field at the horizontal aperture limit. Division by a^2 with a = 35 mm the aperture radius gives the ratio of octupole moment B"/($6 \cdot Bp$) to quadrupole moment B'/(Bp).

From Figure 21 also may be seen, that for some range of octupole component the acceptance is obviously raised beyond that of the error free lattice, at least horizontally. Future investigation will illuminate this phenomenon and check if it will be paying to exploit it for SLS, maybe by installation of octupole magnets as it was done before in other places.

Saturation effects in the quadrupole iron could become a source of dodecapole moments in the quadrupoles. Figure 22 shows the dynamic acceptances as a function of a systematic dodecapole component, measured as the ratio of dodecapole and quadrupole fields at the horizontal aperture limit. Division by a^4 gives the ratio of dodecapole moment $B^{(5)}/(5! - B\rho)$ to quadrupole moment. Only the negative half of Figure 22 is of interest, because saturation effects will decrease the field strength on the poletips and thus the dodecapole field there will be of opposite sign of the quadrupole field. Those relative dodecapole errors were applied to all quadrupoles without any

regard on their field strength, whether they might show saturation effects or not; i.e. the model was pessimistic.

Tolerance requirements

The present status of calculations leads to tolerance requirements as follows obeying the somewhat arbitrary criterion, that each kind of error alone should not decrease the dynamic acceptance by more than 10 % on average, or, in case of statistics runs, that the worst run decreased the acceptance by not more than 20 %:

| Transverse displacements | Δχ, ΔΖ | ≤ | 60 μm r.m.s. |
|---------------------------------|--|---|----------------------------|
| Tilt (rotation around s-axis) | Δψ | ≤ | 2.5 mrad r.m.s. |
| Quadrupole field strength | ΔΒ/Β | ≤ | $3.5 \cdot 10^{-3}$ r.m.s. |
| Systematic octupole component | B _{oct} /B _{quad} _a | ≤ | 3 ⋅ 10 ⁻³ |
| Systematic dodecapole component | B _{dod} /B _{quad} _a | ≤ | 6 ⋅ 10 ⁻³ |

Analysis of other kinds of errors is in progress. Next on the list are longitudinal displacements, rotations around x- and z-axis, higher multipoles in fringe fields of bending magnets and correlated displacement errors from girders.

4. RF System

Considerations of the desired beam characteristics (bunch length, life time), the equipment sizes and the availability of high power RF sources lead us to select 500 MHz as RF frequency.

The design voltage of about 2 MV can be achieved using four single cell cavities operated at a quite moderate level of performance. Typical working conditions are listed in the table below.

Table 6: Typical RF system operating parameters

| | ~~~ <u>``</u> |
|---|-----------------------|
| Energy | 2.1 GeV |
| Energy loss per turn | 500 keV |
| Beam current | 400 mA |
| RF frequency | 500 MHz |
| Harmonic number | 400 |
| Number of cavities | 4 |
| Cavity shunt impedance (V ² /2P) | $3.5~	extsf{M}\Omega$ |
| RF voltage per cavity | 0.5 MV |
| Power dissipation per cavity | 36 kW |
| Input power per cavity | 100 kW |
| | 1 |

The four cavities (including tapers) will occupy about 4 meters within a short straight section of the storage ring, leaving enough space for the installation of a 2 meters long undulator nearby (figure 23). Each pair of cavities will be powered by a 300 kW klystron. Such a system can provide RF voltage larger than 3 MV with a stored beam current in excess of 500 mA.

The choice of monocell cavities was mainly dictated by the need to efficiently load the cavity higher order modes which would be responsible for coupled bunch instabilities. Various cavity shapes and technical solutions (using wave guides or coaxial lines) for strong attenuation of higher order mode impedance are presently under investigation in different laboratories ([19]-[24]). Complementary low power feedback systems (longitudinal + transverse) would finally insure the beam stability up to the design beam current.

5. Intensity Limitations and Beam Instabilities

Previous sections have dealt with basically single particle aspects of the design. Here we examine some of the effects that have to do with beam intensity limitations. Our estimates so far indicate no major obstacles in the way of achieving the design current of 400 mA. Currents per bunch of 10 mA seem to be feasible.

5.1 Impedance model

Electron beam interaction with the surroundings causes the beam parameters such as bunch length, energy spread to depend on current. This interaction can be modelled by describing the beam environment (vacuum chamber, RF cavities, etc.) in terms of impedance. Broad band resonator impedance provides a useful model that can be used for the estimates of the main effects.

Careful design of the vacuum system components should result in a very low value of the equivalent broad band impedance with rather low resonant frequency ($f_r < 3$ GHz). The effective impedance seen by a *short bunch* would then be further reduced [25]. However, there seems to be a lower limit to the effective impedance, due to the so-called "radiation impedance" [26,27]. Using recent estimates [28] of this contribution to the overall impedance we have constructed the following model that we have used to estimate the collective effects such as bunch lengthening.

The model consists of two broad band resonators, the first, with rather low resonant frequency of $f_r = 2$ GHz representing the vacuum chamber and cavities part, and the second, with much higher frequency $f_r = 20$ GHz representing the "radiation impedance".

The parameters of the resonators are given in the Table 7 below.

Table 7: Broad band resonator model for SLS impedance

| Resonator parameter | | Chamber and cavities | "Radiation impedance" |
|--|-------|----------------------------|--------------------------|
| Resonant frequency fr | [GHz] | 2 | 20 |
| Quality factor Q | | 1 | 1 |
| Low frequency limit $\frac{ Z }{ n _0}$ | [Ω] | 1 | 0.04 |
| Effective impedance $\left \frac{Z}{n} \right $ | [Ω] | 0.13 | 0.04 |
| (for bunch length $\sigma_s = 6 \text{ mm}$ | 1) | | |

5.2 Bunch lengthening

Two regimes are distinguishable: potential well bunch lengthening and the turbulent bunch lengthening. In the turbulent regime both bunch length and the energy spread increase with current, starting from some threshold current value. Below the threshold, in the pure potential well regime, the bunch length increases or decreases with current, depending on the character of the overall impedance that the beam sees.

Using the program BBI [29], we have calculated the bunch lengthening as function of current in the presence of the model impedance. The results for two different operating energies of 1.5 GeV and 2.1 GeV are presented in Figure 24.

These results were then used in estimates of the effect of the intrabeam scattering on equilibrium emittance and of the Touschek effect.

5.3 Transverse mode-coupling instability

Careful control of the transverse impedance of the vacuum chamber will insure that the transverse mode coupling instability threshold will be well above the design single bunch current.

5.4 Beam lifetime

The main processes contributing to the loss of particles from the beam include scattering on the residual gas and intrabeam scattering. These effects also change the equilibrium beam distribution away from Gaussian one, namely by populating the tails of the distribution and hardly affecting the core of the beam [30].

Small desired emittances result in a very high particle density in the transverse plane; this leads to a rather short beam lifetime that is dominated by the Touschek effect.

As a result of the scattering process, the particle energy may be altered by large enough amount to be outside the momentum acceptance of the machine. The momentum aperture can be increased by increasing the RF voltage, but is eventually limited by the fact that the dynamic aperture for the off-momentum particles (or particles performing synchrotron oscillations with large energy deviation amplitudes) shrinks to zero. The studies of the SLS lattice energy acceptance indicate that it would be limited to ±3% in relative energy deviation (for more details see the chapter on lattice description). The Touschek lifetime as a function of the RF voltage was calculated with the program ZAP [31] for two different operating energies and for bunch currents of 2 mA and 10 mA. The calculations took into account the bunch lengthening results described above, as well as the equilibrium emittance blow-up (which was below 10% for the worst case of 1.5 GeV operation and the bunch current of 10 mA). The results are presented in Figure 25.

The transverse acceptance of SLS will be limited by the presence of small gap insertion devices. Taking this into account, calculations of the contributions to the beam lifetime from the scattering processes on the residual gas indicate the need for very good vacuum (1n Torr or better).

5.5 Multibunch limitations

Coupled bunch instabilities, caused mainly by the high Q resonances in the RF cavities, will limit the total current in the machine. We plan for a passive damping system for the cavities, complemented by an active feedback system. The power requirements of such a feedback system that will assure stability of the beam up to the design current are expected to be rather modest.

5.6 Control of bunch length

To achieve a longer lifetime in the modes of operation when the short bunch length is not required, we plan to employ a higher harmonic RF system to lengthen the bunch.

On the other hand, when very short light pulses are desired, the same system can be used to reduce the bunch length, e.g. when operating with a single or a few bunches.

5.7 Coherent radiation

A very interesting possibility exists for production of coherent infrared radiation. At wavelengths comparable or longer than the bunch length the particles in the bunch radiate coherently, the intensity of radiation being proportional to the square of the number of particles per bunch. Moreover, the spectrum of such radiation should consist of very narrow peaks spaced at revolution frequency [32]. The effect is largely suppressed in the present day storage rings by the strong shielding provided by the surrounding vacuum chamber. Production of very short bunches as well as special care in the vacuum chamber design may result in very narrow band source of sub-millimeter wavelength radiation.

6. Injection

6.1 Injection into the Storage Ring

Injection from the booster transfer line into the storage ring occurs in a short straight section of 7 m length. The injection method is a classical scheme, as used e.g. in the facilities in Berkeley and Trieste [1,3] and illustrated in figure 26. Four bump kickers with a half-sine wave of 4 μs create a local horizontal displacement of the stored beam by 15 mm towards an injection septum. The newly injected beam is guided with the septum field towards the displaced stored beam.

Figure 27 shows a sequence of an optimised injection process in phase space. The 2 mm thick septum is placed 18 mm away from the ideal closed orbit, giving an acceptance of 40 μ m for the stored beam. Two turns after injection the displaced stored beam is back on its original orbit, whereas the injected beam oscillates around the ideal orbit within a phase space area of 27 μ m, well within an assumed acceptance of 40 μ m. The injected beam eventually joins the stored beam with a damping time of about 7 ms, corresponding to 9000 turns.

A large horizontal beta function at the septum increases the injection efficiency. It is therefore advantageous to have a beta-value of about 8 m in the injection straight (as well as in the opposing straight, for symmetry reasons). In the other straights the beta-values can be made smaller (e.g. 2—4 m) for a better match to the corresponding undulators.

For some special experiments it might be advantageous to install insertion devices, like e.g. crossed undulators or undulators with a short period, which have small apertures. In this case the acceptance might be too restricted for the conventional injection process. A way out of this is to inject the incoming electrons on-axis into the storage ring with a very fast kicker. For this purpose we leave some space for such a kicker after the four bump kickers, as seen in figure 26.

6.2 The injection chain

The injection chain as shown in figure 28 consists of a laser-driven RF-gun, a thermionic stand-by RF-gun, a 100 MeV linac, a possible debuncher and the booster synchrotron.

Electron gun

A laser-driven RF-gun will prepare single bunches (without satellites!) with very high charges up to 10 nC (10 mA/bunch in SLS correspond to 8 nC bunch charge) as well as very short (\sim 1 ps) high-brightness bunches to drive a SASE-FEL (Self Amplified Spontaneous Emission Free Electron Laser) to be operated in the time between injections. One of the possible FELs could work at 3—4 MeV in the sub-mm range ($\lambda\sim$ 100 µm), another one at 50 MeV in the infrared.

Filling of SLS to any number of bunches and any current takes at the most 40 seconds (= SLS-harmonic number x booster cycle). Further reduction of injection time may be possible by distributing the laser pulse power on a couple (~ 10) of bunches by using a laser with long life-time of optical inversion (Ti:Sapphire) or by using stacks of partly reflecting mirrors to split the pulse.

Considering the limited reliability and lifetime of photocathodes it seems sensible to have two guns. The other gun should be a thermionic RF-gun accompanied by an α -magnet for energy-filtering. It covers all tasks of the laser-gun except the on-axis injection in a single shot due to the limited bunch-charge. However concerning filling of SLS with many low-charge bunches, the thermionic gun is even superior to the laser-gun due to its higher repetition rate.

Linear accelerator and debuncher

The 100 MeV linac will be a usual 3 GHz Radio Frequency structure equipped with SLED cavities [33] to minimise linac length and RF-power as well to compensate the beam-loading induced energy-spread of high-charge bunch trains, by means of exploiting the slope of the SLED-pulse.

A debuncher is recommended to improve the injection efficiency, because the longitudinal phase-space at the linac-exit (short bunch, large energy-spread) does not match the longitudinal acceptance of the booster synchrotron (long bucket, small energy acceptance). This device consists of two 3 GHz cavities and a double bend achromat. During acceleration in the booster synchrotron the energy-spread decreases rapidly due to adiabatic and radiation damping as shown in figure 29.

Transverse matching causes no problems, because the emittance at the gun exit is small compared to the linac's transverse acceptance, and the adiabatically damped emittance at the linac exit is much smaller then the booster's transverse acceptance. The SLS storage ring is decoupled from the linac/gun system by radiation damping of the booster.

Booster Synchrotron

The booster takes the electrons from the 100 MeV Linac and accelerates them to the nominal 2.1 GeV energy of the storage ring. The full energy injection into this ring avoids energy ramping, leading to stable and reproducible conditions at injection.

The layout of the booster is similar to the one built for SPEAR in Stanford. The main parameters are given in table 8. The FODO-lattice has 16 periods or 32 half cells. 24 of those are filled with dipoles, each with a bending angle of 15°. This leaves plenty of room for straight sections, some of which are used for injection, extraction and the RF-station. Figure 30 shows a layout of the extraction region.

The booster will be able to accelerate either a single bunch or a train of up to 150 bunches. The repetition rate will be 10 Hz, using a resonant "White-circuit", which allows a rapid filling of the storage ring. The harmonic number is chosen as h=3.59, containing no prime numbers of the storage ring harmonic. This allows for an efficient timing of the injection sequence due to the "cogwheel"-effect.

Table 8: Main parameters of booster synchrotron

| Circumference Harmonic number (500 MHz) Minimum energy Maximum energy Cycling frequency Horizontal emittance (2.1 GeV) | [m] [GeV] [GeV] [Hz] [µm·rad] | 106.2 177 = 3.59 0.1 2.1 10 0.28 |
|--|---|---|
| Relative energy-spread (2.1 GeV) | μιπτασ | 8.3·10-4 |

7. Vacuum System

7.1 Introduction

There are some basic requirements common to all storage ring vacuum systems [36]:

- Stored beam lifetimes due to residual gas must be >10 hours.
- Good lifetime must be achieved soon after start-up and after sections are vented and opened up for changes; i.e. short "conditioning time".
- "Smooth" chamber wall design to minimise electromagnetic fields and losses induced by the beam.
- Ease of modification for new developments, i.e. new insertion devices, beam ports etc.

In order to achieve a good beam lifetime it is necessary to have operating pressures in the nano-torr range. Pressures of this order are easily obtained in stainless-steel or aluminium chambers, but must be maintained in the presence of synchrotron radiation originating from the circulating beam.

Radiation striking components in the vacuum chamber desorbs gas molecules from the material. This photon induced desorption is expected to dominate the gas load in the chamber. In recent years photodesorption yields (number of desorbed molecules per incident photon) have been measured in extensive experiments for many materials; these values, together with some suggestions for pretreatments like chemical cleaning and bake-out under vacuum may be found in references [37]–[40]. The photodesorption yield decreases with the photon dose (time integrated photon flux) of the desorbing material, which is called the "beam cleaning" effect. As a result, the vacuum system pressure improves with the time integrated stored beam current.

Measured outgassing rates, after an appropriate conditioning period, appear to be about the same for many metals such as stainless steel, aluminium and copper. Hence, the choice of material for the vacuum chamber is not strongly connected with the operating pressure requirements.

For the vacuum system design of recent light sources [4]–[7] the radiated photon fan will be absorbed at discrete locations rather than by distributed absorbers along the beam chamber as on most former machines. Discrete absorbers have two main advantages, (i) the pumps may be mounted close to the photon absorbers (the source of the gas load) and (ii) gives a short "conditioning time" due to a high photon flux on the desorbing surfaces.

7.2 Vacuum chamber constraints

For SLS the vacuum system is severely constrained by the lattice design. Due to the short bending magnets and having a separation angle of only five degree between the photon beam and the electron trajectory, the separation of the photon and electron beams is small. Also, the dense packing of quadrupoles and sextupoles give a very limited access for discrete absorbers, beam ports and pumping. Consequently an antechamber which extends over the whole of a straight section is the presently favoured solution [41]. This is shown in figure 31.

7.3 Design implications

The antechambers allow the photons to pass the quadrupole sections, hence into the separate photon beam-lines and also acts as a pumping channel for the electron beam vacuum. Such antechambers can be designed to accommodate large pumps mounted beside the magnet system.

Two discrete photon absorbers are located within each antechamber. These act as a collimator for the photon beam line and also prevent completely radiation directly impinging on the chamber wall. As a consequence of this antechamber solution, the focusing magnets will require a splittable figure-of-eight yoke to allow the insertion of the vacuum chamber (see figure 32).

Further consequence of this antechamber solution is, that aluminium would have to be the material of construction, because of the complicated structure. This has disadvantages as commercially available standard UHV-components such as flanges and bellows, being made from stainless-steel, could not be used.

The final decision on chamber design for SLS (including the choice of material of construction) will require further careful study, considering the needs of magnet design, safe photon absorption, vacuum requirements and thermal and structural stability.

7.4 Photon absorbers

The main synchrotron radiation sources are the ring bending magnets. (Additional sources of synchrotron radiation are the Insertion Devices (ID's) placed in the straight sections. The synchrotron radiation of ID's has a very small horizontal opening angle so that it does not strike any components in the vacuum system.) In SLS, the discrete photon absorbers block all synchrotron radiation except that going to the beam lines, as shown in figure 31. This means that synchrotron radiation does not strike any portion of the chamber directly.

The power distribution on the absorbers as well the photon induced gas load are basic data for the design of both the absorbers and the vacuum system. The photon induced gas desorption and the peak power density on the surface of a discrete absorber downstream of a bending magnet have been calculated [42]. The results for SLS operating at 2.1 GeV and 400 mA are shown in figure 33 for an absorber which stops a 5° photon fan emitted from a superconducting-bend and for the absorber layout shown in figure 31 give the following values:

| | Absorber position | Inclined angle | Peak power density W/mm ² | Photon induced gas desorption (100Ah) nTorr·liter/s |
|--------------------------------------|-------------------|-------------------|---|--|
| s.cbend: Absorber 1 Absorber 2 | 0.65 3.4 | 18 90 | 150 15 | 200 350 |
| n.cbend: Absorber 3 Absorber 4 | 0.2 2.8 | 45 90 | 90 4 | 150 350 |

A total photon intensity of $\approx 2 \cdot 10^{19}$ /s is radiated from a 10° bending magnet. The total radiated power from a superconducting bend is ≈ 13 kW and from a normalconducting bend ≈ 4 kW. The peak power density of 150 W/mm² on the first absorber downstream of a superconducting bend is the same as that for the high power absorber of ESRF at 6 GeV and 200 mA operation. Therefore the design of the ESRF absorber [43], which is in operation, can be taken as a reference for the SLS high power photon absorber.

7.5 Pumping system

High gas loads will be produced by the absorbers and it is proposed to increase the pumping speed in these regions with a combination of lumped ion pumps and non-evaporable-getter(NEG) pumps, which have been used successfully at CERN [44] and ESRF. Combining NEG and ion pumping is effective for all the common residual gases such as argon, CO, CO₂, CH₄ and water vapor. In addition to the gas load released by the photon induced desorption from the absorbers, an almost equal contribution comes from thermal induced gas desorption. Assuming a desorption rate of 10⁻¹¹ Torr·liter/s/cm² and a total vacuum surface of 4.5·10⁴ cm² for each chamber, this gives an additional load of 450 nTorr·liter/s to be handled.

To meet the pressure requirement of one ntorr at 400 mA operation and after a "conditioning" period of 100 Ah one needs a pumping speed of 1000 liter/s for each chamber. This may be achieved by a 400 liter/s StarCell [45] ion pump with NEG at each absorber and two additional 120 liter/s StarCell ion pumps in each antechamber region. This means for the storage ring vacuum system, there will be a total installed pumping speed of 44000 liter/s. Some additional small pumps are required for the insertion device chambers and the injection section.

8. The Superconducting Dipole

As mentioned earlier we want to offer hard X-rays, produced by the 2.1 GeV SLS storage ring, in order to attract a wider user community. The radiation from normal conducting bends with a field of 1.4 T has a critical energy of 4.1 keV, too low for the X-ray region above 15 keV. By using superconducting bends with a field of 4.7 T we can increase the critical energy to 13.8 keV, assuring thus a reasonable flux up to about 50 keV.

To guarantee a low emittance of the circulating electron beam we have to integrate these s.c.-bends carefully into the magnet lattice. In an earlier lattice version, published in our conceptual study report, a combined function magnet was required, i.e. the s.c.-dipole had to provide a field gradient for vertical focusing. Detailed calculations [34] with 2D- as well as 3D-magnet codes showed, that such a magnet is indeed feasible.

In the meantime a new and simpler lattice has been worked out, where only a homogeneous dipole field is needed. The properties of such a dipole are summarised in the table below.

Table 9: Properties of the superconducting bending magnet

| bend angle | 10° |
|---------------------------|-------------|
| magnetic length | 0.26 m |
| radius of curvature | 1.49 m |
| energy range | 1.0-2.1 GeV |
| magnetic field | 2.2—4.7 T |
| good field region x and y | ±20 mm |
| homogeneity | ±0.04 % |

8.1 General magnet design considerations

P. Vobly from Novosibirsk, who originally proposed the use of s.c.-dipoles for a compact storage ring, has worked out the geometry shown in figure 34 for our case. A combination of four coils, all fed by the same power supply, guarantees a very homogeneous magnetic field around the beam axis. Figures 35, 36 confirm this claim.

We add here some comments by P. Vobly to the design of such a s.c.-dipole: The choice of the superconducting dipole magnet for SLS was made in two stages. First, the advantages and disadvantages of the magnet with iron pole pieces were compared with its iron-free analog.

1. Magnet with iron pole piece:

Advantages:

- lower number of Ampere-turns in the main coils
- lower stored energy
- reduced ponderomotive forces on the coils

Disadvantages:

- needs 2 power supplies to have a homogeneous field at different field levels
- each coil (with the exception of the main coil) has two sections, which increases the number of soldered contacts between the s.c.-coils
- the iron pieces lead to tighter tolerances on the magnet components

2. Magnet without iron pole pieces:

Advantages:

- Use of single section coils
- · use of single power supply

Disadvantages:

- higher ponderomotive forces acting on the coils (by a factor of three)
- thicker coils needed (by a factor of two)

Taking into account that at the field level of 4.7 T the magnetic pressure does not exceed 90 bars, and that clamping of such a coil is not very difficult, the magnet with iron-free pole pieces was chosen. A decisive factor in making this choice was the fact that the magnet needs only one power supply. This is a very significant advantage in the case that each dipole is powered by individual power supplies, since it halves the number of cryogenically cooled leads. In addition it would allow the use of superconducting transformers in powering such magnets (in this case the current flowing in the cold leads can be reduced by an order of magnitude).

After the choice of the magnet with iron free pole pieces was made, two versions of such a magnet were considered: One version is a magnet with racetrack coils. Such coils are relatively easy to wind compared to the saddle shaped coils. The disadvantage of this version is the rather strong dependence of the magnetic field on the longitudinal and transverse coordinates. Final determination of the integral properties of such a magnet requires detailed 3-D field calculations.

In a second and better version, a magnet with modified saddle shaped coils is proposed. Winding of such a coil in this version is significantly simplified, at the same time retaining all the advantages of the saddle shaped coils, i.e. no gaps in the coil at the medium plane, which significantly improves the homogeneity of the field compared with the racetrack version. In this version the magnetic field depends in a first approximation only on the longitudinal coordinate. This allows estimation of the integral properties of such a magnet using 2-D field calculations.

8.2 Cryogenic design

For the superconducting dipole the wedge coil structure of Vobly was chosen as the one which gives the highest field homogeneity with the simplest means. Because of the request to operate the magnet with only one current source, the solution without iron core was chosen which imposes stringent conditions on the statics of the whole construction with the corresponding consequences for the cryogenic design.

As a result of a preliminary study [35] of the cryogenic aspects, the solution with centralised cryogenic system was eliminated, attention being given to the local cryogenic system with three variations:

- a cooling system with continuous supply of LN2 and LHe
- b elimination of LN₂ cooling by using a two stage cryocooler
- c two stage cryocooler and He recondensation system

In cases **b** and **c**, additional complexity is added to the whole construction by the need of one (case **b** or two (case **c**) Gifford-McMahon cryocoolers. The second cryocooler in case **c** comes as an integral part of the so called He recondensation unit. The increase in complexity is however overwhelmed by the advantage of very low LHe consumption and the long term operation of the magnet. For all cases the possibility and the advantage of using retractable current leads should be analysed.

The thermal loads on the s.c.-dipole cryostat are shown in Table 10 together with the cryogenic consumption appropriate for the variant **a** at steady state. It is worth noting that also the cryogenic system for the variant **a** is local in principle, it is (or should be) also centralised in respect to the He recovery. This will have a central gas bag, a central high pressure compressor to compress the used He back into the high pressure cylinders and a small low pressure compressor with the suction side connected to the gas bag bus and the pressure side connected to the gas space (low pressure bus) of the LHe delivery container.

Figures 37 and 38 show a transversal section through the cryostat which emphasises the magnet support system (and the cryostat design for variant \mathbf{c}).

The cooling of the s.c.-dipole

The coil windings of the s.c.-dipole and the iron yoke are bath cooled with LHe. In order to eliminate the need of additional field-coupling coils, the whole iron yoke is immersed in the helium bath, a solution which however increases the overall dimensions of the cryostat. The windings are mechanically supported by a laminate structure consisting of alternating, good thermal conducting Al perforated plates intercalated with G-11 fibre-glass reinforced epoxy plates. The perforated holes build axial channels which help increasing the contact surface to the LHe bath and the Al plates assure a good thermal conductivity transversally to the magnet axis to the innermost windings. A detailed thermal stress analysis is however needed in order to optimise the proposed solution.

Two plate heat exchangers connected in series are attached to the upper and bottom faces to the iron yoke. Circulating LN_2 through the two plate heat exchangers assures a cheap and rapid cool-down of the magnet from 300 K to 80 K. After this cool-down stage the magnet is cooled down to 4.2 K by filling the cryostat with LHe. The cool-down sequence is in general the same for all constructive alternatives. Differences occur only for the steady state cooling i.e. normal operation of the magnet. In the variant $\bf a$ the cryostat is continuously supplied with LN_2 to cool the 80 K radiation shield and with LHe to recuperate the natural boil-off of the cryostat. Eventually a PID control loop is attached between the level-metre in the cryostat and a valve on the LHe transfer line to maintain the helium level between acceptable limits.

In the variant $\bf b$ and $\bf c$, the refilling with the LHe could take place one or two times per year as a consequence of the very low boil-off of the cryostat. No LN₂ to cool the radiation shield is needed. All that is achieved with the help of a two stage Gifford-McMahon refrigerator which cools two concentric radiation shields at 80 K and 20 K.

A helium recondensation system (figure 39) in the variant $\bf c$ gives the lowest LHe boil-off (theoretically zero). Only that helium must be added to the cryostat which could not be reliquified because of the fluctuation in the magnet operation or uncontrolled heat sources.

An important reduction (ca. 50 %) in the LHe consumption is possible due to the use of retractable current leads i.e. with the magnet operated in the permanent mode. A more detailed analysis is however necessary in order to investigate the possible consequences of the natural decay rate of the current in the short-circuited magnet winding on the homogeneity and stability of the magnetic field.

Table 10: Parameters for the s.c.-dipole cryogenic system

Cryostat

| Nominal temperature levels | 80 K, 4.2 K |
|-------------------------------------|-------------|
| Overall length [mm] | 800 |
| Outer diameter [mm] | 1000 |
| Overall height [mm] | 1510 |
| Cold mass (Magnet & iron yoke) [kg] | 1300 |
| Number of support posts | |
| - compressive: | |
| stainless steel | |
| Ø 30x1, 80 K station at $z = 100$ | 4 |
| - tensile: | |
| E-Glass Fabric Bisphenol A, G-10CR | |
| Ø 8x767, no 80 K station | 4 |

Thermal Load

| | 80 K [W] | 4.2 K [mW] |
|---------------|----------|------------|
| Radiation | 1 | 84 |
| Supports | 10 | 450 |
| Piping | 1 | 20 |
| Current leads | | 543 |
| Total | 12 | 1097 |

Cryogen consumption

| | l/hour | l/day |
|-----------------|--------|-------|
| LHe | 1.52 | 36.42 |
| LN ₂ | | 6.5 |

9. Representative Photon Sources

To calculate the peak brightness produced by a bending magnet or an undulator one has to determine the photon distribution in transversal phase space as outlined e.g. in [46]. One has to take into account, that there are two different contributions to the effective photon source.

- diffraction effects from a single electron
- finite emittance of the electron beam

To simplify the picture we assume that the corresponding distributions can be approximated with Gaussian distributions, which in turn are represented by rms phase space ellipses. The effective source ellipse is thus the convolution of the beam ellipse and the diffraction ellipse, which we assume both to be upright. The emittance of the diffraction limited source depends on the chosen wavelength λ and is given by

$$\varepsilon_{\rm r} = \frac{\lambda}{4\pi}$$

The beam ellipse can be represented by either pair of parameters:

$$\begin{split} &\sigma_{x,y} = \text{rms} - \text{amplitude} \\ &\sigma_{x,y} = \text{rms} - \text{divergence} \\ &\epsilon_{x,y} = \sigma_{x,y} \cdot \sigma_{x,y} = \text{rms} - \text{emittance} \\ &\beta_{x,y} = \sigma_{x,y} \, / \, \sigma_{x,y}' = \beta - \text{function at source point} \end{split}$$

In the following we show two examples, one for a typical undulator in the VUV- region, the other for the superconducting bend. As a reference we take an SLS-lattice with the following parameters:

$$E=2.1~\text{GeV},~I=0.4~\text{mA}$$

$$\epsilon_{xo}~(1~\text{GeV})=0.75~\text{nm} \qquad \epsilon_{x}=3~\text{nm} \qquad \epsilon_{y}=0.3~\text{nm} \qquad 10\%~\text{coupling}$$

a) Undulator

The wavelength of the undulator radiation is given by

$$\lambda = \lambda_u \frac{(1 + \frac{1}{2}K^2 + \gamma^2\theta^2)}{2n\gamma^2}$$

with the parameters

 λ_{ii} =period

N = number of periods

L = $N \lambda_u$ = total length

K =strength

n =harmonic of radiation

 θ = "average" emission angle = $\sqrt{\Sigma_{\chi}^{2}} + \Sigma_{y}^{2}$

(see below for definition of $\Sigma_{x,y}$)

The wavelength resolution $\Delta \lambda / \lambda$ is given by

$$\frac{\Delta\lambda}{\lambda} = \frac{\gamma^2\theta^2}{1 + \frac{1}{2}K^2} = \frac{\lambda_u}{2n\lambda}\theta^2 = \frac{1}{nN} + \frac{\lambda_u}{2n\lambda} \left(\frac{\epsilon_x}{\beta_x} + \frac{\epsilon_y}{\beta_y}\right)$$

For a zero emittance beam this is reduced to $\Delta \lambda / \lambda = 1/(nN)$.

As an example we take for SLS an undulator with L = 5 m, λ_u = 50 mm, N = 100, n = 1, K = 1.4

This gives a wavelength of $\lambda=3$ nm, corresponding to a photon energy of 400 eV. For an undulator the β -function for ideal matching to the diffraction limited source should be $\beta_r=L/(4\pi)\approx0.4$ m for our case. We choose for the undulator section a β -value of 2 m, taking into account a slight mismatch. (In the injection section it is advantageous to have a higher β of about 8 m.)

In the following lines we show how we arrive at the effective photon source parameters and the corresponding brightness.

Beam ellipse:

Diffraction ellipse:

$$\begin{array}{lll} \beta_{r} & = & L/(4\pi) & = 0.4 \text{ m} \\ \epsilon_{r} & = & \lambda/(4\pi) & = 0.25 \text{ nm} \\ R & = & \sqrt{\lambda L/(4\pi)} & = 10 \text{ }\mu\text{m} \\ R' & = & \sqrt{\lambda/L} & = 25 \text{ }\mu\text{rad} \end{array}$$

Photon source:

The corresponding ellipses in the horizontal and vertical phase space are shown in figure 40.

The formula for the spectral brightness F_1 is given by the ALS-handbook [47]:

$$F_1 = 1.431 \cdot 10^{14} \text{ N} \cdot \text{Q}_1 \cdot \text{I}$$
 [ph/(s · 0.1 % BW)]

With $Q_1 \approx 0.75$ we have for the peak brightness B

$$B = \frac{F_1}{(2\pi)^2 \varepsilon_{tx} \varepsilon_{ty}} \approx 4 \cdot 10^{19} \frac{\text{photons}}{\text{s} \cdot \text{mm}^2 \cdot \text{mrad}^2 \cdot 0.1\%BW}$$

It is interesting to note, that for our special case we have, for constant coupling, an approximate scaling law for the brightness with undulator length and emittance:

$$B \sim \frac{L^{1.5}}{\varepsilon_x^{1.4}}$$

The "average" emission angle θ is given by

$$\theta = \sqrt{\Sigma_X^{'2} + \Sigma_V^{'2}} = 54\mu \text{rad}$$

which leads to a wavelength resolution of

$$\frac{\Delta \lambda}{\lambda} = \frac{\lambda_{\rm u}}{2\lambda} \theta^2 = 2.4\%$$

This has to be compared with a value of 1/N = 1% for the case of zero emittance, where $\Sigma_x^{'} = \Sigma_y^{'} = R^{'} = \sqrt{\lambda/L}$.

b) Superconducting bend

For the s.c.-bend we assume the following parameters:

| Length | L | = | 0.26 m |
|---------------------|----------------|---|--------|
| Bend angle | θ | = | 10° |
| Field | В | = | 4.7 T |
| Radius of curvature | ρ | = | 1.5 m |
| Critical energy | ϵ_{c} | = | 14 keV |

The maximum flux occurs at 0.3 \cdot $\epsilon_c \approx 4$ keV and is given by eq. 3-17 in [47]

$$\frac{dF_b}{d\theta} = 2.457 \cdot 10^{13} E \cdot I \cdot G_1$$

With G_1 (0.3) = 0.92 we get

$$\frac{dF_b}{d\theta} \approx 2 \cdot 10^{13} \text{ ph/(s·mrad·0.1 \% BW)}$$

For the peak brightness we have to calculate first the effective source amplitudes Σ_x , Σ_y . Due to the small divergences involved, the source broadening, from the curvature of the trajectory, can be neglected.

The maximum brightness occurs at 0.8 \cdot ϵ_c = 11 keV, corresponding to λ = 0.11 nm.

Beam ellipse:

Diffraction ellipse:

$$eta_r = 0.8
ho/\gamma = 0.3 \ mm$$
 $\epsilon_r = \lambda/(4\pi) = 0.009 \ nm$
 $R = 0.65/\gamma = 160 \ \mu rad$
 $R' = \epsilon_r/R' = 0.06 \ \mu m \approx 0$

Photon source:

$$\begin{split} \Sigma_{x} &= \sqrt{\sigma_{x}^{2} + (D\frac{\Delta p}{p})^{2}} = 35 \; \mu m \qquad \qquad \Sigma_{y} \qquad \approx \; \sigma_{y} = 55 \; \mu m \\ \Sigma_{x}^{'} &= \sqrt{\sigma_{x}^{'2} + R^{'2}} = 188 \; \mu rad \qquad \Sigma_{y}^{'} \qquad \approx \; R^{'} = 160 \; \mu rad \\ \epsilon_{tx} &= \Sigma_{x} \Sigma_{x}^{'} = 6.6 \; nm \qquad \qquad \epsilon_{ty} = \Sigma_{y} \Sigma_{y}^{'} = 8.8 \; nm \end{split}$$

We have a large mismatch between the β -values of the beam- and the diffraction-ellipses with $\beta_x \approx 1300~\beta_r$ and $\beta_y \approx 3 \cdot 10^4~\beta_r$! The increase in the emittance is relatively modest in x (120 %), but substantial in y (from 0.3 to 8.8 nm).

The maximum in the angular photon distribution is given by eq. 3-15 from [47]:

$$\frac{d^2F}{d\theta d\psi} = 1.327 \cdot 10^{13} I \cdot H_2$$

With H_2 (0.8) = 1.5 we get

$$\frac{d^2F}{d\theta d\psi} = 3.5 \cdot 10^{13} \frac{\text{photons}}{\text{s} \cdot \text{mrad}^2 \cdot 0.1\% \text{ BW}}$$

and the peak brightness is from eq. 3-22 in [47]:

$$B = \frac{\frac{d^2F}{d\theta d\psi}}{2\pi\Sigma_{x}\Sigma_{y}} = 2.9 \cdot 10^{15} \frac{\text{photons}}{\text{s} \cdot \text{mm}^2 \cdot \text{mrad}^2 \cdot 0.1\% \text{ BW}}$$

c) Normal conducting bend

For the n.c.-bend we assume the following parameters:

| Length | L = | 0.88 m |
|---------------------|-------------------------|---------|
| Bend angle | θ = | 10° |
| Field | B = | 1.4 T |
| Radius of curvature | ρ = | 5.0 m |
| Critical energy | $\varepsilon_{\rm c} =$ | 4.1 keV |

The maximum flux occurs at 0.3 \cdot $\epsilon_{\text{C}} \approx$ 1.2 keV and has the same value as for the s.c.-bend:

$$\frac{dF_b}{d\theta} \approx 2 \cdot 10^{13} \text{ ph/(s} \cdot \text{mrad} \cdot 0.1 \% \text{ BW)}$$

The maximum brightness occurs at 0.8 \cdot ϵ_c = 3.3 keV, corresponding to λ = 0.38 nm.

Beam ellipse:

Diffraction ellipse:

$$eta_r = 0.8
ho/\gamma = 0.3 \ mm$$
 $\epsilon_r = \lambda/(4\pi) = 0.009 \ nm$
 $R' = 0.65/\gamma = 160 \ \mu rad$
 $R = \epsilon_r/R' = 0.06 \ \mu m \approx 0$

Photon source:

$$\begin{split} \Sigma_{x} &= \sqrt{\sigma_{x}^{2} + (D\frac{\Delta p}{p})^{2}} = 35 \; \mu m \\ \Sigma_{y} &\approx \sigma_{y} = 55 \; \mu m \\ \Sigma_{x}^{'} &= \sqrt{\sigma_{x}^{'2} + R^{'2}} = 189 \; \mu rad \\ \varepsilon_{tx} &= \Sigma_{x} \Sigma_{x}^{'} = 6.6 \; nm \\ \end{split}$$

$$\Sigma_{y} \approx R' = 160 \; \mu rad \\ \varepsilon_{ty} &= \Sigma_{y} \Sigma_{y}^{'} = 8.8 \; nm \end{split}$$

It turns out that the peak brightness is the same as for the s.c.-bend:

$$B = 2.9 \cdot 10^{15} \frac{\text{photons}}{\text{s} \cdot \text{mm}^2 \cdot \text{mrad}^2 \cdot 0.1\% \text{ BW}}$$

The complete brightness curves as a function of wavelength are shown in figure 3 for both bending magnets and undulators.

10. Alignment and Stability

10.1 Introduction

A high brightness, low emittance machine like SLS is very sensitive to positioning errors of the magnets of the ring (dipoles, quadrupoles and sextupoles). This is especially true for the quadrupoles because of their high magnetic field gradients. Both, misalignment as well as movements of the magnets lead to distortions of the closed orbit, which in turn result in decrease of brightness and dynamic aperture.

Slow movements of the magnets can be introduced by thermal deformation of the ring or its components and by motions of the hall floor or parts of it, caused amongst other reasons by a varying ground water level. Faster periodic movements with a frequency up to, say, 100 Hz can be induced by vibrations whose sources may lay either within the SLS hall or outside. The former must be minimised by thorough engineering and placing of machines like cranes, pumps, compressors etc. The latter, as for instance traffic on the public road or other "cultural noise" or general Ground Tremor (micro earthquakes etc.) are out of our control. We have to know their intensities and characteristics in order to take appropriate countermeasures.

10.2 Survey and alignment

Very critical is the matching of the electron beam and the central axis of the insertion devices and the superconducting magnets. This has to be done to micron accuracy in order to achieve the high brightness and low emittance, which will be the trademark of this novel machine. This poses requirements to the precision of the survey and the alignment of the ring elements and the beam position measuring probes which are significantly more stringent than in the existing PSI accelerators. However, the expertise gained in this domain as well as in the high precision L3 LEP experiment at CERN [48] where PSI is participating in the solution of delicate alignment problems, will be a valuable base from which further necessary steps can be taken.

We plan to arrange subsets of ring elements on solid and stiff girders on which these elements will be prealigned using an appropriate alignment stand. Following the well established example of the European Synchrotron Radiation Facility ESRF, each girder will be positioned on three remotely controlled high precision hydraulic jacks.

Survey and primary alignment of the girders will be done by high precision but classical triangulation. For this a primary survey net has to be established for which a set of concrete pillars has to be erected. They must be based on the natural rock below the ground water level. The primary survey grid and the positioning of the girders with reference to this grid will be done with the MEKOMETER 500 (a most modern computer controlled laser based telemeter system by LEICA) and classical WILD theodolites. With this instrumentation position precision of < 50 μ over the relevant distance of ca. 50 m and

direction precision of 10⁻⁴ newgrade will be achieved. This was recently demonstrated by the alignment of the gantry of the proton therapy facility currently under construction at PSI.

From this we conclude, that we can achieve an initial positioning of the most sensitive ring elements (quadrupoles, s.c. dipoles and insertion devices) with an accuracy of 50 μ . Such a misplacement induces an electron beam displacement which is approximately 40 times bigger, i.e. 2 mm. Probes will measure this actual displacement and a feedback system using correction magnets will apply a closed orbit correction, which will bring the beam very near to the ideal closed orbit. The beam width in the undulators and the s.c. dipoles will be σ_{χ} =50 μ . The closed orbit inside those most important elements must not deviate more than 10 % of σ_{χ} from the ideal orbit. This calls for an accuracy of the relative beam positioning of < 5 μ and this in turn asks for a measurement accuracy of about 1 μ and a similar precision in knowing the relative position of the probes!

The initial positioning precision can be corrupted by movements described above. Slow movements will be measured with a Hydrostatic Levelling System similar to that of the ESRF. Appropriate corrections will be applied, say, several times a year, using the hydraulic jacks m. a. Vibrations with frequencies of 0.01 to 100 Hz will be counteracted by the correction elements controlled by a fast feedback system.

10.3 Measurements of Ground Tremor at PSI

As described above, the source of vibrations can be Ground Tremor. With the help of the Schweizerischer Erdbebendienst of ETH Zurich [49] we undertook first investigations in order to measure the Ground Tremor at PSI near the prospective site of the SLS. Figure 41 shows the part of the PSI-West area which is relevant for the SLS project. Indicated are the spots where measurements were taken using highly sensitive seismometers including the locations 2' and 4', close to the foreseen SLS site. Here the seismometer probes were placed in the natural soil 30 cm below the surface.

Figure 42 gives for location 2'– in about 5 meter distance from the public road (Kantonsstrasse) – the measured lateral displacement as a function of time and the corresponding frequency spectrum. Displayed are three orthogonal components of the response to a heavy vehicle passing by on the public road. Note that the maximum induced amplitudes are 0.1, 0.3, and 0.5 μ , respectively. These are truly small and very promising values which would even be diminished had we measured on the foreseen floor of the SLS hall!

Figure 43 shows the "normal" Ground Tremor, i.e. without vehicle passage, at locations 2' and 4'. The maximum amplitudes are smaller, of course, and range from 0.1 down to 0.05 μ .

Figure 44 shows vibrations measured at location 5 on the floor of the existing experimental hall during normal operation, but without crane movement. The maximum deflections of 0.06 to 0.1 μ again are very encouraging. These and many other measurements we took show:

- Amplitudes of soil vibrations at the foreseen SLS site are smaller than 1 μ , even when they are caused by the passage of heavy vehicles.
- The frequency spectra show a broad continuum between 0.02 and 0.5 Hz. Isolated events show sharp lines of the frequency spectrum between 8 and 30 Hz.

From this we conclude:

There is measurable Ground Tremor at the prospective site of the SLS. However, the comparison with results of similar measurements undertaken at the sites of other Electron Storage Rings, as ALS (Berkeley), APS (Argonne), ELETTRA (Trieste), ESRF (Grenoble), SPring-8 (Japan), show comparable values. This indicates that appropriate countermeasures can be taken to prevent significant emittance growth induced by the ground vibrations.

11. Infrastructure

11.1 Site

The new SLS facility will be built on the south-west corner of the present PSI west site, within the territory of Villigen, on the left side of the river Aare. It will be partly on a free area of the present PSI site, partly on two adjacent lots 602/603. These lots are agricultural areas; they must be classified as industrial areas previous to a purchase by PSI.

The existing internal roads and the networks of electrical power, cooling water, sewage, etc. can be easily extended towards SLS.

SLS will be included in the present radiation controlled zone. Access will be through the existing access controls.

Situation of SLS

The precise location of SLS has been chosen to fulfil the following requirements:

- Leave enough space between the existing facilities and SLS for future extensions.
- Provide a possible extension of one beamline outside the SLS hall in the direction of the neutron facility SINQ.
- Take into account the possible extensions of the annexes
- Provide access to all sides of SLS on a small truck road
- Maximise the distance from the highway.

Therefore, the facility will be oriented parallel to the highway, placed as far SE as possible, taking into consideration the legal minimum distances from the area boundaries, as shown in Figure 41. The unpaved roads outside the future PSI area will be improved for the current agricultural use of the adjacent areas. The altitude of SLS must not be related to the altitude of the other experimental facilities. The altitude of the hall floor has been chosen from minimum cost considerations as 347.5 m above sea level. That is 2 m above the floor level of the present experimental halls.

Stability problems

The requirements on the mechanical stability, especially for the storage ring and for the experimental areas are far more stringent than usual: Differential settlements < 0.1 mm and vibration amplitudes at low frequencies < 1 μ m. Such small values cannot be fulfilled by the construction of the hall floor alone. The support structures for the components of the storage ring and of the experimental apparatus must be designed in a way to provide the required stability.

Nevertheless, the building must be designed to minimise the instabilities.

The main potential causes of instabilities are:

- A. Unstable geological layers, that may lead to settlements
- B. Variations of the water table
- C. Earthquakes
- D. Artificial vibrations both from outside (cultural noise) and from inside the facility

Two studies are under way with the help of laboratories of ETH Zurich:

- To A/B : Consultant Prof. H.J. Lang (Institut fuer Geotechnik ETHZ); 7 bores on the future SLS area.
- To C/D: Consultant Dr. D. Mayer-Rosa (Institut fuer Geophysik ETHZ); Vibration measurements within the present PSI facilities and on the SLS area (see section on alignment).

The results available to date suffice for the following basic conclusions:

- To A: The geological conditions under the SLS area are very convenient. The subsoil consists of compact sand/gravel layers (Aareschotter), 15–30 m deep, over a rockbed. The foundation will be placed on the Aareschotter after having removed the upper layer of loose clay of approx. 2 m thickness. The range of settlements of these compact layers is small, and the settling times after loading/unloading are short. Figure 45 shows the lines of equal altitude (isohypses) of the rockbed as found in 7 bores. There is a continuous slope of about 15 % towards the river Aare, contrasting with the abrupt terrace found in the northern part of the PSI west area. Therefore we do not expect differential settlements within short distances on the SLS site.
- To B: The ground water table is rather deep under the surface, i.e. deeper than 20 m. The levels shown in Figure 46 have been recorded in August 1993. The hillside water table slope consists of small amounts of water trickling through the permeable parts of the gravel layers. This water varies with rainfall, and feeds the ground water table. The ground water expands under the whole SLS area and can not be avoided by shifting the facility. Movements and settlements of the floor slab are not caused by the presence of a water table itself, but by variations of its level. The amplitude of these variations is estimated not to exceed 2 m. From theoretical calculations, vertical surface movements of 0.1 mm per 1 m water level

change are expected. Therefore it is important to investigate further the variations of the ground water level due to changing meteorological conditions and to the operation of the nearby well of PSI. Measurements are planned in 1994. We already know from pumping tests in test wells and in the PSI well that a pumping rate of 2000 liters/min lowers the water level by 0.5 m at 5–10 m distance and by a few cm at 100–150 m distance. The validity of the theoretical predictions on vertical surface movements will be controlled by high precision geodetical levelling.

To C: Villigen is situated in the zone of smallest earthquake probability within Switzerland (SIA-Norm 160, zone 1, MSK VI–VII).

To D: Cultural noise has been measured (see the section on alignment). In general, the cultural noise at the SLS site is not more intense than at other similar facilities. Vibrating machines at PSI, for example some of the present helium compressors, have to be isolated from the ground. Within SLS, the floor slab will be decoupled from the foundations of the hall and of the annexes, in order to minimize the transmission of noise to the storage ring and to the experiments.

Conclusion

The site of PSI in Villigen has ideal conditions within Switzerland as a site for an SLS building. The effects of small residual instabilities will be minimised by a careful building design.

11.2 Building layout

The building consists of an experimental hall, with annexes for offices, laboratories, technical supplies and control rooms.

The hall is 115 m \times 115 m, with a single central pillar. The floor consists of a 40 cm thick reinforced concrete slab. The roof is made of 4 thin reinforced concrete domes (system Isler) supported on 8 peripheral pillars and on the central pillar. The foundation of each pillar is 4–5 m deep and is independent from the floor slab.

A crane of 12 tons capacity is supported at one end on the central pillar, and at its other end on a circular rail suspended by the roof structure. The height of the hall is defined by the requested height of the crane. The height of the side walls (10.5 m) is well suited for annexes 2 to 3 stories high. The hall will house the whole accelerator complex, i.e. the linac, the booster and the storage ring, their magnet and RF power supplies, the areas for experiments using synchrotron light, and an area for free electron laser experiments. The annexes consist of conventional multipurpose buildings, built in an industrial standard type similar to the other buildings of PSI-west. A standard grid of 3.6 m length will be used. The present layout comprises a

complete annex at the NW corner of the hall, with two wings, one for office/lab type rooms and one for heavier technical equipment. A second annex is planned at the SE corner. It will be built first at the minimum size required for technical equipment, with the provision for later extensions. The presently planned capacity of the annexes is for 100 persons.

The existing supply tunnel system at PSI-west will be extended towards SLS, then diagonally under the whole SLS facility. This tunnel will distribute the electrical power, the cooling water, the heating water, etc. from the existing networks to the annexes of SLS and to the center areas of the booster and of the storage ring. The tunnel is furthermore the main emergency escape way from these center areas.

11.3 Supplies

Prof. K. Daniels (Lehrstuhl für Haustechnik, ETH Zürich) has led a general study for the SLS facility ("Grobkonzeptstudie Gebäudetechnik"). The study shows that the supplies for electrical power, cooling and heating water available on the site are sufficient.

Airconditioning

The requirements for the mechanical stability, mainly of the storage ring and of the experimental set-ups, imply constant temperatures. The present specifications for temperature stability at SLS have been derived from data worked out at other synchrotron light sources. Further detailed studies will include a review of the specifications on temperature stability in connection with the alignment concept, with the aim of relaxing the requirements.

Electrical Power

The high voltage transformers for 16 kV installed at present in the transformer substation at PSI-West can provide the estimated 6–7 MW to SLS, even with some reserve. 5 transformers with a total power of 8000 kVA are foreseen on the SLS site to transform 16 kV down to 380/220 V. The magnet power supplies and the RF power supplies will be installed in the center areas of the booster and of the storage ring.

Heating

The regional REFUNA network provides hot water at 120°C to the PSI facilities. The reserve of installed power on the PSI-west area is 1.2 MW. The max. simultaneous needs for heating and for cold water processing are 0.94 MW, i.e. the on-site available REFUNA power is sufficient.

Cooling water

- As in other facilities of PSI, two sorts of cooling water are needed: Demineralized water in a closed loop to remove the heat load from the magnets and other similar equipment. The water will have a slight radioactive contamination. The closed loop is cooled through heat exchangers by the water of the Aare. The temperature is maintained at 30°C, to avoid condensation. The space and the existing installations in the SG-building of PSI-west can accomodate 3 additional heat exchanger units of 2.8 MW each for SLS needs. The pipes will run from SG-building to SLS in the extended existing tunnels.
- Cold water (approx. 12°C): In the existing facilities of PSI, ground water from a well is used. We cannot expect a license to pump additional ground water for SLS needs. Therefore, cold water for SLS has to be processed in refrigerators. The study for heating and ventilation foresees to use the hot water from the REFUNA network as a power source for the refrigerators. A maximum hot water power consumption of 600 kW is assumed. This is a desirable way to use waste heat in summertime, when the needs for cold water are highest.

11.4 Radioactivity and radiation protection

We present here only a resumé of these problems. A detailed presentation will be included in a future safety report directed to the control authority HSK (Hauptabteilung fuer die Sicherheit von Atomanlagen). The safety report will be due after SLS has been approved and the technical details has been worked out. It will include the safety devices and procedures needed to comply with the legal limits as well as with the guidelines of HSK. The potential radiological hazards at SLS are lower by several orders of magnitude than at the existing facilities of the accelerator complex situated on the PSI west area, on the territory of Villigen. Therefore the radiation protection at SLS will be realized within the frame of the experience already accumulated at PSI, using the same monitoring procedures.

The protection has to fullfil the legal requirements valid inside the controlled area delimited by the fence of the PSI west area, as well as those applicable outside. A few examples of the max. permissible values in the design of the shielding:

- At places of short time access restricted to occupationally radiation exposed persons: 0.1 mSv/h
- At places of unlimited stay of occupationally radiation exposed persons: 0.002 mSv/h
- The dose integrated over one year at any place outside the PSI area shall not exceed 5 mSv.

Not only the maximum permissible individual dose is fixed by law.
 In accordance with the new swiss radiation protection law STRAVO, the control authority will define as well a limit for the admissible collective radiation burden to the persons occupied at SLS.

Concerning induced radioactivity two important limits have already been fixed:

- The limits for emissions to the air and to the waste water are set for the whole of PSI, including any future facility like SLS. Since the expected emissions from SLS will be negligible compared to these limits, they will cause no new problem.
- At the time of the future decommissioning of the facility, the earth under the building must be inactive according to the legal limits of STRAVO.

Operating conditions and protection

Under normal operation some high energy electrons will get lost mainly during extraction from one of the accelerator stages (linac or booster), during injection into the next stage (booster or storage ring) or during collisions with the atoms of the residual gas in the storage ring. Depending on the operating mode (batch or top-up injection) different loss rates are expected. In table 11 below the losses are calculated for the worst case scenario, where the lifetime in the storage ring is assumed to be as low as 30 min. In this mode we need top-up injection to keep the beam current approximately constant. The average beam loss in the storage ring is then given by the ratio between the injected charge (including the charge lost at injection) and the beam lifetime.

In the long lifetime mode the storage ring is refilled about 1–4 times per day. During a typical filling time of 1 minute the losses are about a factor 30 higher than the values in the table.

Table 11: Beam losses

| Injection efficiency into storage ring | 80 | % |
|--|-----|----|
| Extraction efficiency from booster | 90 | % |
| Storage ring current | 400 | mΑ |
| Accumulated charge in storage ring | 320 | nC |
| Continuous losses in storage ring (320 nC in 30 min) | 160 | pΑ |
| Injection losses in storage ring (80 nC in 30 min) | 40 | pΑ |
| Extraction losses in booster (40 nC in 30 min) | 20 | pΑ |
| Injection losses in booster during tests (100 MeV) | 1 | nΑ |
| Losses at the gun-to-linac transfer during tests (3 MeV) | 4 | nA |
| Linac current at FEL mode (100 MeV, 100 Hz) | 500 | nA |

Approximately 12 hours per week will be needed for test runs to optimize and develop the facility performance. As often as possible,

these runs will be performed at reduced intensity. Sometimes however, tests at maximum intensity with increased beam losses will be unavoidable. To keep the radiation burden to the operating crew as low as possible, the planning of such tests includes the following rules:

- Minimize the duration of tests with high beam losses
- Close the access to the areas with high dose rates.

At the commissioning of the booster and at further booster beam tests, access to the storage ring should be permitted without restriction for the personnel. A beam dump is planned in the injection path from the booster to the storage ring. The shielding of this beam dump is designed for a permanent loss of 5 nA at max. energy.

The shielding of the FEL area should allow unrestricted access to all other areas (booster, storage ring, supply areas) for the personnel.

Some failures, for example an accidental shut-off of a bending magnet, may throw the full electron beam off its stable orbit. The localized collision of the electron beam with material inside the shielding walls will give a local high dose rate outside the shielding. A system of ionisation chambers will detect such excursions and shut off the beam within milliseconds, so that the average dose rate should not increase, provided such accidents are relatively rare.

One potential consequence of an accident must be absolutely prevented: The electron beam of the storage ring shall not possibly be led outside the shielding wall through one of the experimental beam lines. If the detailed failure analysis shows such a possibility, preventive passive devices will be installed, for instance:

- a reduction of the spatial angle of the experimental beam with additional local shielding
- a permanent deflection of the experimental beam with mirrors placed inside the main shielding
- a permanent magnet to deflect any accidental electron beam out of the direction of the experimental beam

Radiation sources and shielding

The interaction of high energy electrons with matter produces different radiations, of which the three following components are important in shielding design. (Muons are not relevant at the relatively low energy of SLS)

 High energy gammas are produced in the electromagnetic cascade. The cascade has a strong forward peak. An other source of forward peaked gammas is the bremsstrahlung from interactions of the storage ring electrons with the residual vacuum chamber gas.

- Fast neutrons (E < 10 MeV) are produced by giant resonance reactions of gammas in matter. The emission is practically isotropic. This radiation is relevant to lateral shielding.
- High energy neutrons (E from 10 MeV to a few 100 MeV). The emission is weakly peaked forward. The production rate is relatively low. However, this radiation determines the dose outside thick shields, due to the large absorption length in shielding material.

Different radiation protection groups have developed semi-empirical formulae for the calculation of high energy electrons (for instance at DESY). They start with source terms of the dose flux from each radiation type. The sources are located at the starting points of electromagnetic cascades. The source terms for gammas are angle dependent. The attenuation in shielding material is exponential. For gammas, dose build-up in the innermost shielding layer is taken into account by adding a build-up layer (mostly Pb) to the shielding thickness calculated using the exponential attenuation.

These semi-empirical methods give the shielding thicknesses summarized in table 12, based on the beam losses of table 11. For the calculation of the storage ring shielding, we made the conservative assumption that the losses are concentrated at six source points.

Table 12: Shieldings

| Storage ring outer wall | 1 m baryte concrete |
|------------------------------------|--------------------------------|
| Storage ring forward direction | 12 cm Pb + 1 m baryte concrete |
| (vicinity of the experimental bear | |
| Storage ring inner wall | 0.6 m normal concrete |
| Storage ring roof | 0.5 m normal concrete |
| Beam dump forward | 25 cm Pb + 2 m normal concrete |
| Beam dump side shielding | 2.5 m normal concrete |
| Booster outer wall | 1.1 m normal concrete |
| Booster inner wall | 0.5 m normal concrete |
| Booster roof | 0.5 m normal concrete |
| FEL area side walls*) | 2 m normal concrete |

^{*)} Assuming an electron beam dump without side shielding effect

The basic design for the shielding of the storage ring and of the booster will be the same as has already been applied with good success at other light source facilities:

 Inner walls of poured in place concrete, on which electric cabling, cooling water pipes, ventilation channels etc. can be mounted. These lines cross the through mazes. Power supplies and main distributions are installed on the inner side of each ring.

- The outer wall is built of one layer of movable concrete blocks with rounded sides, as the examples of Elettra (Trieste) and of Bessy II (Berlin). The interlock of adjacent blocks provided by their rounded sides allows a maximum flexibility for the lay-out of such a onelayer shielding wall. The outer wall of the storage ring will be placed as close as possible to the ring, in order to minimize the length of the experimental beams inside the shielding.
- The roofs will be of movable concrete beams. If the beams can be placed in a way to avoid large cracks, one layer, 0.5 m thick, will be sufficient. Otherwise two interlocked layers of 0.25 m thickness may be used.

Induced radioactivity

Air: Ar⁴¹, as well as the short-lived positron emitters O¹⁵ and N¹³ will be produced in the air inside the shieldings. The emission of these isotopes will depend strongly on the rate of air exchange and release. A precise calculation will be made, after the ventilation system has been optimized and finalized. Provisional calculations under conservative assumptions (i.e. an air exhaust rate of 10 volumes per hour) give values lower by 6 orders of magnitude than the permissible emissions of these isotopes from the exhausts of PSI west area. The final values will be even much lower.

Earth: The earth under the hall floor shall be inactive at the demolition of the SLS facility, assuming a delay of 3 years after the definitive shut-down. Earth inactivity is granted wherever the flux of high energy neutrons has been lower than 8000 neutrons/cm²sec during a supposed 20 years operation. Under the 40 cm thick concrete floor, the maximum flux may reach 4 n/cm²sec, so that the requirements are safely fullfilled.

Water table: A radioactive contamination of the water table is excluded. This has already been shown for the PSI facility SINQ, where the water level is at 8 m below the building. At SLS site, the water level is approx. at 18 m below the building, and the neutron flux in vertical direction is 2000 times lower than at SINQ, i.e. we have even far safer conditions.

Water and waste water: Components inside the shieldings are cooled by closed demineralized water circuits permanently cleaned by ion exchangers. The radioactive contamination of the water, mainly from corrosion products from activated parts, is almost totally fixed in the ion exchangers. The activity of the water will be at a similar level as in the present secondary water circuits of PSI. The radiation protection procedures will be the same as at present:

 A permanent on-line control of the activity of the water circuits.

- The waste water from cooling circuits is collected in the existing retaining tanks system.
- The activity is controlled and the waste water is processed, if necessary, before leading it into the river Aare. Permissible values of water activity emissions have been defined by the control authority HSK for the PSI as a whole. SLS cooling water will contribute only a small fraction to the activity of all PSI waste waters.

Activated components: The components at the places of high beam losses (e.g. injection into the storage ring and extraction from the booster) and in their immediate vicinity will be activated. Through carefull design of the components and of local shielding, the dose received by the personnel during maintenance procedures will be minimized. PSI has a wide practical expertise in such techiques. With SLS, the problems of activated material will be comparatively easy to solve, since the production will be lower by several orders of magnitude than at other existing and future facilities of PSI.

Radiation protection and monitoring systems

The proven systems in operation at the present accelerator complex of PSI will be used at SLS. The health physics section of PSI is responsable for monitoring the radiations and implementing the safety rules.

Three permanent monitoring and safety systems will be installed:

- The already mentioned system of ionisation chambers inside the shielding vaults to detect high beam losses and to eventually shut off the beam. 60 ionisation chambers are needed.
- A system of approx. 20 neutron "Rem counters" will monitor the neutron dose leaking from the shieldings into the hall. This is in some respect redundant to the ionisation chamber system.
- The same access safety system PSA (Personen-Sicherheits-Anlage) as at the PSI accelerator complex, but as an independent second system. The PSA prevents the access to shielded enclosures whenever a beam production is allowed therein, and locks any beam port as long as a person is inside the enclosure. The number of accesses to the rings is dictated by emergency exit requirements. The total number of accesses to be monitored by PSA amounts to 8 (4 to the storage ring, 2 to the booster, one each to the linac and to the FEL area).

12. Budget Estimate

12.1 Project costs

The budget estimates are based on a layout which consists of the following items:

- Linear-Accelerator for electrons, 100 MeV; the electron gun and a first acceleration section will be carried over from a test stand
- Booster Ring, 0.1–2.1 GeV, 106.2 m circumference
- Storage Ring, 2.1 GeV, 240 m circumference
- "hexagon lattice": 6 achromats, each with 6 normal bends and 1 superconducting bend.
- long straight sections (18 m) and 4 medium straight sections (7 m)
- Initial operation with 3 Insertion Devices
- Initially only 4 out of possible 6 s.c.-bends will be installed
- beamline infrastructure, optical components and instrumentation for 5 "Beam lines", 3 from undulators and 2 X-ray lines from superconducting bends. In a second phase one has to increase this infrastructure.

The budget estimates are based on detailed numbers from the BESSY II Proposal and the ESRF Foundation Phase Report. The costs were scaled with the size of the facilities.

The investment costs were split into three parts as shown in tables 13 and 14

- A sum of about 160 MSFr., which has to be requested from the government through a "Botschaft", which in turn has to be approved by the Swiss Parliament. To build SLS we need an additional 2 ha of land adjacent to PSI (not included in the budget).
- For the beamlines 23 MSFr. will be provided by PSI (with hopefully some external help from Industry). This sum would have to come out of the regular operating budget.
- On the experimental chamber and detector side we hope that the "Nationalfond" will contribute in the order of 5 MSFr during the construction phase of four years.

12.2 Operating Costs

To get a rough idea about the operating costs of **SLS** we used as main items:

- power bill
- maintenance
- developments

Different "items" like: general services, lab usage, library, transport services, travel, general safety, central computing services etc. were not taken into account.

The operating costs for maintenance and developments will be covered by the normal annual research budget of PSI.

As a basis for the power bill we took an average power consumption of 6 MW during 6000 h per year and a unit price of .08 SFr/kWh. Maintenance and development costs were deduced from the project costs. The numbers are given in the table 15

12.3 Manpower Requirements

Construction Period:

Based on experience from similar projects (ALS in Berkeley, BESSY II in Berlin) we estimate, that about 500 man-years are needed to construct the SLS facility. This is under the assumption, that practically all accelerator components are ordered from industry, but put together and commissioned by PSI staff.

Operation Period:

To operate the completed SLS facility we need about the following manpower:

| accelerator facilities | 50 persons |
|------------------------|-------------|
| beamline facilities | 35 persons |
| technical support | 30 persons |
| total | 115 persons |

These numbers are based on the assumption, that the SLS-users expect a full support and continuing upgrading of the beamlines by the PSI staff. As seen from this table the operation of SLS will require a substantial technical support by the technical division B8 of PSI for civil engineering, workshop, design and engineering, vacuum system, power supplies, cooling etc.

The required manpower for SLS will be obtained by changes of the internal structure of PSI.

Table 13: Total investment costs of SLS

| | "Botschaft" | PSI | Nat. | Total |
|---|-------------|------|--------------|-------|
| | MSFr | MSFr | Fond MSFr | MSFr |
| Accelerator Complex Research Facilities | 77.0 | 23.0 | 5.0 | |
| 3. Conventional Facilities | 73.0 | | | |
| 4. External Manpower | 10.0 | | | |
| SLS Total costs | 160.0 | 23.0 | 5.0 | 188.0 |

Table 14: Investment Costs of SLS

| | MSFr | | MSFr |
|--|--|---|--|
| 1. Accelerator Complex | 77.0 | 3. Conventional Facilities | 73.0 |
| 1.1 INJECTOR SECTION 1.1.1 Electron Linac+Transfer 1.1.2 Booster (2.1GeV) 1.1.3 Transfer Lines 1.2 STORAGE RING 1.2.1 Magnets + Supports 1.2.2 Power Supplies 1.2.3 Supercond. Bends (4) 1.2.4 Vacuum System 1.2.5 RF System 1.2.6 Septa, Kickers 1.2.7 Diagnostic, Alignment 1.2.8 Control System 1.2.9 Instr. + Electronics | 24.0 6.0 17.0 1.0 53.0 16.0 6.0 4.0 7.0 6.0 2.0 3.0 6.0 3.0 | 3.1 Experimental Hall 3.2 Technical Buildings 3.3 Laboratory Buildings 3.4 Electrical Power 3.5 Cooling System 3.6 Heating System 3.7 Air-conditioning 3.8 Shielding 3.9 Security System 3.10 Infrastructure 3.11 Site preparation 3.12 Varia 3.13 Fees, consulting | 26.3 4.8 4.5 4.8 5.0 1.9 6.3 2.5 1.0 4.1 2.0 1.8 8.0 |
| 2. Research Facilities | 28.0 | 4. External Manpower | 10.0 |
| 2.1 INSERTION DEVICES (3) | 4.0 | | _1 |
| 2.2 BEAM LINES (5) | 24.0 | | |
| 2.2.1 Front Ends 2.2.2 Optics 2.2.3 Experim. chambers 2.2.4 Detectors 2.2.5 Control Systems 2.2.6 Cryogenic Systems 2.2.7 Ancillary Equipment 2.2.8 Radiation enclosure | 4.5 7.5 3.8 1.2 2.0 1.0 1.0 3.0 | | |

Table 15: Operating costs of SLS

| | MSFr/Jahr |
|--|-------------------|
| 1. Power bill | 3.0 |
| 2. Maintenance | 3.0 |
| Accelerator Experiments Infrastructure | 1.5 1.0 0.5 |
| 3. Developments | 5.0 |
| Accelerators Experiments | 2.0 3.0 |
| 4. Personnel costs | 12.0 |
| Total | 23.0 |

Figures

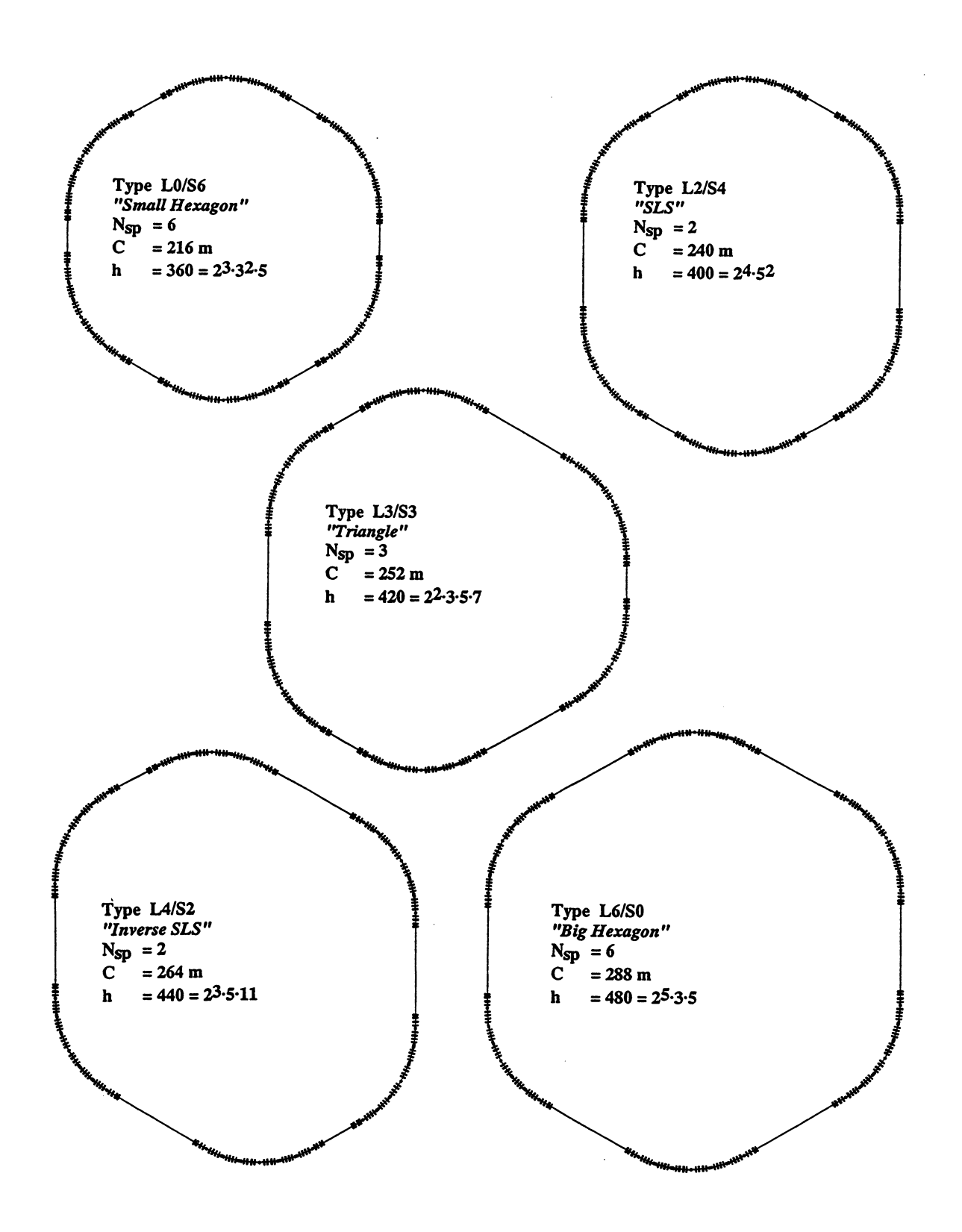


Figure 5: The SLS-"Isomers"

Five possible hexagon-lattices with different numbers of short (7 m) and long (18.48 m) straight sections may be composed from the 60° achromatic arcs.

They all have nice harmonic numbers, a large dynamic aperture and only slightly different optical functions for adjusting proper tune values. The proposed lattice for the SLS is shown in the upper right. (N_{so} is number of super periods, C is circumference, h is harmonic number)

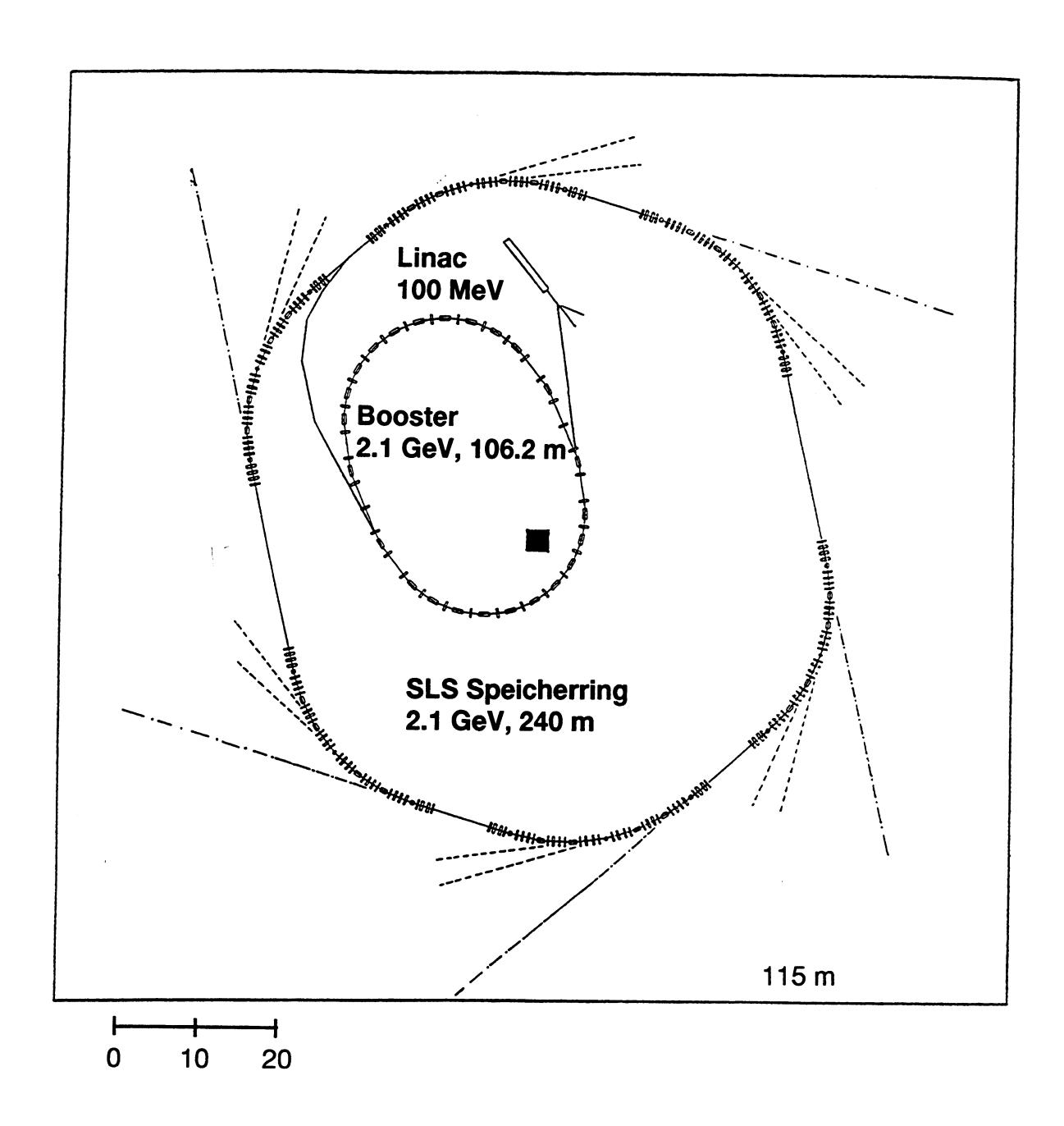


Figure 6: SLS Hall

Possible arrangement of storage ring, booster synchrotron and injector linac in a $115 \, \text{m} \times 115 \, \text{m}$ square hall, providing sufficient space for the photon beamlines. The beamlines based on the superconducting bending magnets (dashed lines) and undulators (dash-dot lines) are shown. One of the short straight sections is reserved for injection.

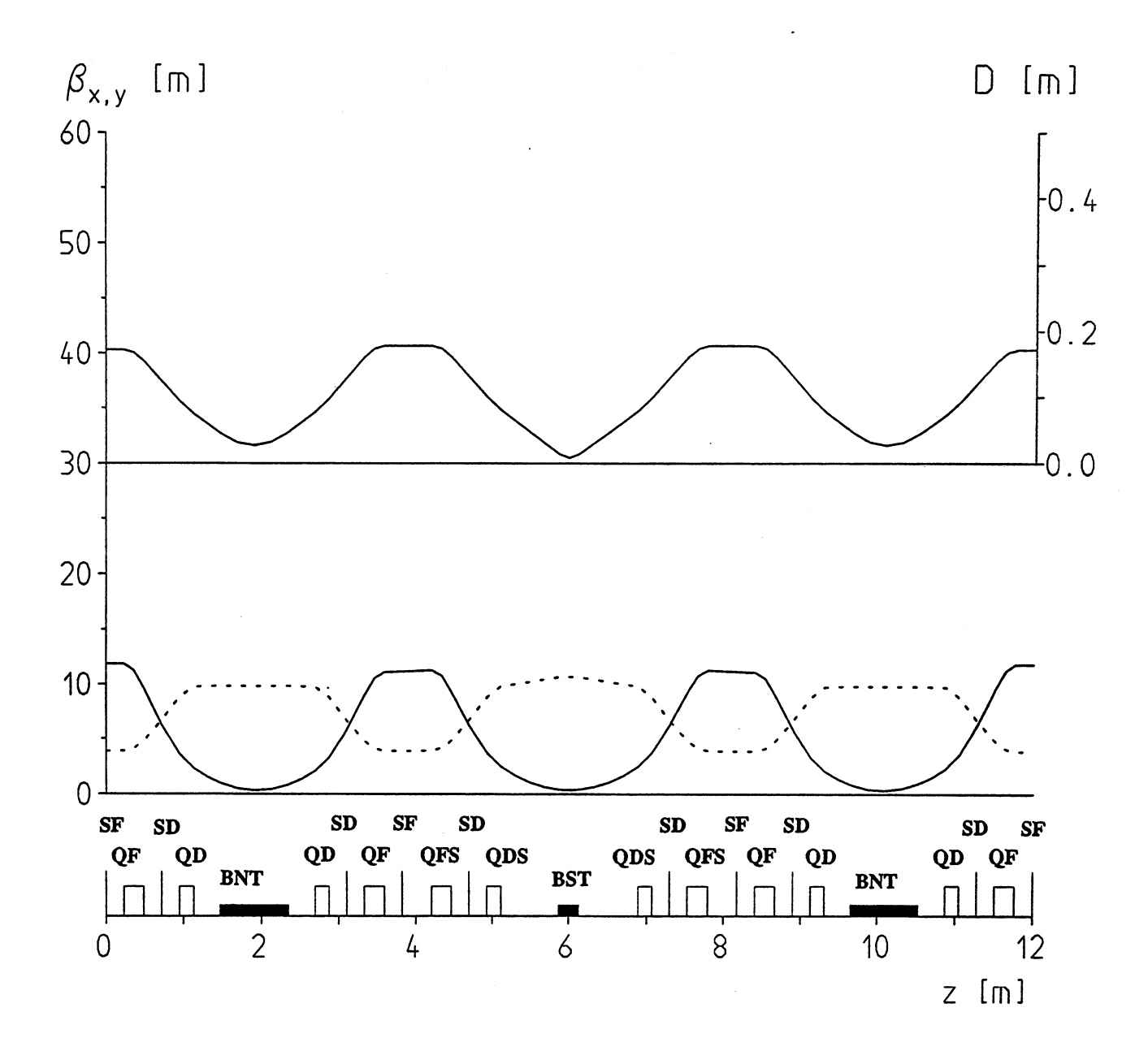


Figure 7: Optics of the three middle cells

Horizontal (solid line) and vertical (dotted line) beta functions and dispersion for the cell with the superconducting bending magnet BST and the adjacent cells with normal conducting bending magnets BNT. Four quadrupole families are used to adjust the emittance.

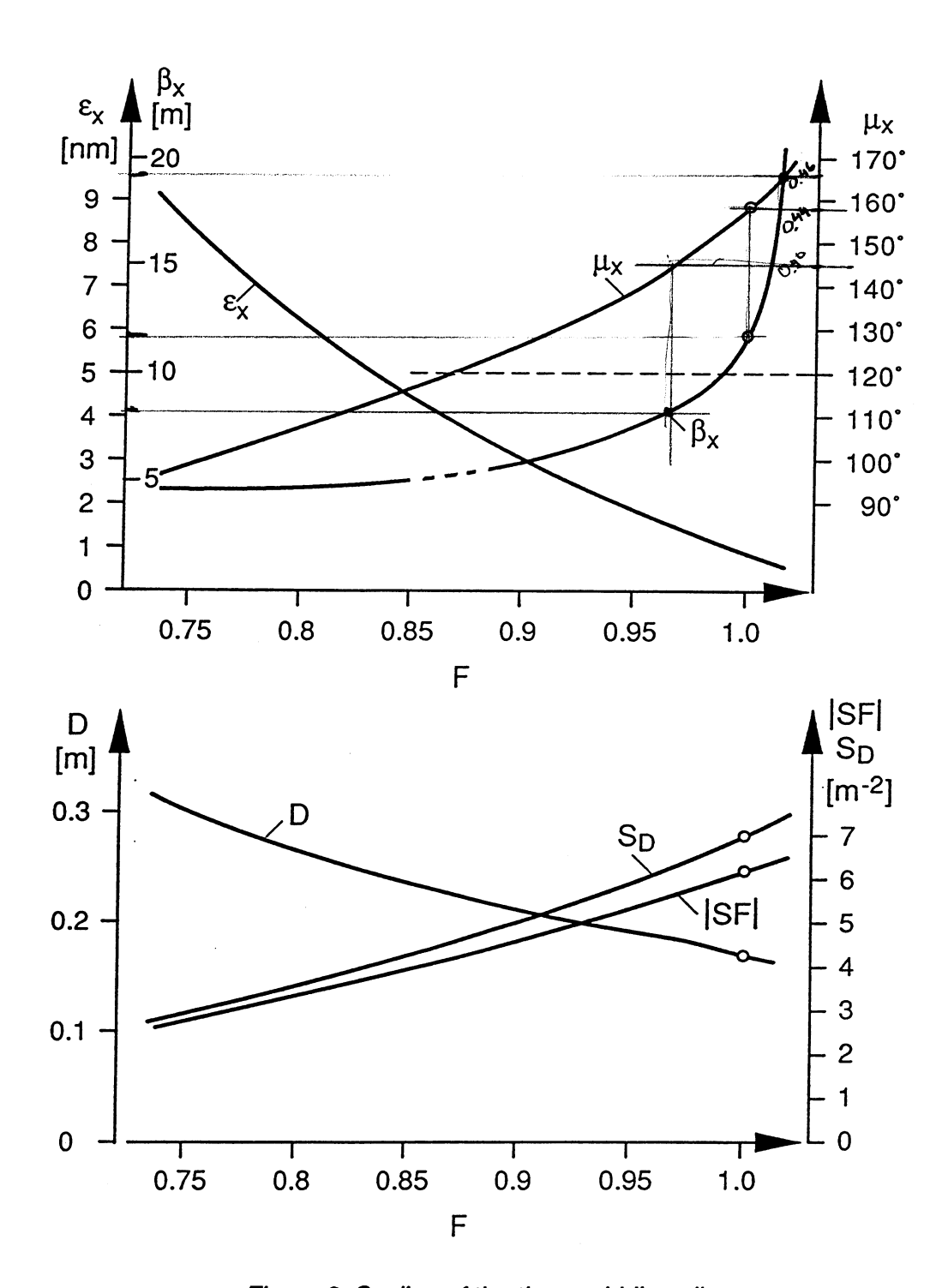


Figure 8: Scaling of the three middle cells

The scaling factor F is applied to the quadrupoles QF, QD, QFS, QDS of the 60° achromatic arc as shown in Figure 7. F = 1 corresponds to the low emittance mode. With this scaling β_Z is kept almost constant at β_Z = 10 m in the bending magnets and the dispersion is periodic. ϵ_X is the natural emittance normalised to 1 GeV, μ_X is the horizontal phase advance per cell

The sextupoles with integrated strengths SF, SD compensate the chromaticity of the three middle cells; the contribution to chromaticity from the quadrupoles in the straight sections requires significantly stronger sextupoles in the final lattice. Note: Sextupole-strength = $2 \cdot B^*/(2 \cdot B\rho)$ (DESY-convention)

For a phase-advance of 120° per cell, corresponding to 360° for the three cells, β_x is not quite periodic (broken section of β_x -curve).

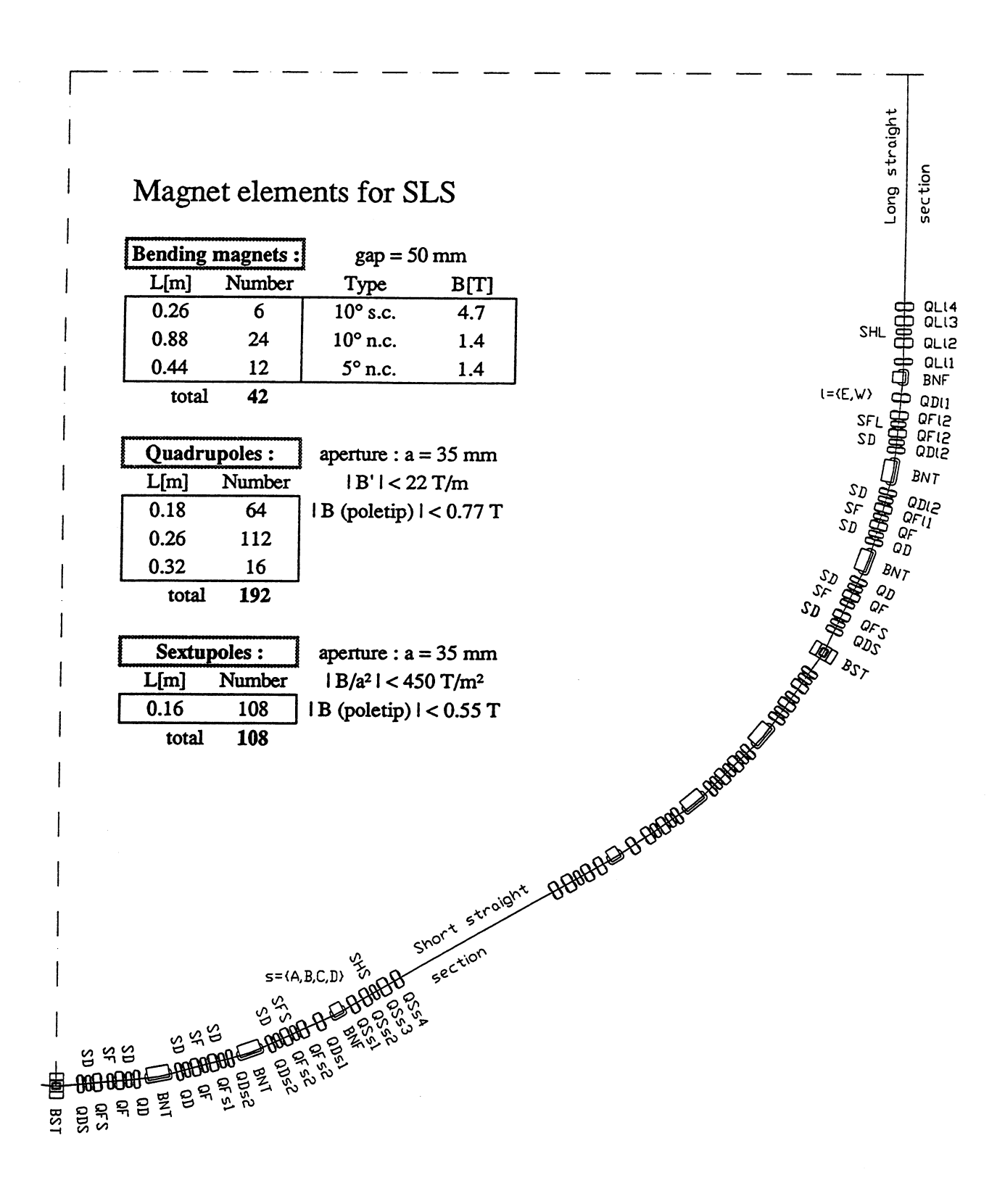


Figure 9: One quarter of the SLS storage ring

The corresponding optical functions are shown in Figure 10. Three types of quadrupoles with different lengths will be used to avoid saturation effects in any operation mode of the lattice.

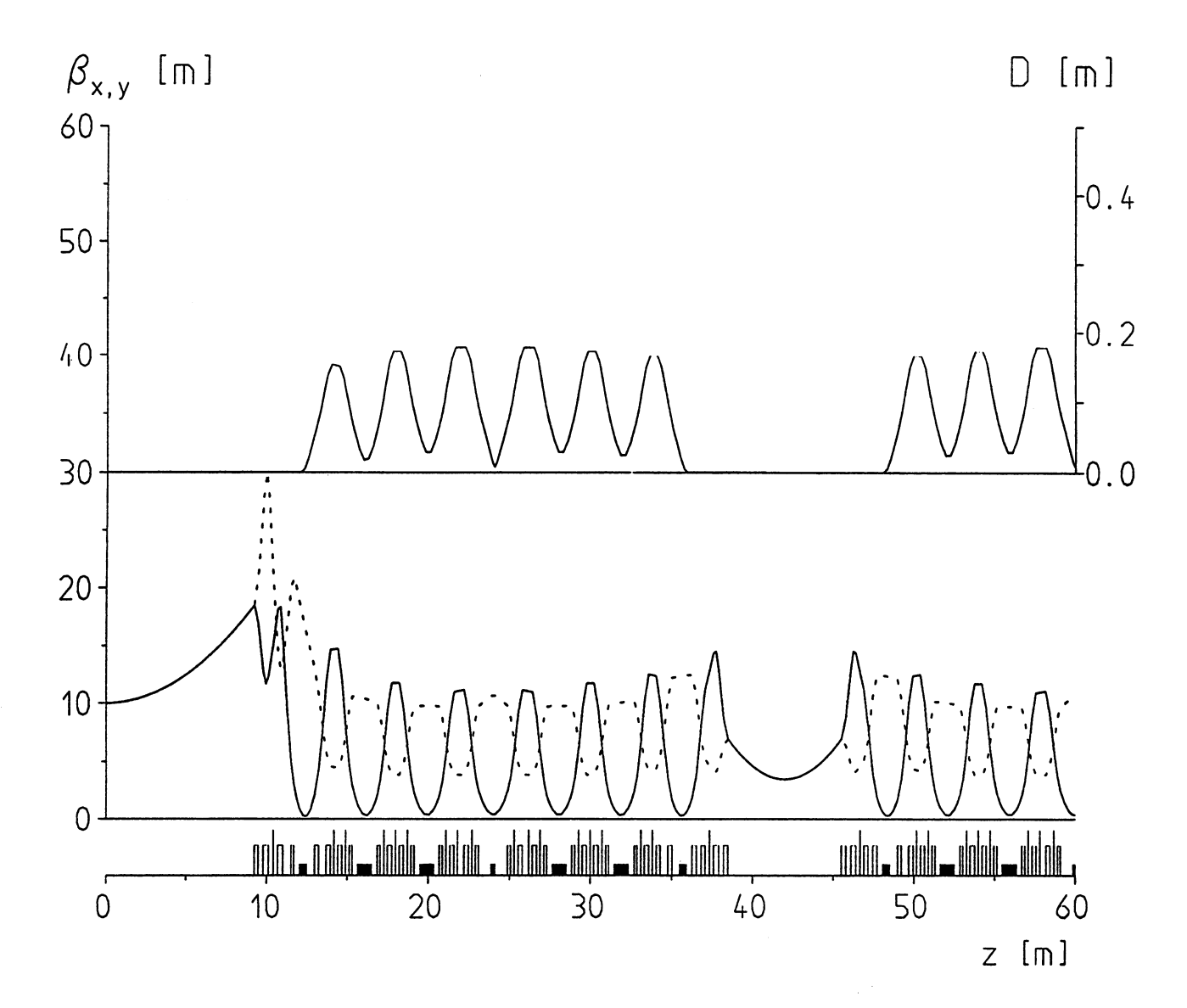


Figure 10: Optics of a quarter of SLS ring

Horizontal (solid line) and vertical (dotted line) beta functions and dispersion for one quarter of the SLS lattice in the low-emittance mode.

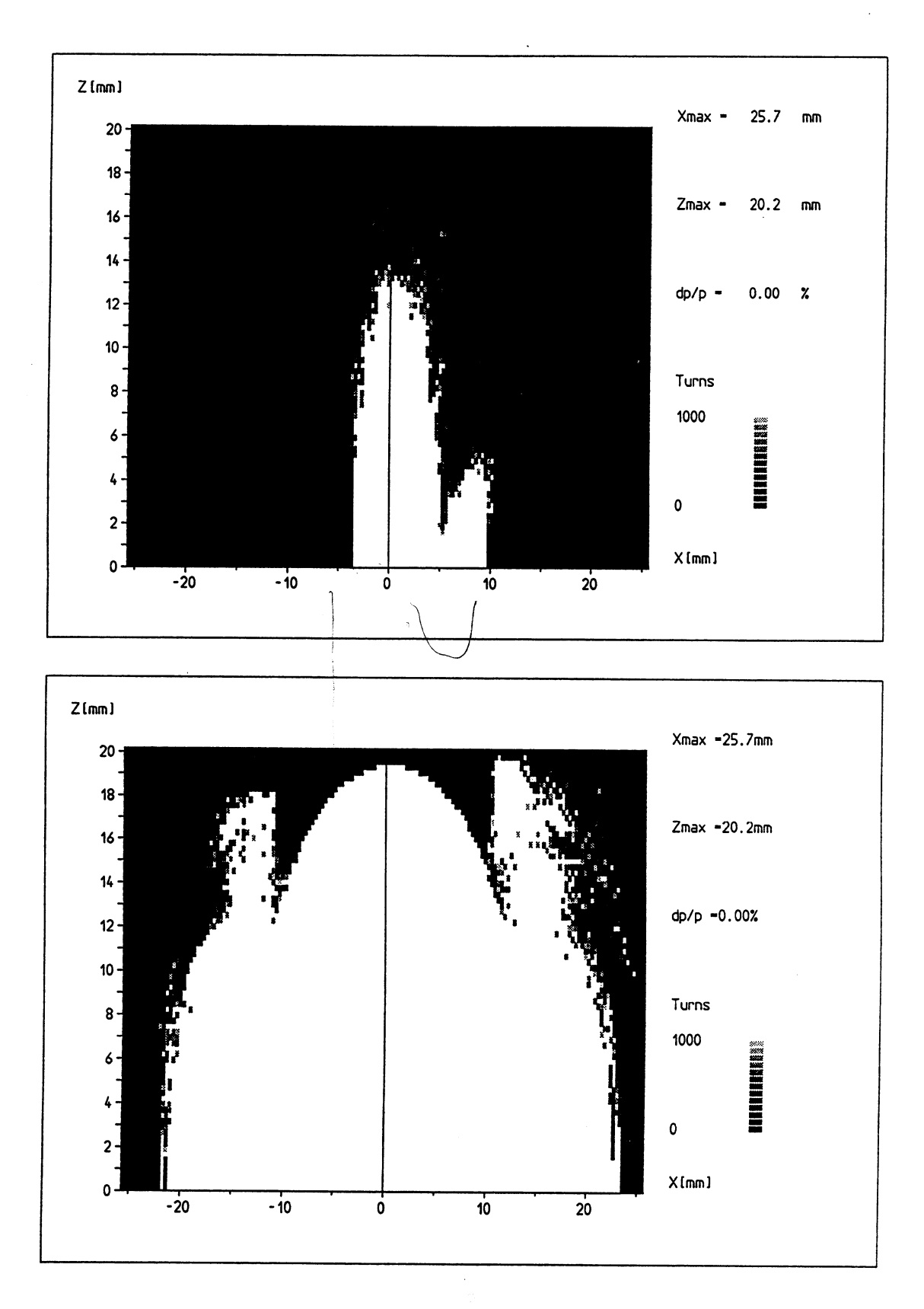


Figure 11: Dynamic aperture for on-momentum particles

Trackpoint was in the center of the long straight section ($\beta_x = \beta_z = 10$ m).

Above: Dynamic aperture after chromaticity correction with two sextupole families SF and SD. **Below**: Dynamic aperture after chromaticity correction and harmonic compensation of sextupole-resonances with six sextupole families: The horizontal chromaticity-sextupoles SF were divided into three families SF, SFS, SFL and two more families SHS, SHL in the dispersion-free regions were added (also see Figure 9).

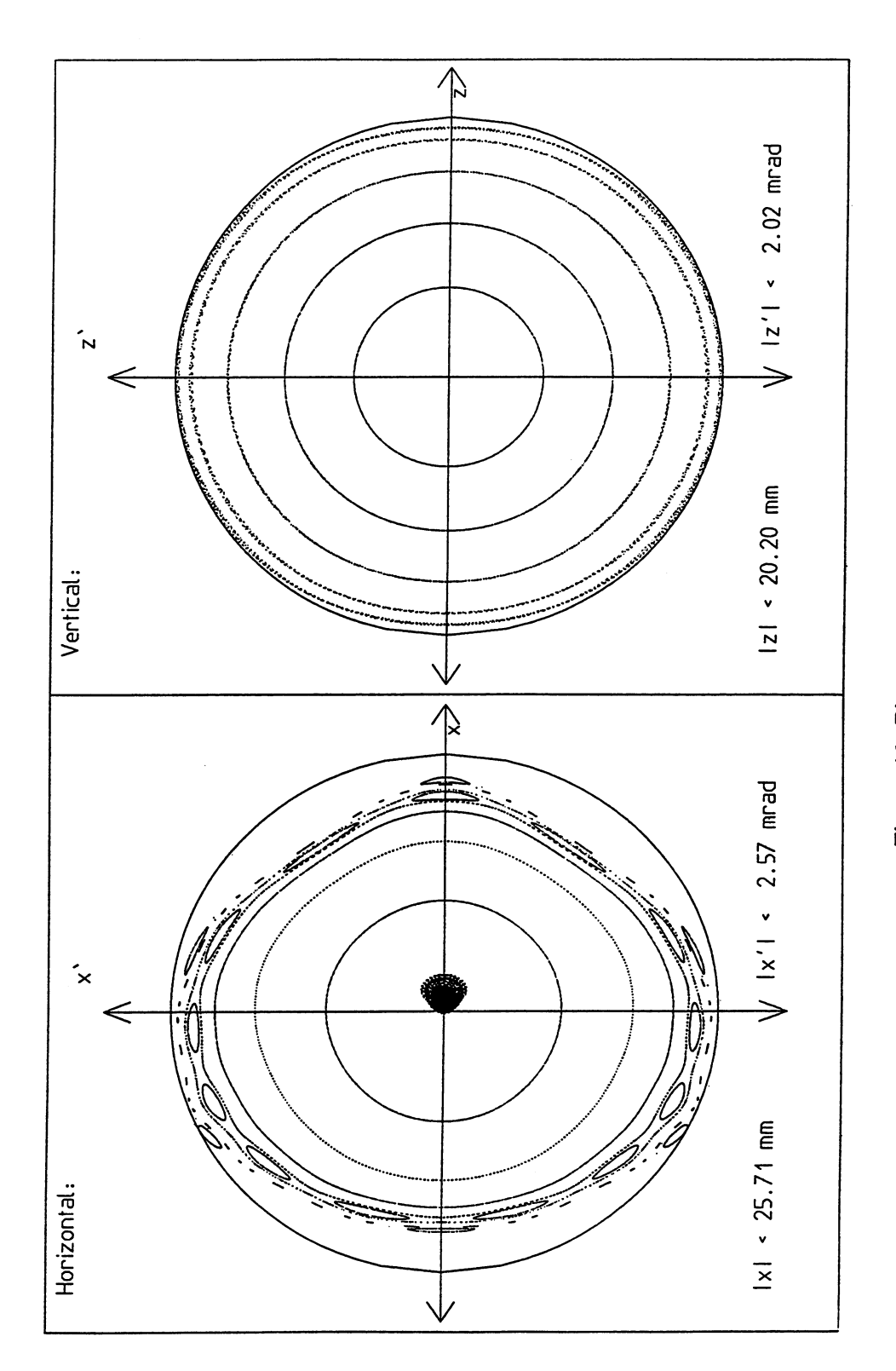


Figure 12: Phase space motion

of the long straight section ($\beta_x = \beta_z = 10$ m). Limitations for |x| and |z| denoted in the plot indicate the geometric aperture from a 35 mm radius beam pipe. Poincaré plot of motion in phase-space after harmonic compensation, taken at the center

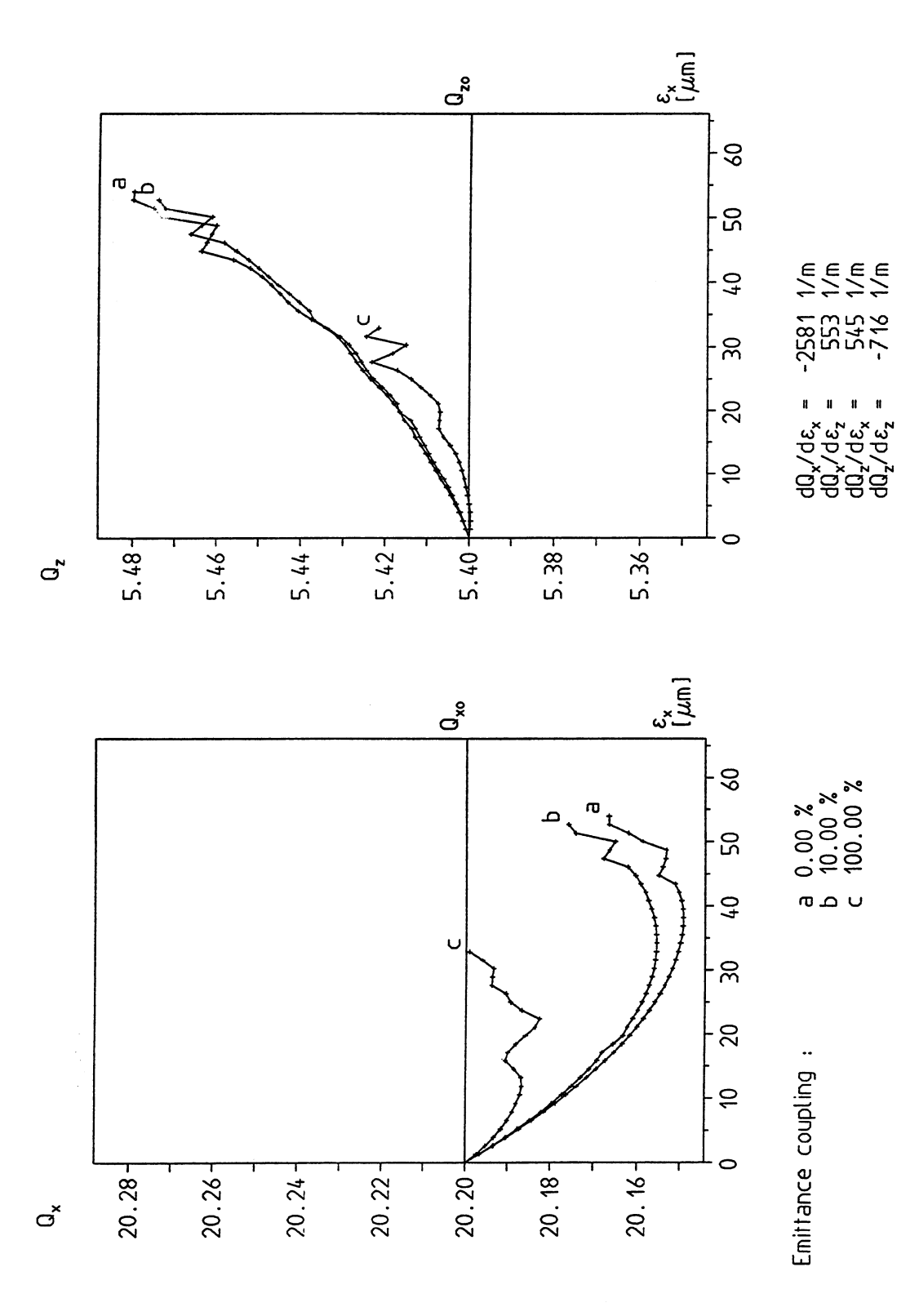


Figure 13: Amplitude-dependent tune-shift

Variation of horizontal and vertical tune with horizontal amplitude for three values of emittance-coupling. The gradients given at the lower right were minimised by harmonic compensation.

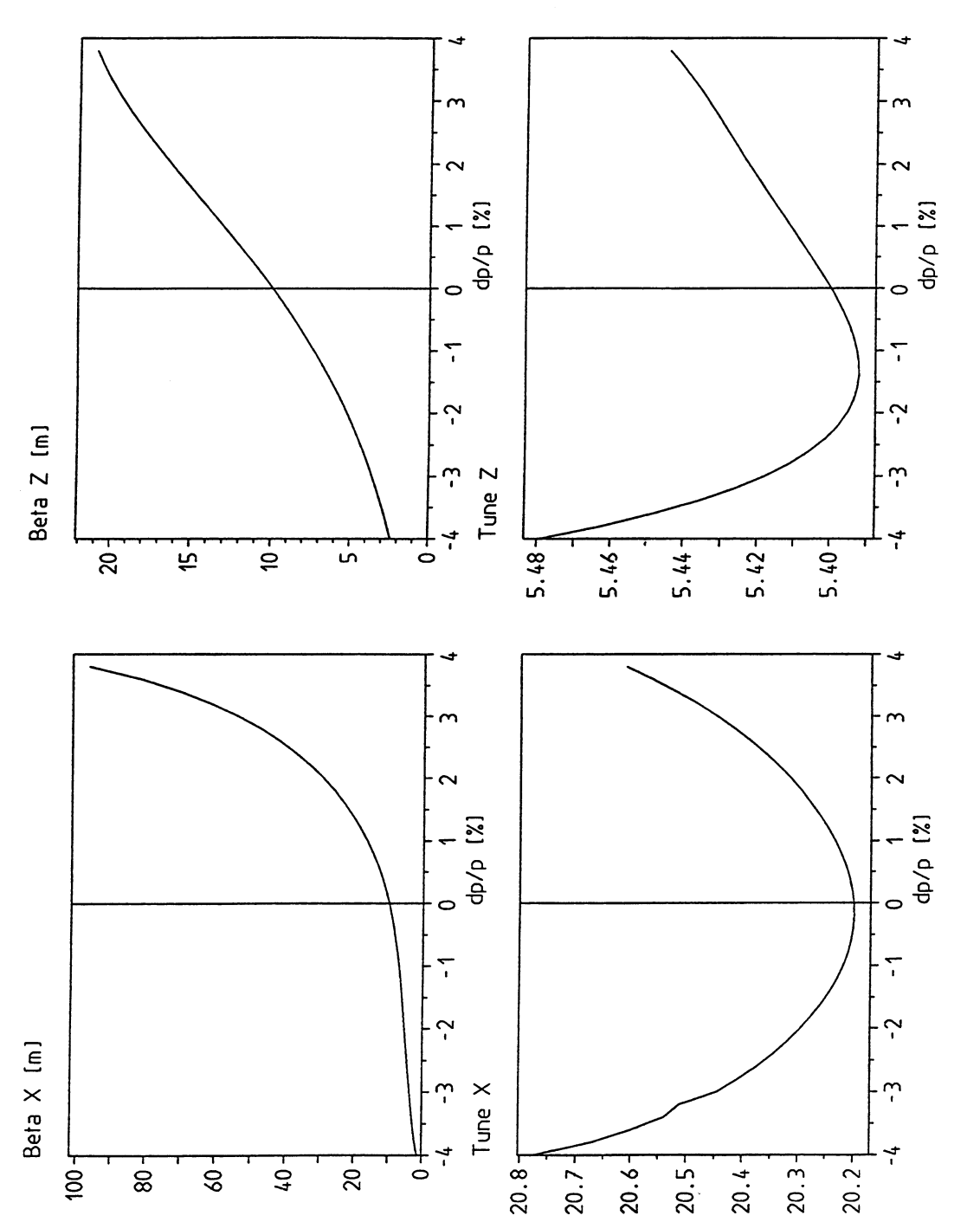


Figure 14: Momentum dependent beta functions and tune shift

Variation of beta functions (at the center of the long straight) and tunes with momentum deviation. Despite the rather large second-order chromaticity the momentum acceptance of the lattice amounts to \pm 4 %.

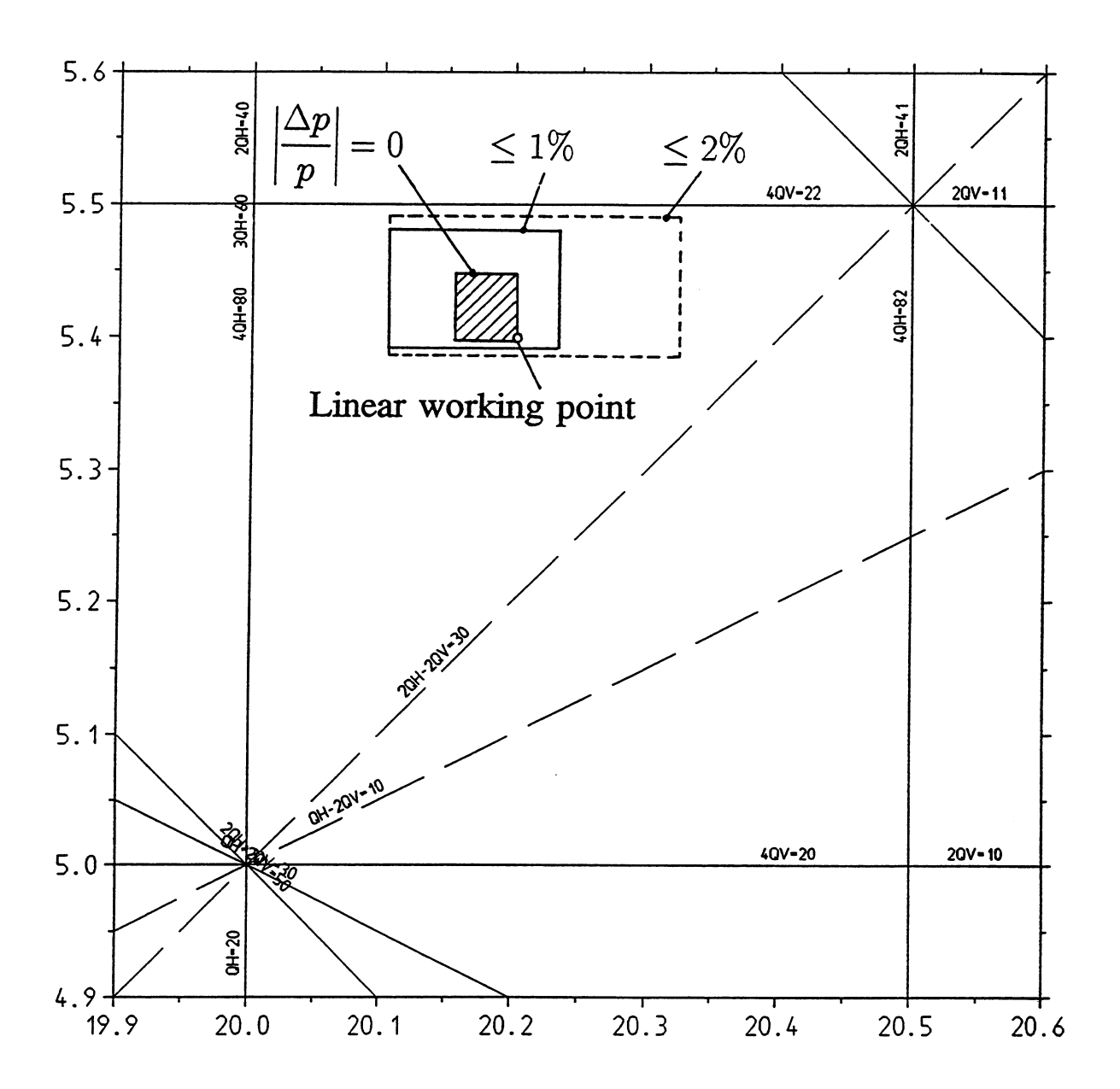


Figure 15: Beam footprint

Location of the working point in the resonance diagram of up to 4^{th} -order. Skew and non-systematic ($n_xQ_x+n_zQ_z=$ odd) resonances are not shown. The boxes enclose the beam footprints (tune spread areas) for different values of momentum deviation (without synchrotron oscillation).

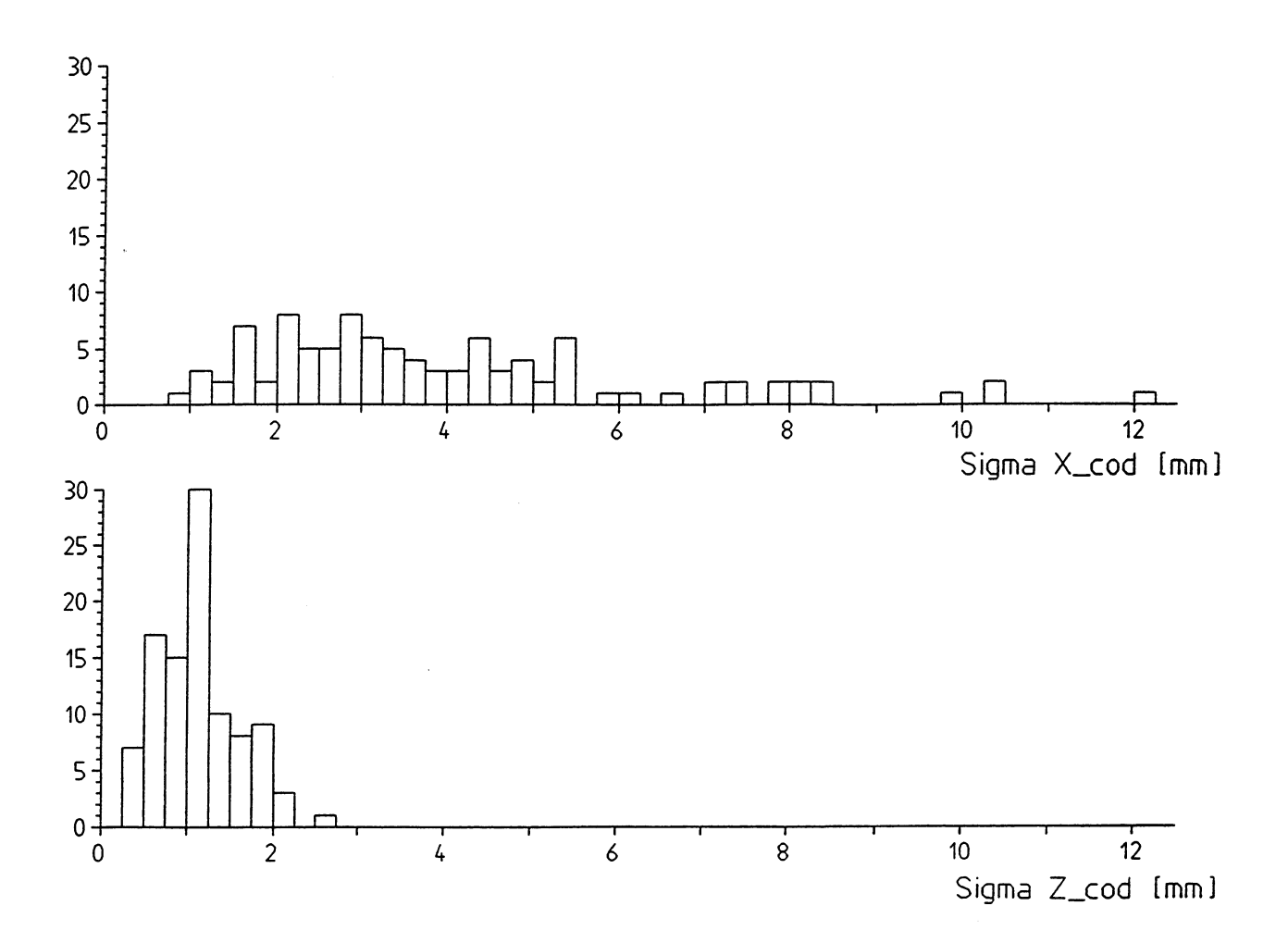


Figure 16: Closed orbit distortions

Distribution of r.m.s. closed orbit distortions for 100 sets of Gaussian distributed (cut at 2σ) transverse positioning errors in quadrupoles, bending magnets and sextupoles. Error amplitude was $\sigma = 100~\mu m$. The mean amplification factors were found to be 40.3 horizontal and 11.4 vertical.

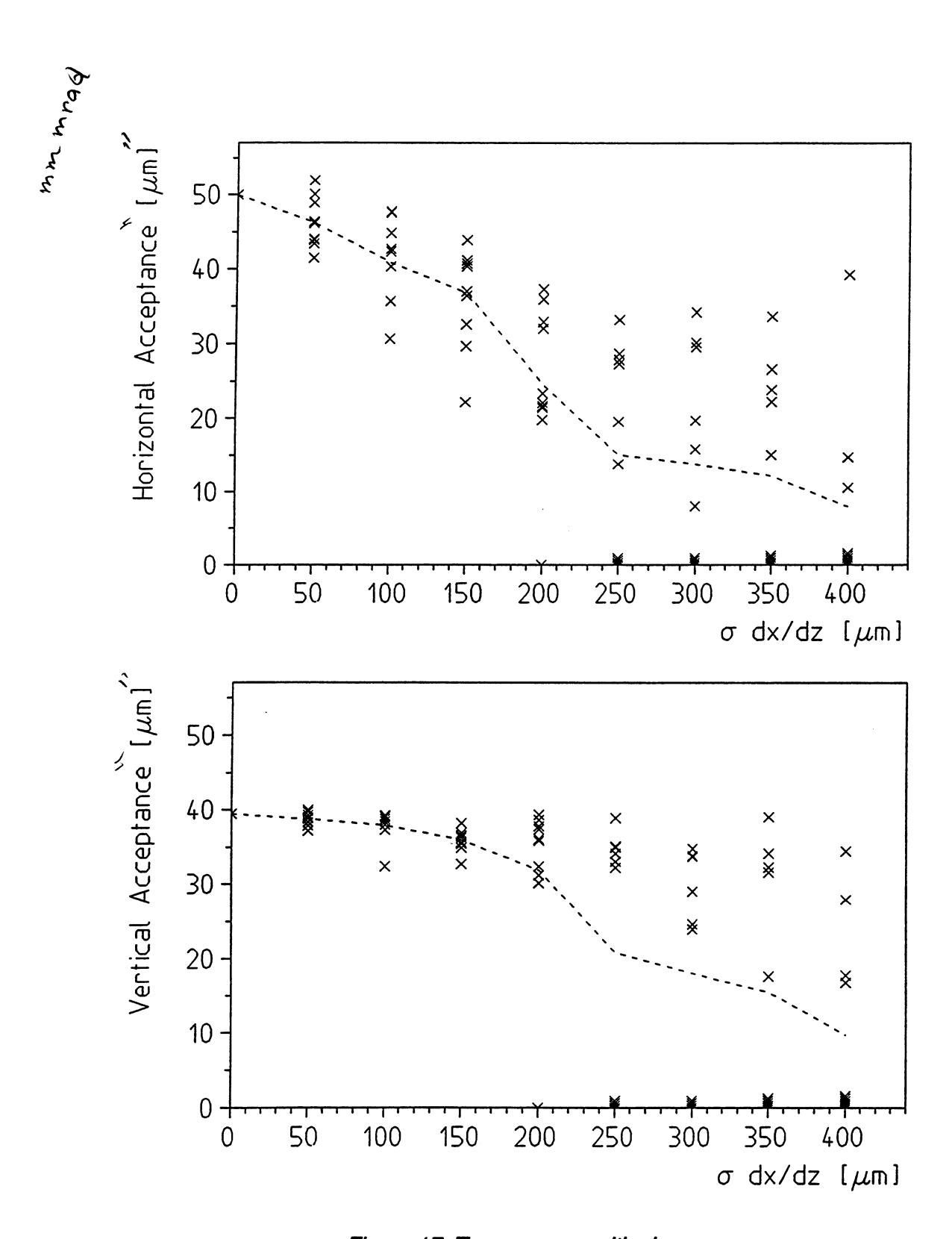


Figure 17: Transverse positioning errors

Sensitivity of the acceptances to transverse positioning errors in quadrupoles, bending magnets, sextupoles and monitors (Gaussian distribution, cut at 2 σ).

Closed orbit correction with the local bump method was done before calculating the acceptance by binary search for largest stable amplitude and ellipse-fit to the Poincaré-section of the corresponding eigenfigure in phase space. If no closed orbit was found, the acceptance was taken to be zero. The dotted line connects the average results. (Calculated with TRACY).

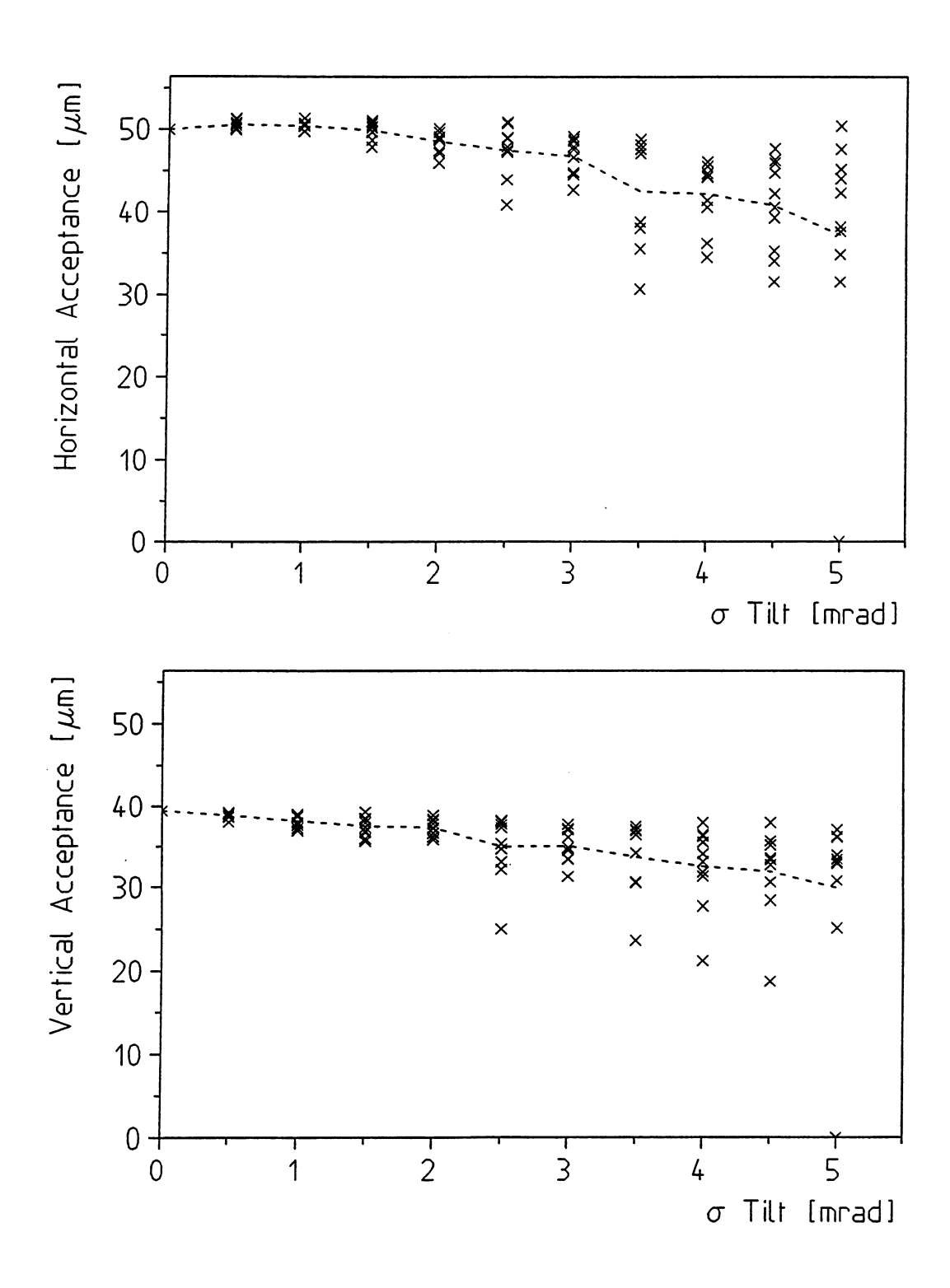


Figure 18: Tilt errors

Sensitivity of the acceptances to the tilt errors (rotation around beam-axis) in quadrupoles, bending magnets, sextupoles and monitors (Gaussian distribution, cut at 2σ). Closed orbit correction was performed before every run. The dotted line connects the average values.

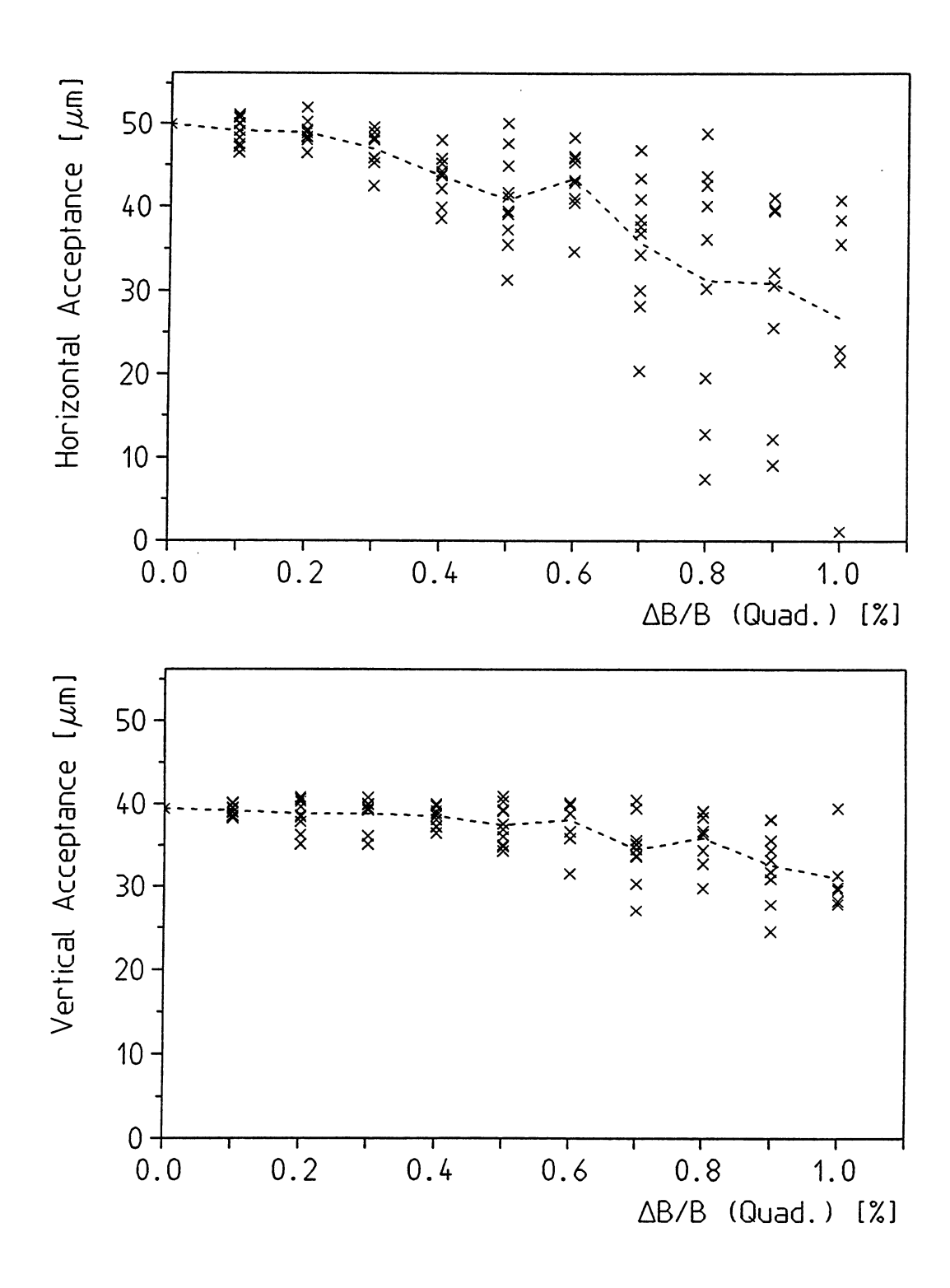


Figure 19: Quadrupole tolerances

Sensitivity of the acceptances to errors in the quadrupole field strengths (Gaussian distribution, cut at 2σ). The dotted line connects the average values.

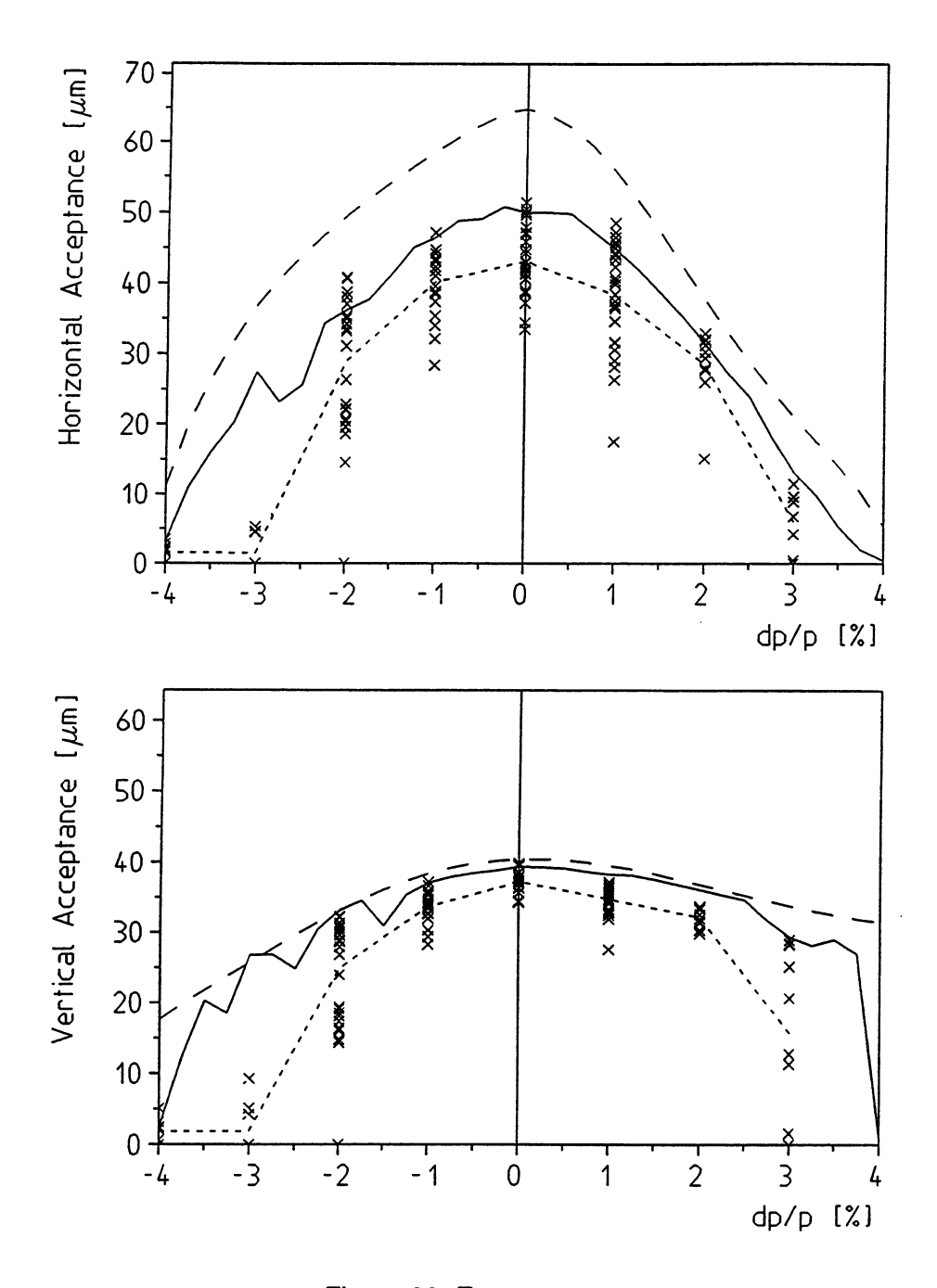


Figure 20: Error acceptances

Acceptances of the SLS-lattice as a function of momentum deviation (no synchrotron oscillations). Acceptances were calculated by binary search for the outermost stable particle and ellipse-fit to its eigenfigure.

Dashed line: Geometric acceptance limit due to the chromatic variation of beta functions as shown in Figure 14, assuming a beam pipe with radius 35 mm.

Solid line: Dynamic acceptance for the error-free lattice.

Dotted line and crosses: Dynamic acceptance of a lattice with Gaussian distributed (cut at 2σ) combined errors: Transverse displacement of quadrupoles, bending magnets, sextupoles and monitors with $\sigma = 100~\mu m$. – Tilt (rotation around beam-axis) of quadrupoles, bending magnets, sextupoles and monitors with $\sigma = 1~m rad$. – Relative deviation from design field strength of quadrupoles and sextupoles with $\sigma = 10^{-3}$. The dotted line connects the average values for each set of runs (crosses). A closed orbit correction was done before calculation of the acceptance (TRACY).

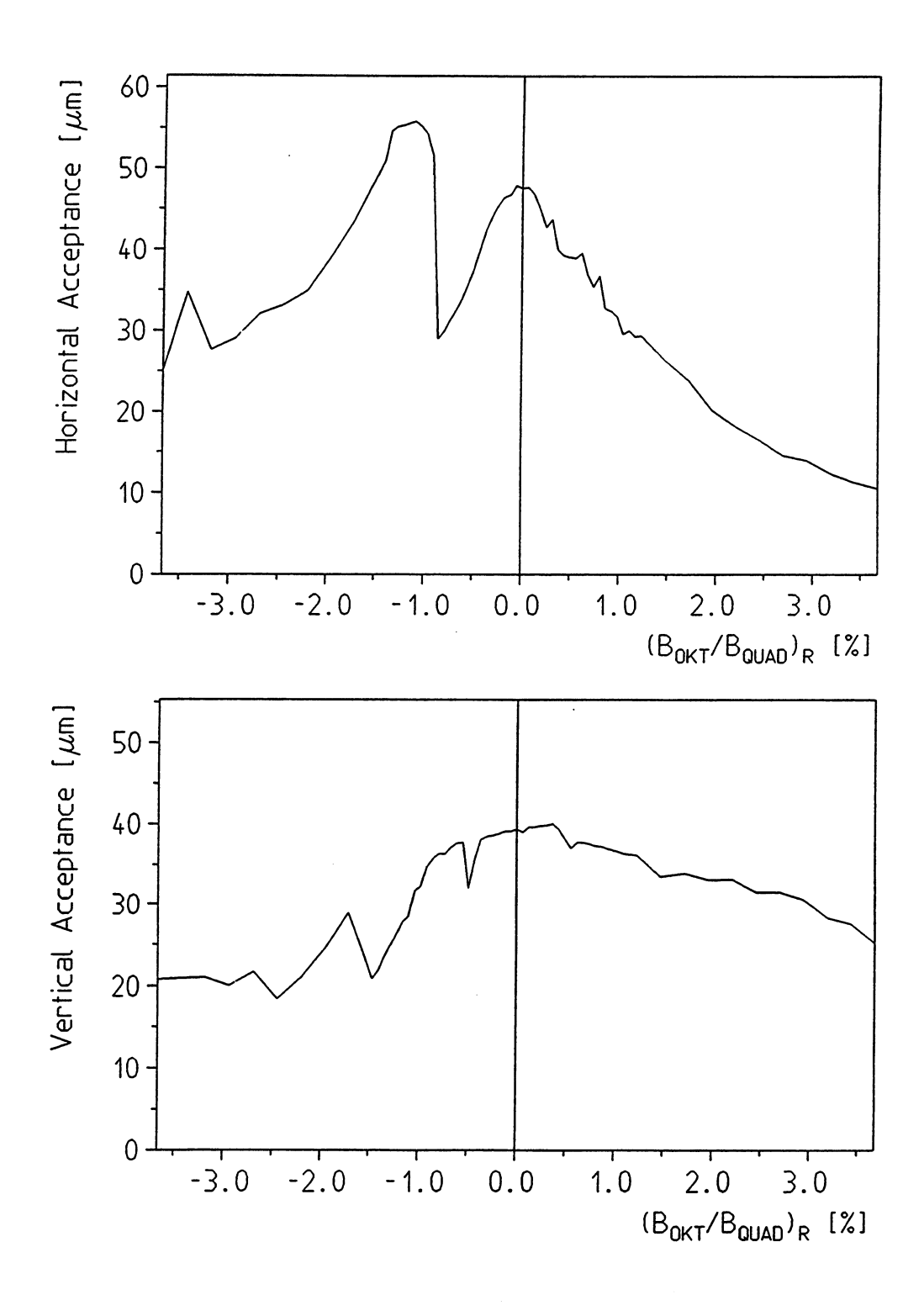


Figure 21: Systematic octupole errors

Sensitivity of the dynamic acceptances to systematic octupole components in the quadrupoles. Abscissa is the ratio of the octupole component to the quadrupole component at the horizontal aperture limit (x = a = 35 mm, z = 0).

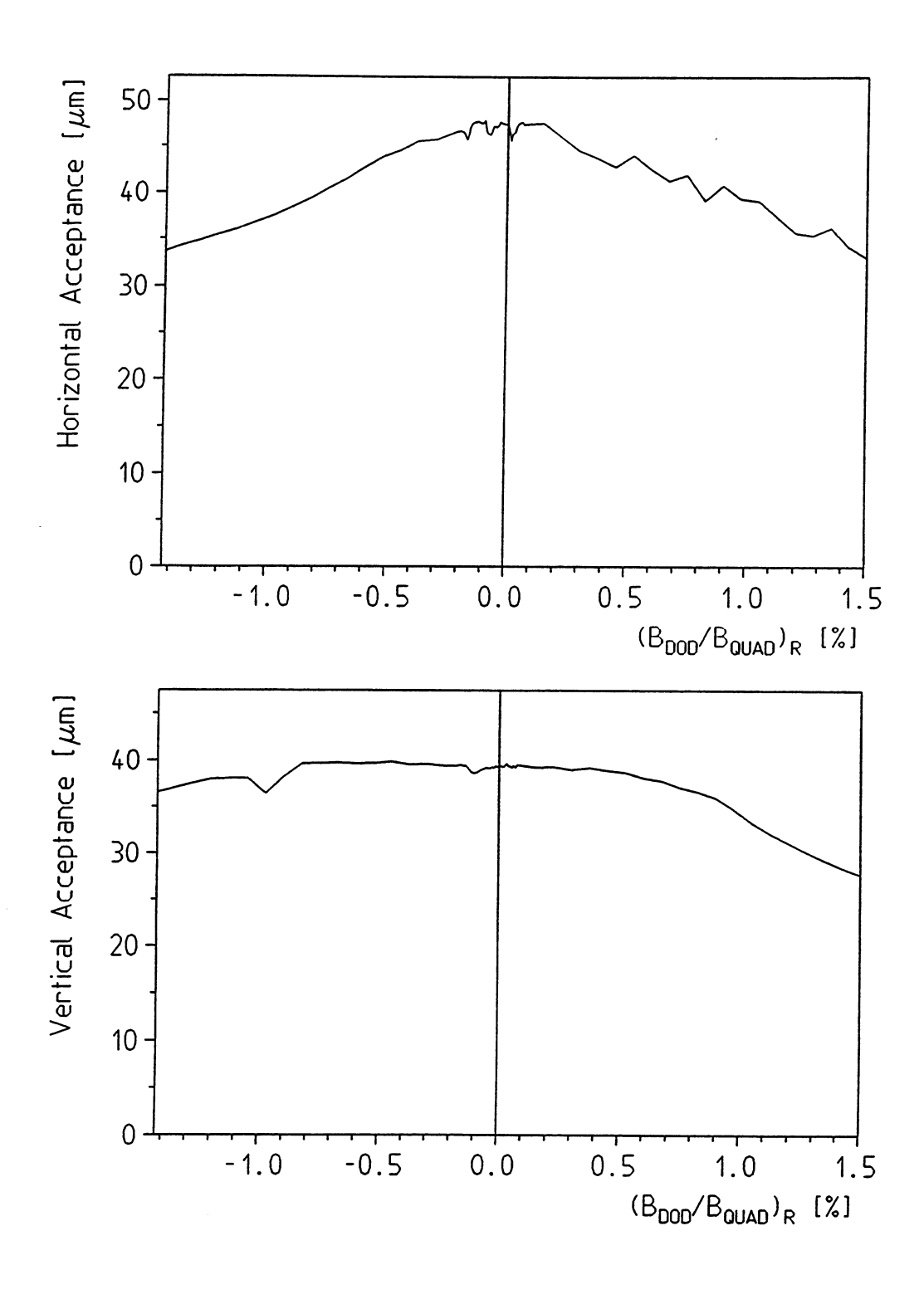


Figure 22: Systematic dodecapole errors

Sensitivity of the dynamic acceptances to systematic dodecapole components in the quadrupoles. Abscissa is the ratio of dodecapole component to quadrupole component at the horizontal aperture limit (x = a = 35 mm, z = 0).

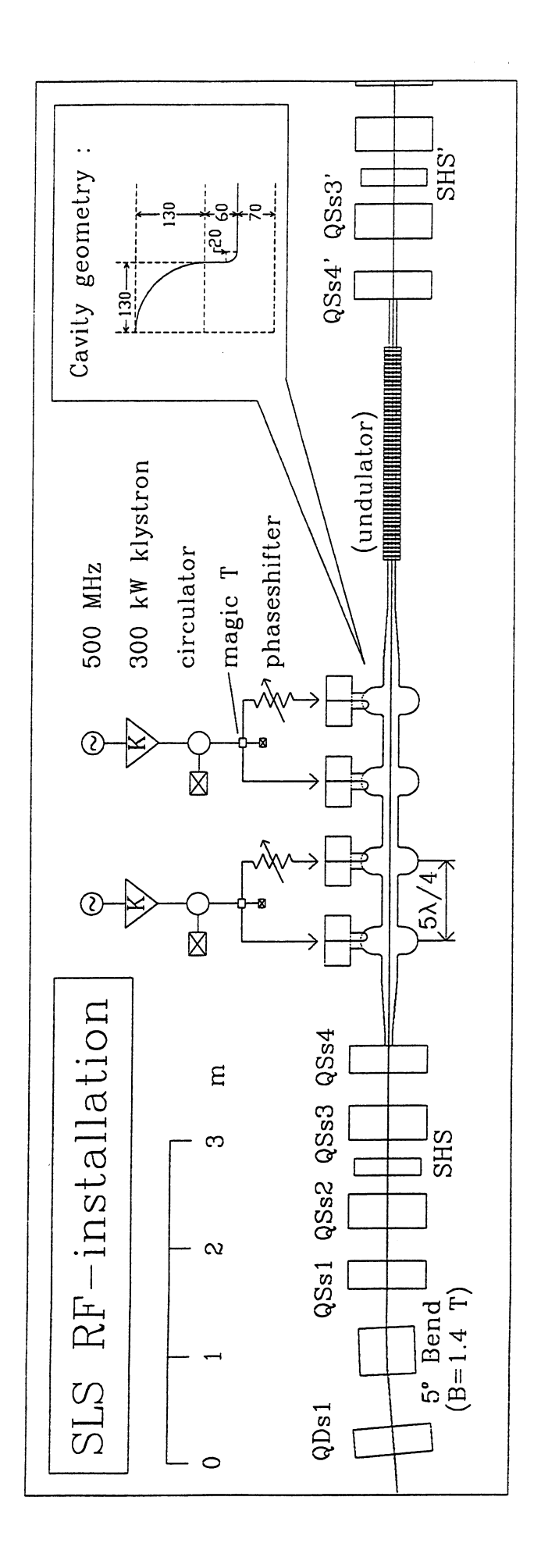


Figure 23: SLS RF Installation

The four cavities (including tapers) will occupy about 4 m within a short straight section of the storage ring, leaving enough space for a 2 meter long undulator nearby.

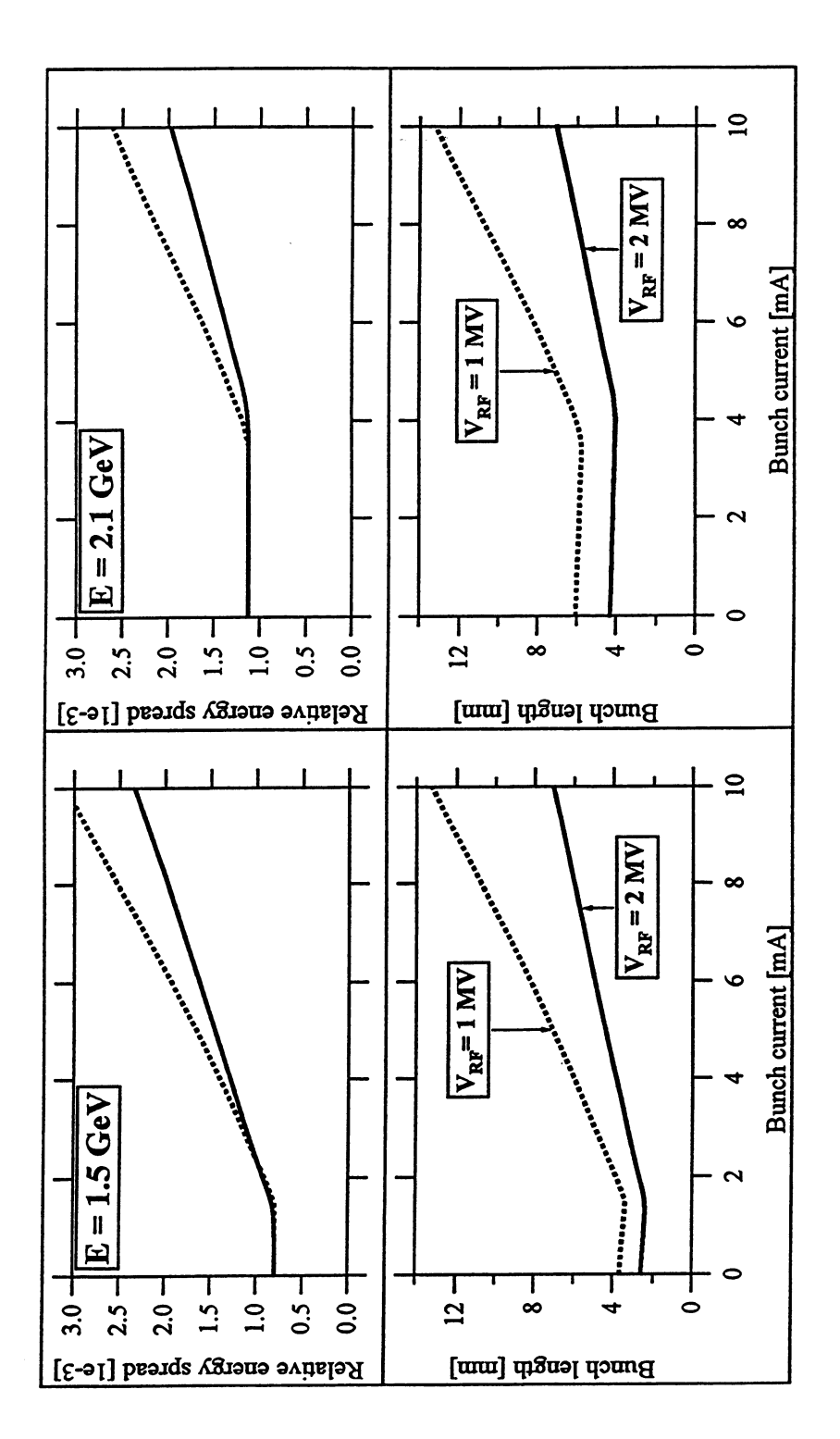


Figure 24: Bunch lengthening at E = 1.5 GeV and E = 2.1 GeV.

(potential well regime) and bunch length is seen to actually shorten, due to the capacitive character of the effective impedance. Bunch length and relative energy spread are plotted as a function of bunch current. The calculations were done using two broad band resonators model of the impedance. Below the turbulent bunch lengthening threshold current the energy spread remains constant

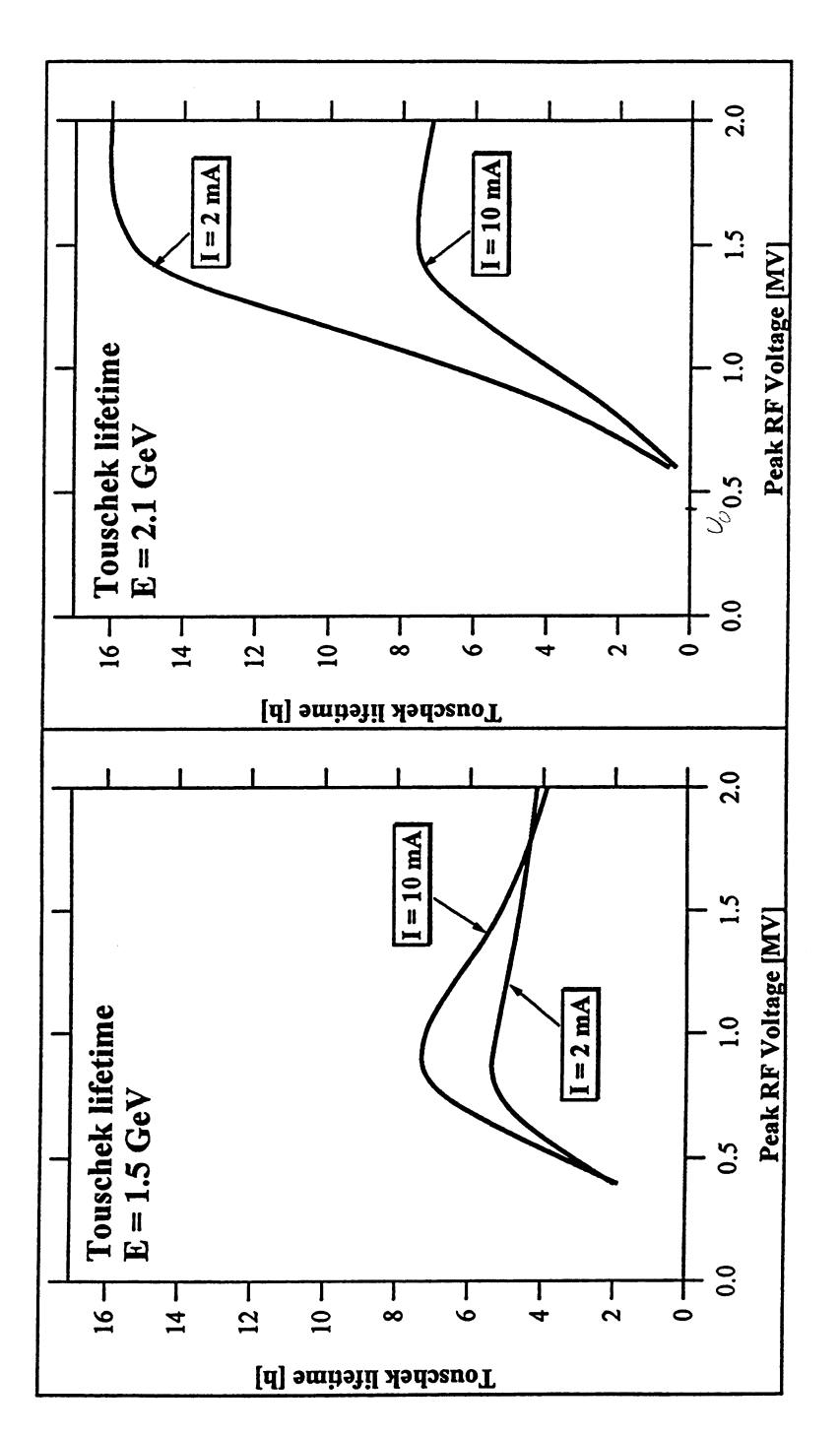


Figure 25: Touschek lifetime vs. peak RF voltage.

Due to very small equilibrium emittance and short bunch length, Touschek effect will be function of the ring energy acceptance, which can be increased by increasing the limiting the beam lifetime in most modes of operation. Touschek lifetime is a steep the lifetime in these plots occur at the values of RF voltage corresponding to the RF bucket size reaching \pm 3 % in relative energy deviation. The fact that the Touschek lifetime at 1.5 GeV is longer for 10 mA bunch than for 2 mA, is due to significant bunch available RF voltage. However, the energy acceptance of the SLS ring will be limited by the shrinking dynamic aperture for off-momentum particles to about \pm 3 %. The maxima of engthening at that current

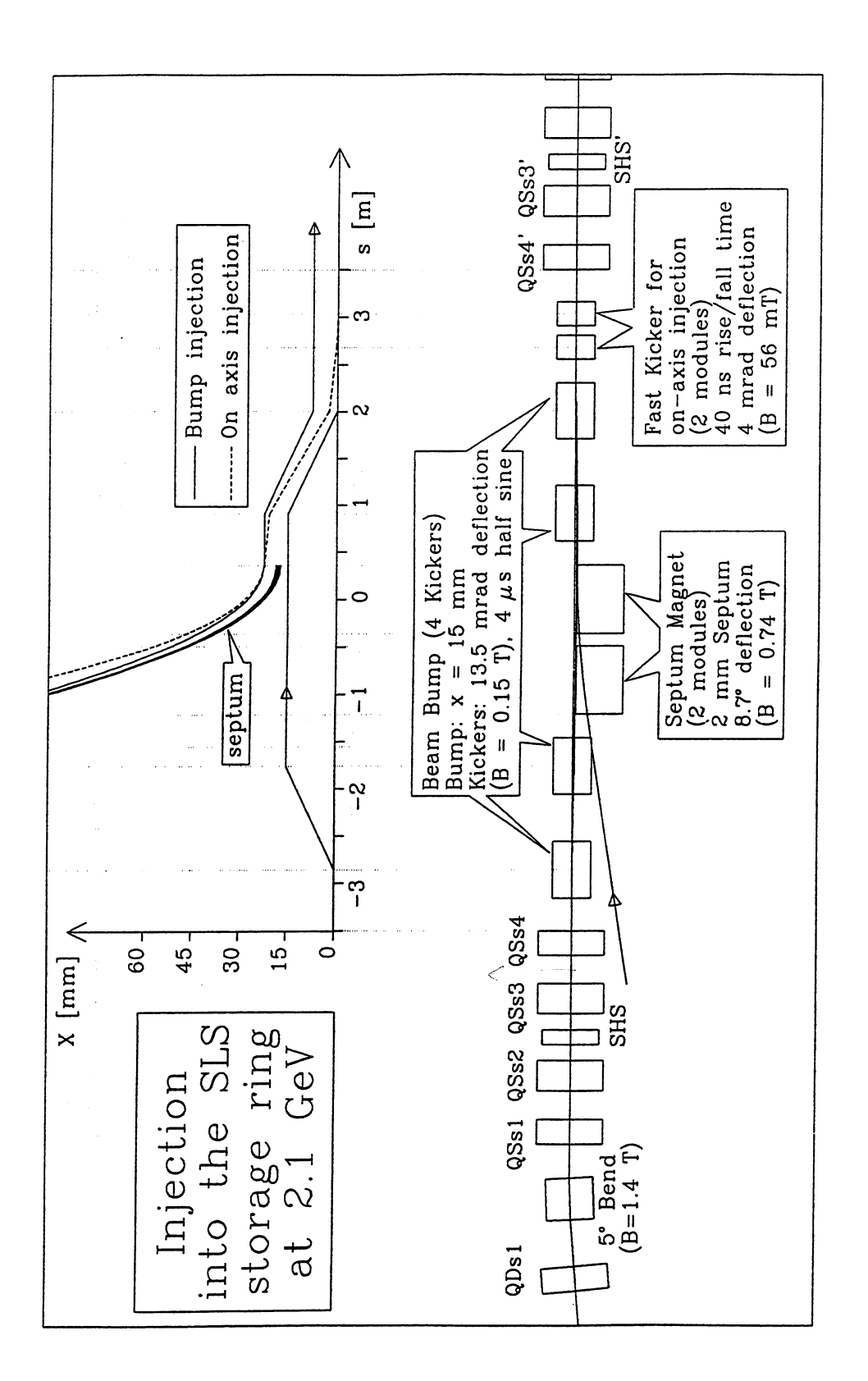
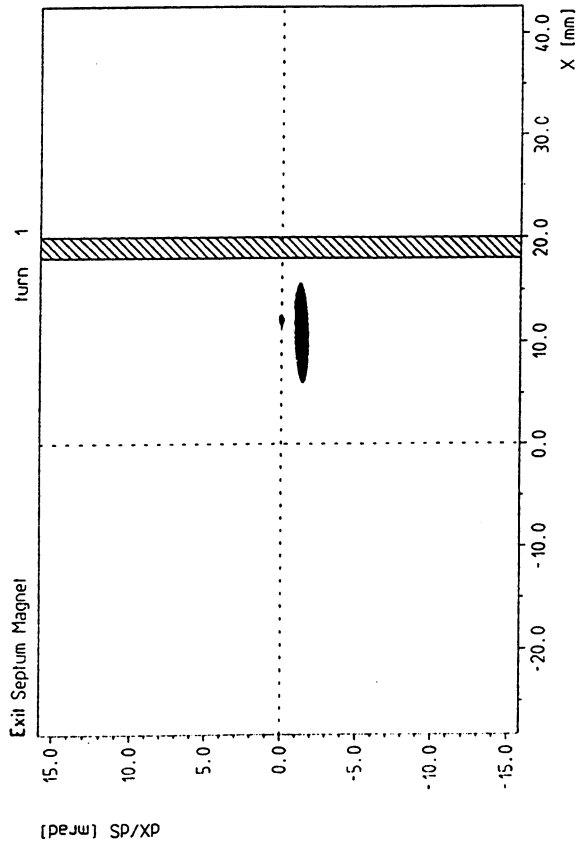


Figure 26: Layout of the injection components

The top figure shows the orbit bump of 15 mm for the stored beam and the orbit of the the quadrupoles QSs4 and QSs4. Besides the four kickers for the orbit bump some space new injected beam. Below is a layout of the injection straight with 7 m free space between is reserved for an alternative "on-axis"-injection with a fast kicker.





and after the last kicker. Turn 0 starts at the peak of the kicker

displaced by 15 mm, and the injected beam with the 3 sigma contour 1 mm away from the septum. One turn later the orbit bump is reduced to 12 mm, and the fractional tune of 0.2 has helped the injected beam to stay clear of the septum by 2 mm.

field. We see the 2 mm thick septum, the stored

injection process for turns 0, 1 and 2 at the exit of the septum

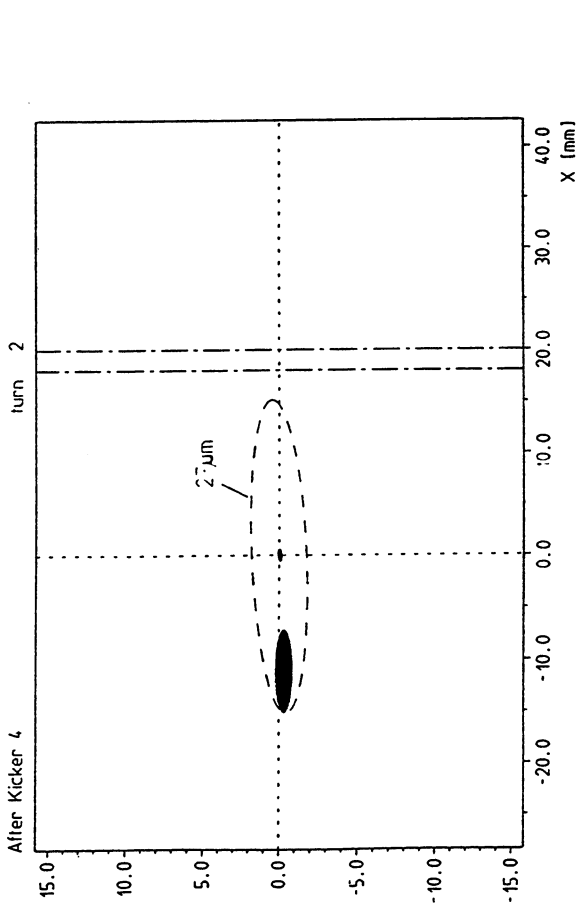
Sequence of horizontal phase space plots showing

The bottom picture shows the situation after 2 turns with the

stored beam back on its centered orbit. The injected beam is

captured into an eigenellipse of area 27 µm, well within the

acceptance of about 40 µm.



(mm) × 0.07 30.0 injected septum beam 20.0 0 5 stored Deam 0.0 0.0 - 10.0 Exit Septum Magnet -20.0

-5.0-

0.0

5.0

10.0

[benm] Sb/Xb

15.0

-10.0-

-15.0-

[benm] Sb/Xb

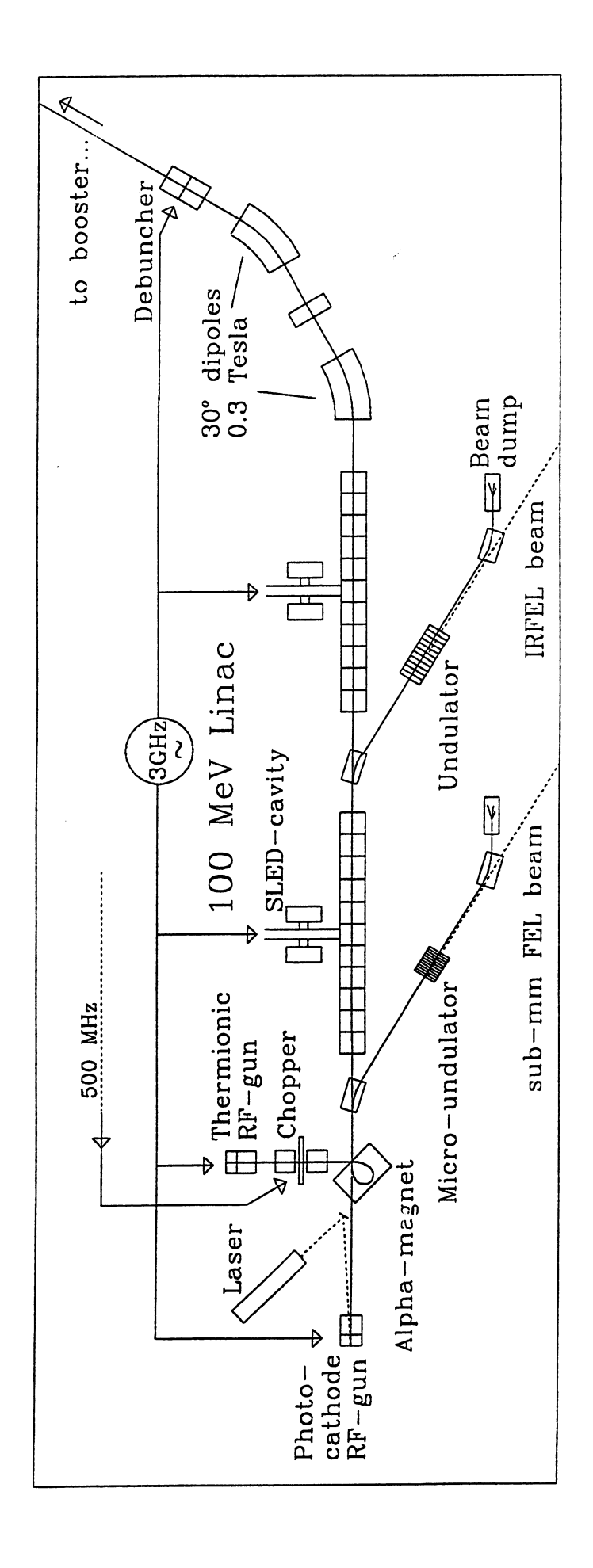


Figure 28: Schematic view of the injection chain

applications. A thermionic RF-gun with an α -magnet for energy filtering is on stand-by. The linac is equipped with SLED cavities to save length and RF-power. A debuncher is recommended for longitudinal matching of the high charge bunches to the acceptance of A laser-driven RF-gun delivers high charge bunches for single-shot injection and FEL the booster synchrotron

Relative energy-acceptance (RF-amplitude constant during cycle)

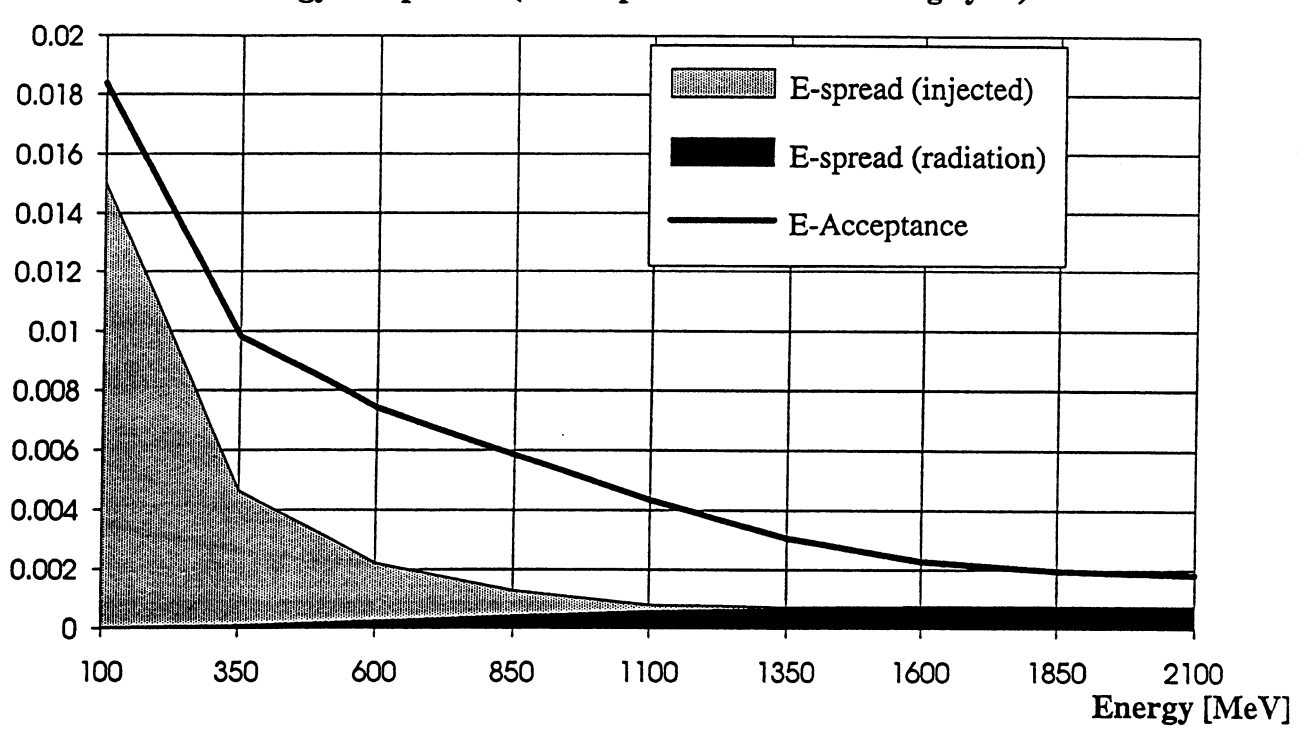


Figure 29: Energy spread damping in the booster.

At low energies the adiabatic damping mechanism dominates, while at higher energies the energy spread levels off to an equilibrium value, given by radiation damping and quantum fluctuations.

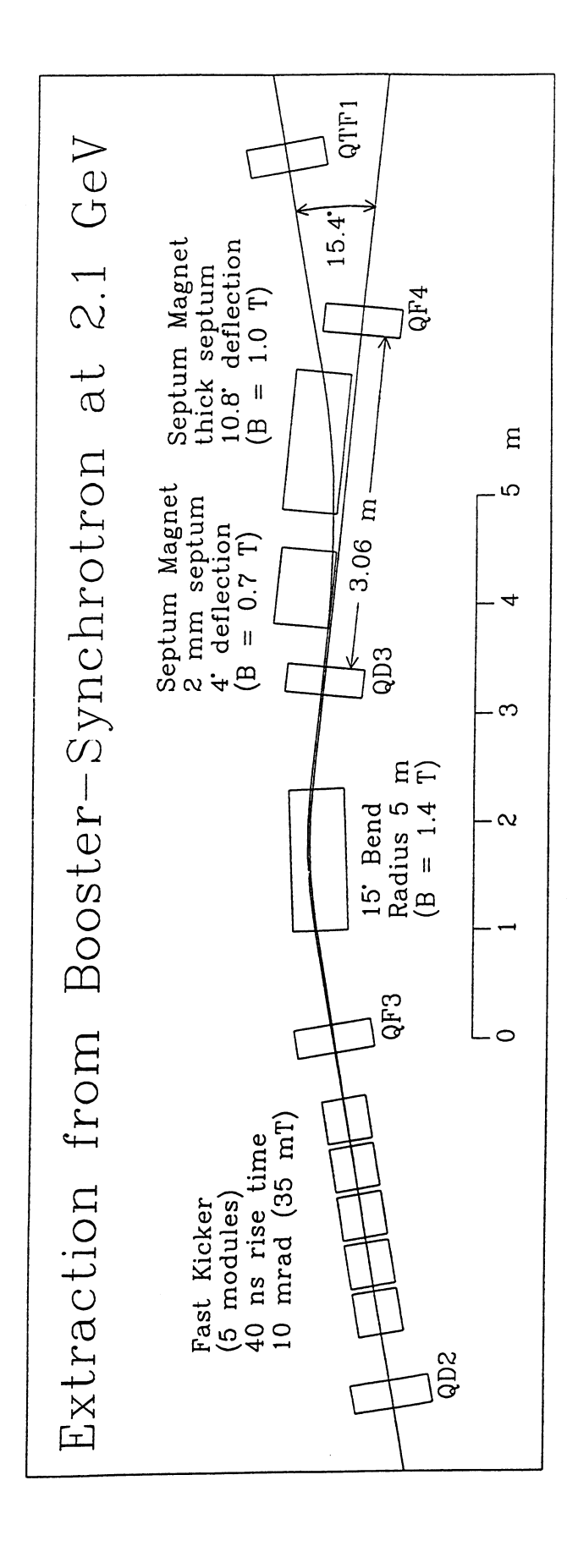


Figure 30: Extraction scheme for the booster synchrotron

between two quads, deflects the beam by 10 mrad. This gives a displacement of about 25 mm at the entrance to the extraction septum, located in the next free sector. The extraction process occurs in two stages: A fast kicker, placed in a straight section

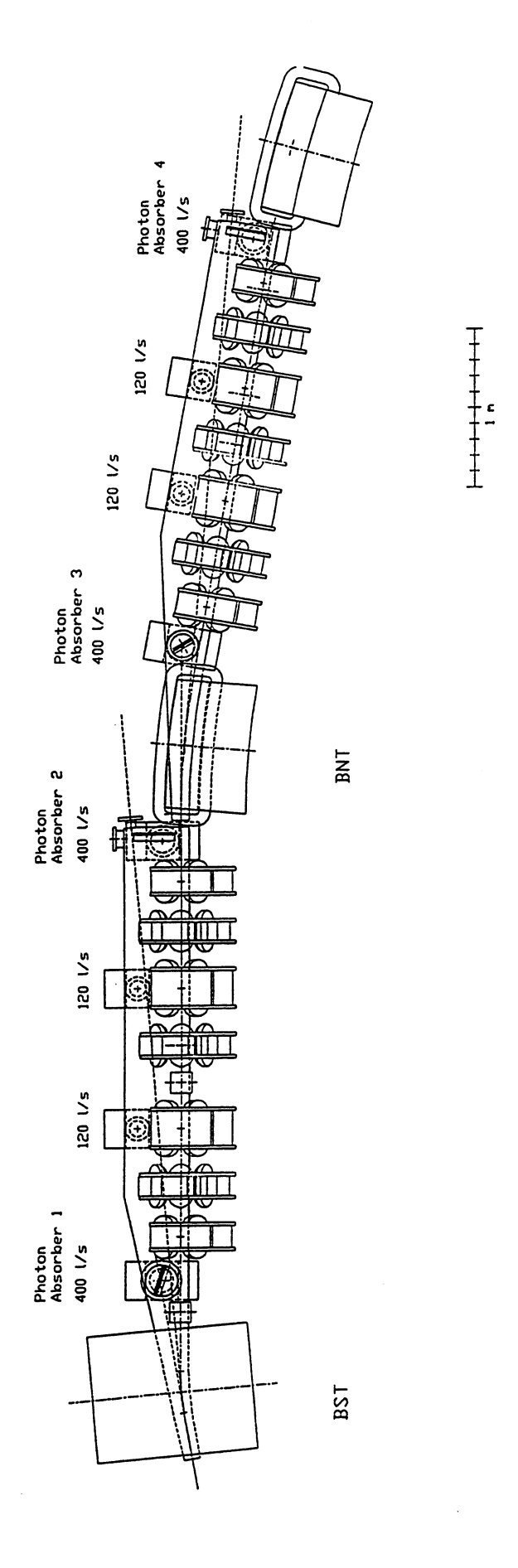


Figure 31: Vacuum chamber layout

the beam line. Each absorber region is pumped by a 400 l/s ion pump with NEG. Two additional 120 l/s ion pumps are needed to meet the pressure requirement of one nano-Torr at 2.1GeV, 400mA operation and a beam 'conditioning' period of 100Ah. Layout of the vacuum chambers for a 10° superconducting and a 10° normalconducting bend for the antechamber solution. Two photon absorbers in the antechamber block all synchrotron radiation except that coming from the center of the dipole and going down

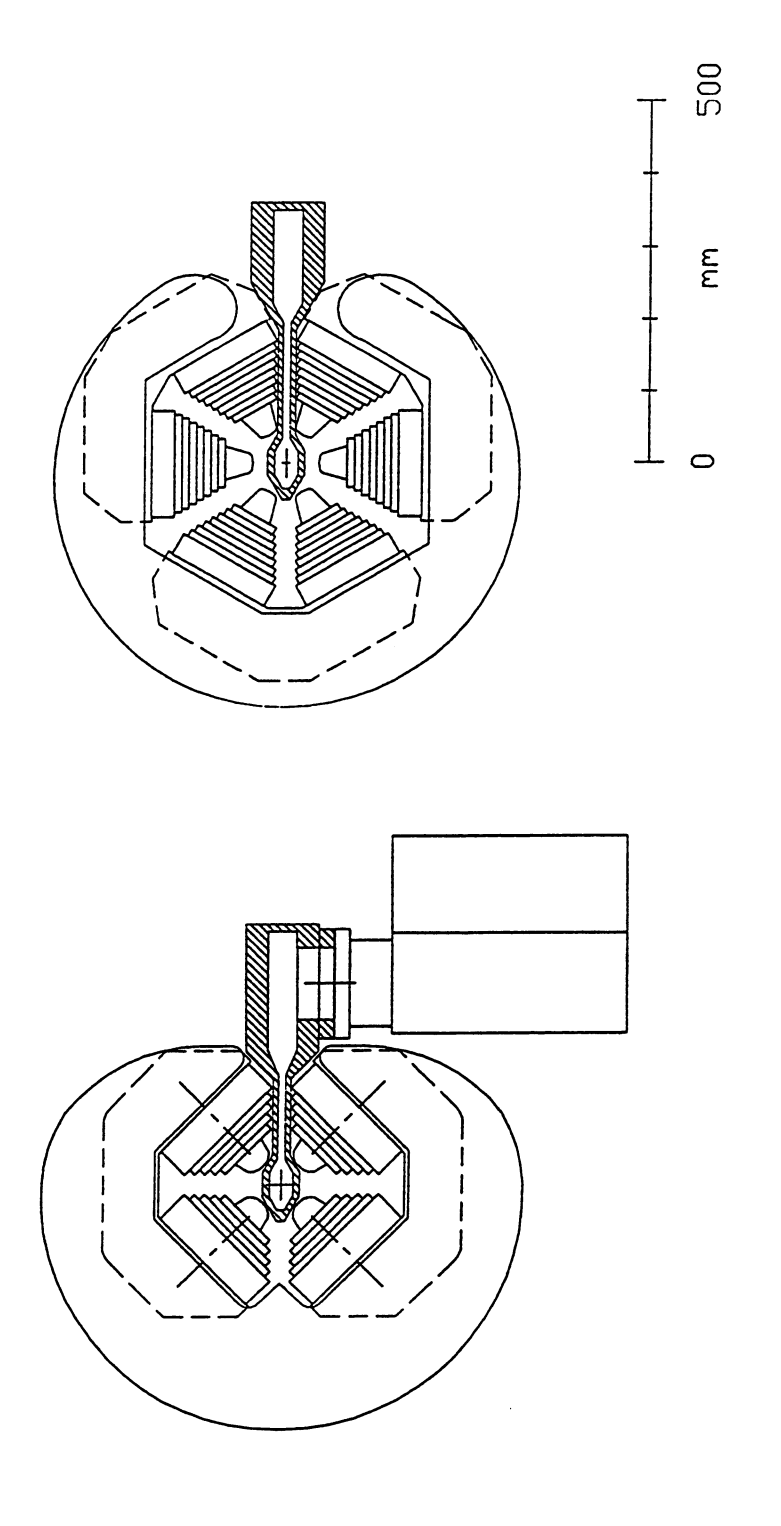


Figure 32: Quadrupole and sextupole face views and vacuum chamber cross-sections for the antechamber solution

vacuum chamber. The yokes could be supported by a C-shaped structure or by a frame around the chamber to minimise the distortion from the magnetic field forces. In order to gain space on the outside of the 'C-structure' the pole axes may be turned by a angle of 3-degree as introduced by ELETTRA [2]. The focusing magnets will need a splittable figure-of-eight yoke to allow insertion of the

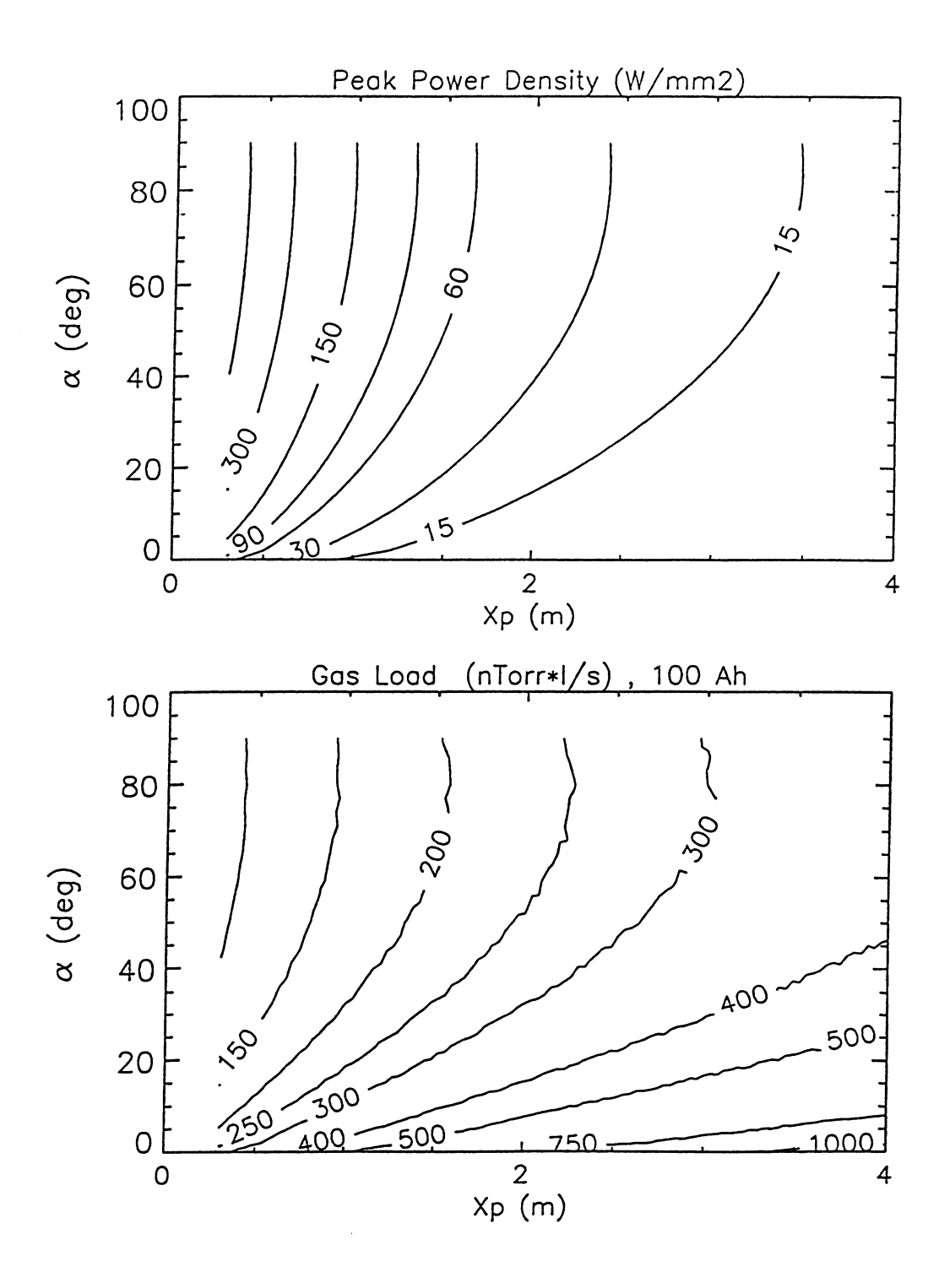


Figure 33: Peak power density and photon induced gas desorption load for a discrete photon absorber at 2.1GeV and 400mA operation

The absorber stops a 5-degree photon fan emitted from a super-conducting dipole. In the figures, the absorber surface is defined by the absorber edge at a distance X_P from the exit of the dipole and by the inclined angle α of the absorber surface to the electron beam axis. With increasing distance and decreasing inclined angle the photon flux on the desorbing surface decreases, resulting in a lower peak power density and a higher gas desorption for a given beam 'conditioning' period.

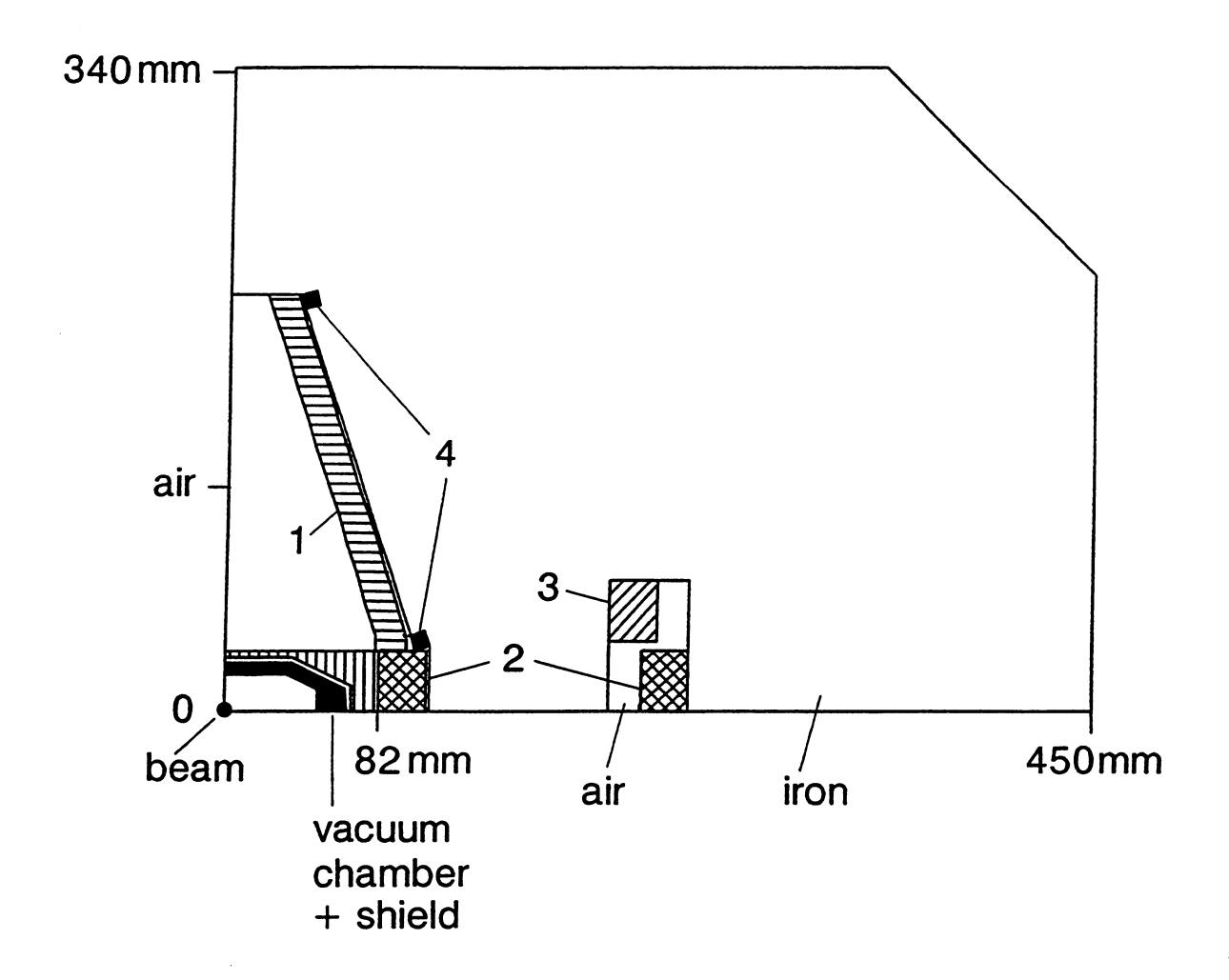


Figure 34: Cross-section of superconducting dipole

Shown is the geometry of one quadrant with iron, four s.c.-coils and the vacuum chamber. The iron is cold while the vacuum chamber is at room temperature (warm bore). The coil configuration has been worked out by P. Vobly of Novosibirsk. Coil 1 is tilted to give a homogeneous field of 4.7 T in air, while keeping the field in the iron below saturation. Coil 2 is a continuation of coil 1 towards the medium plane. Coil 3 compensates the return current of coil 2 inside the iron and thus simulates a saddle coil. Coil 4 finally compensates the finite thickness of coil 1 to give a highly homogeneous field around the beam axis. The current density in all coils is below 240 A/mm².

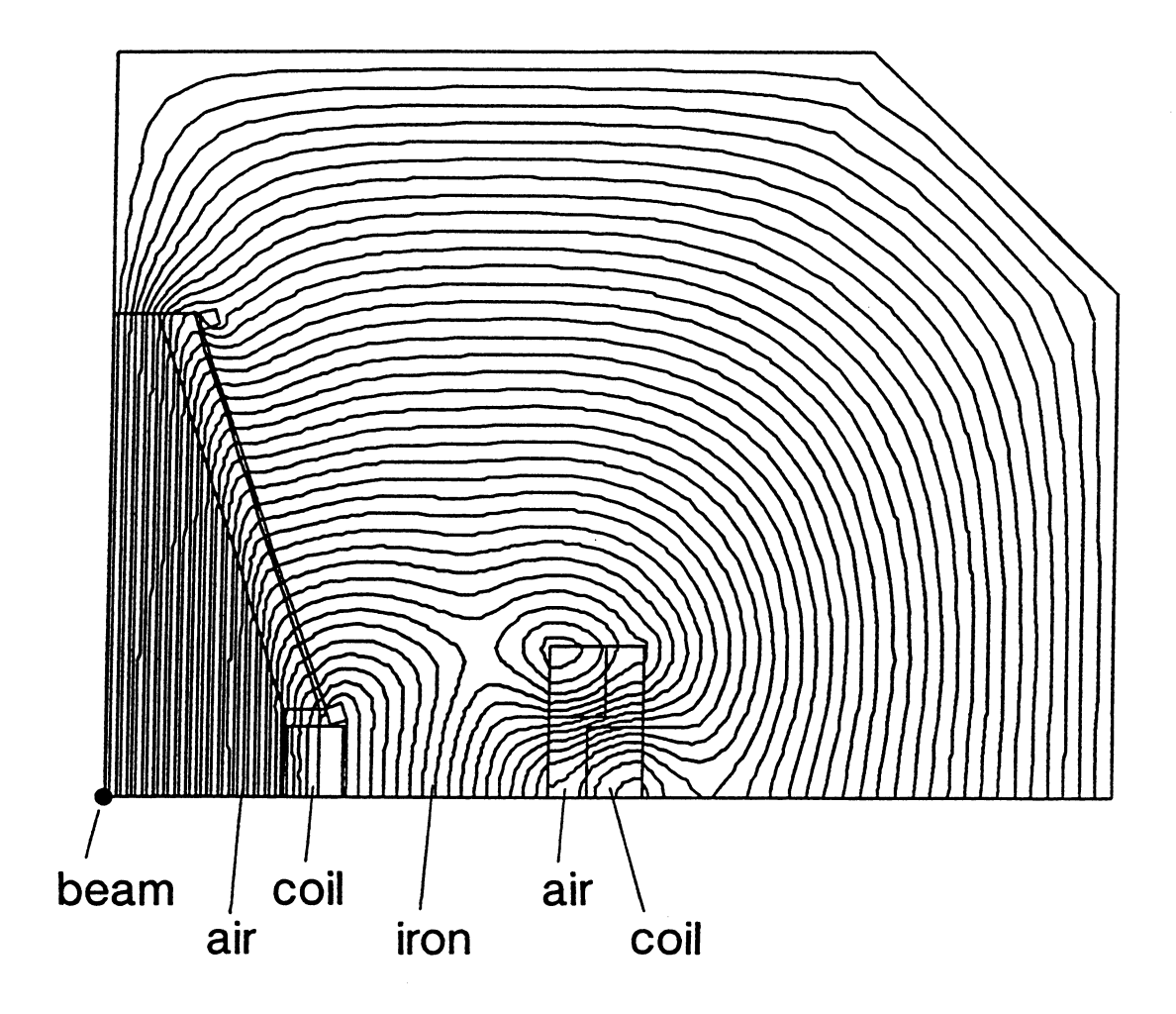


Figure 35: Flux-lines in the superconducting dipole

The field of 4.7 T around the beam center is very homogeneous. The field in the iron is 1.5 T or less, except close to the two coils inside the iron, where it is 2 T.

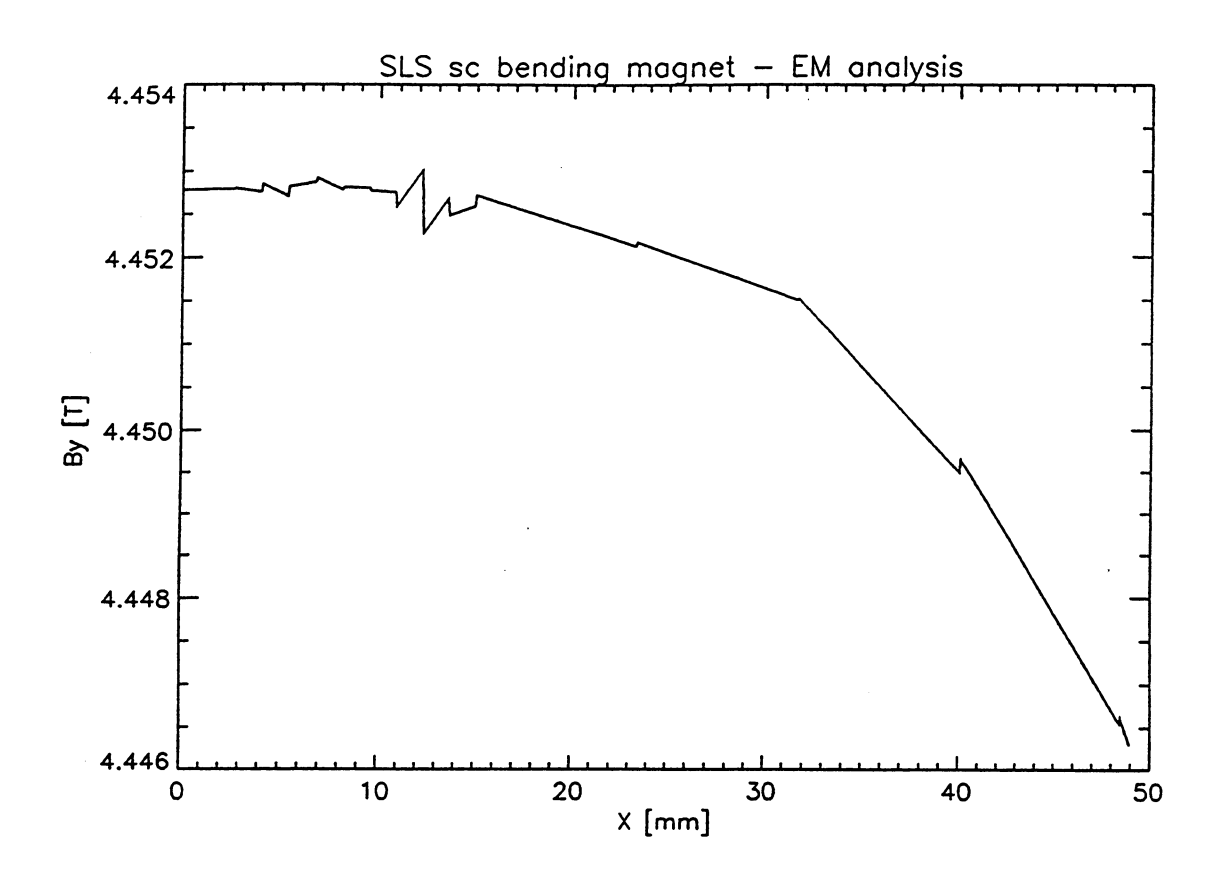


Figure 36: Field homogeneity of the superconducting dipole

Vertical field B_y in the median plane is plotted versus the horizontal displacement x from the beam axis. The curve is not smooth due to the finite mesh size used in the calculations. The field is homogeneous to better than \pm 0.02 % for x < 20 mm.

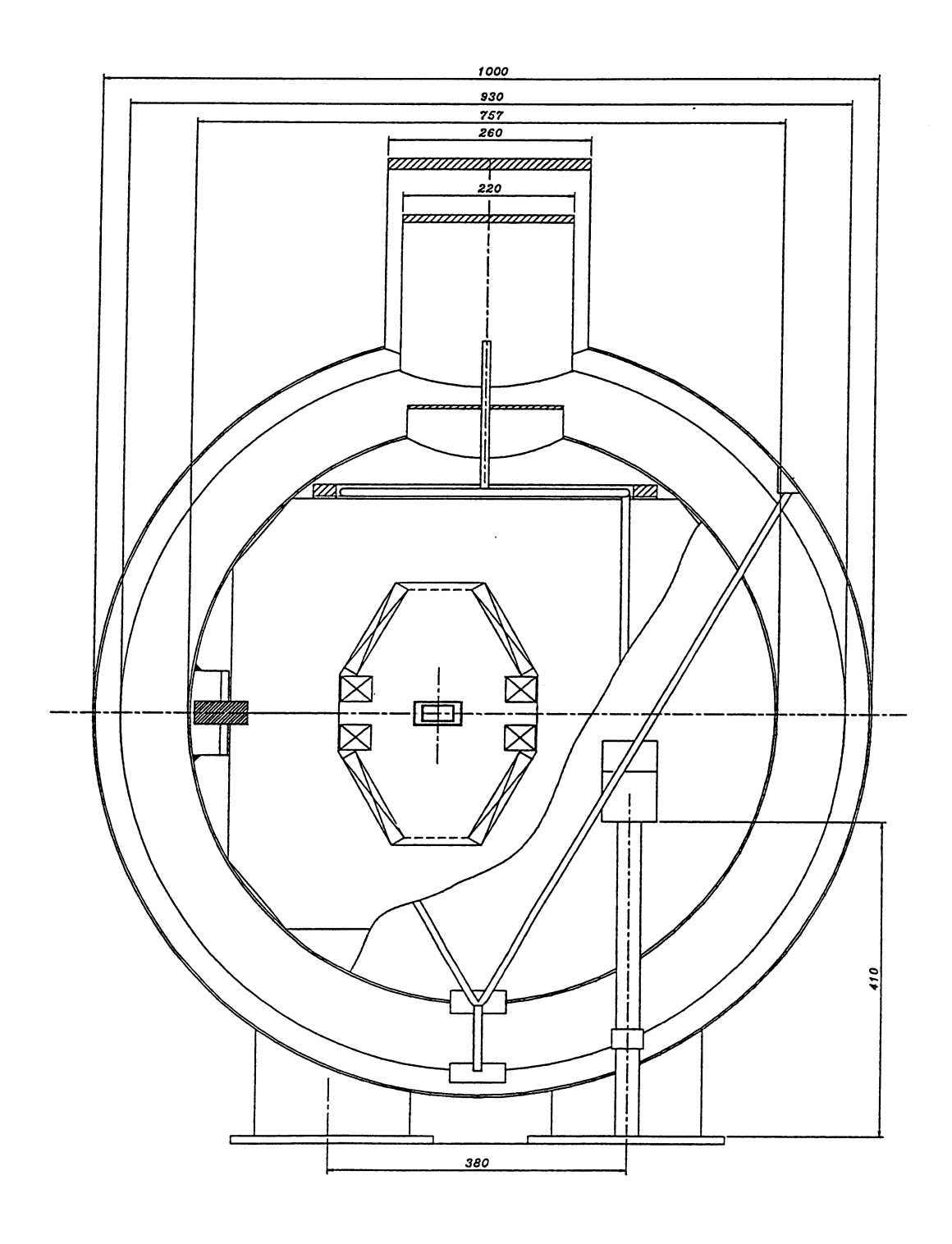


Figure 37: Transversal section through the cryostat of the superconducting-dipole

The iron and coil configuration corresponds to an earlier version and has since been modified to the one shown in Figure 34

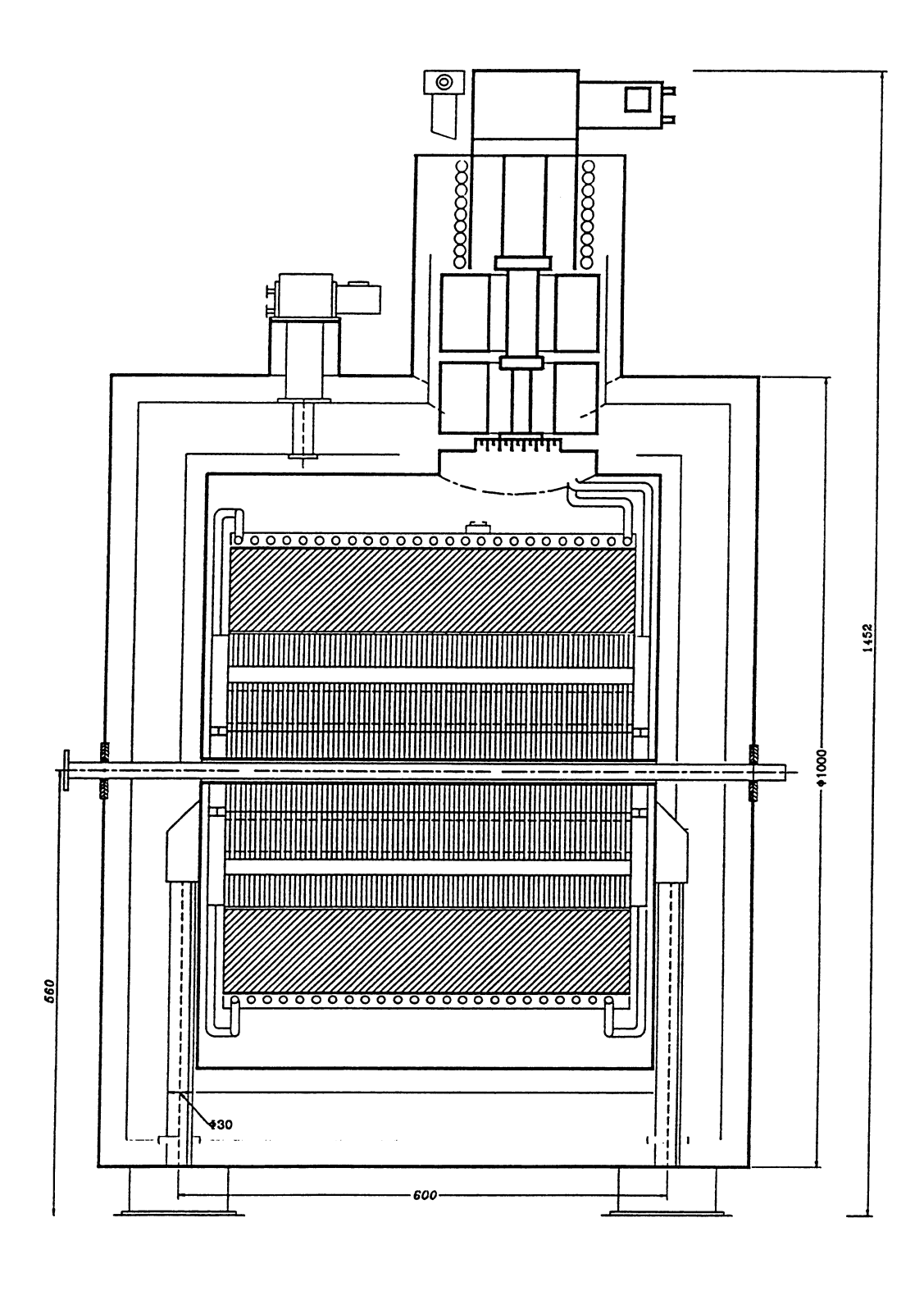


Figure 38: Longitudinal section through the cryostat, with dimensions indicated in mm

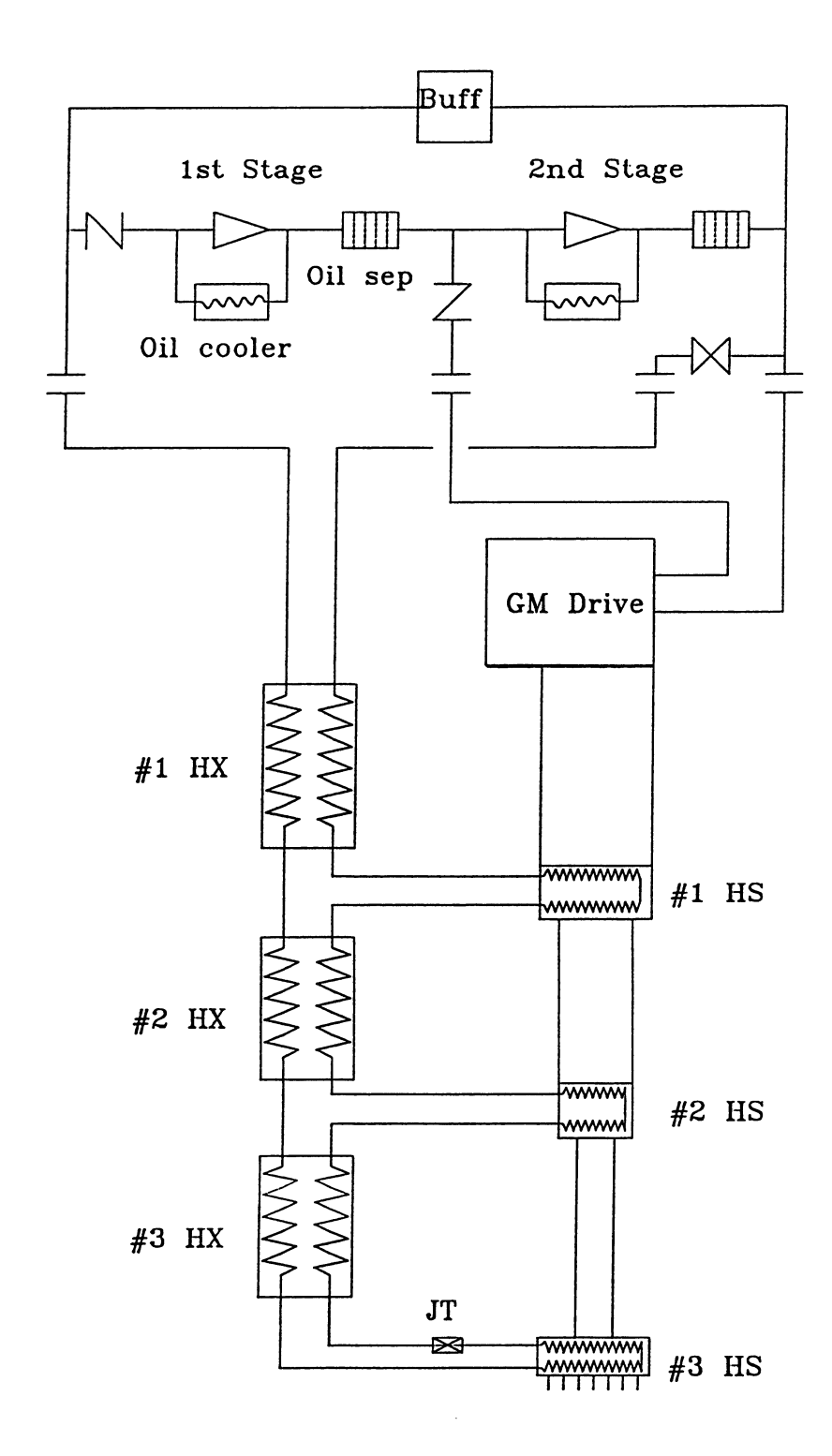


Figure 39: Helium recondensation system for variant with a two stage cryocooler

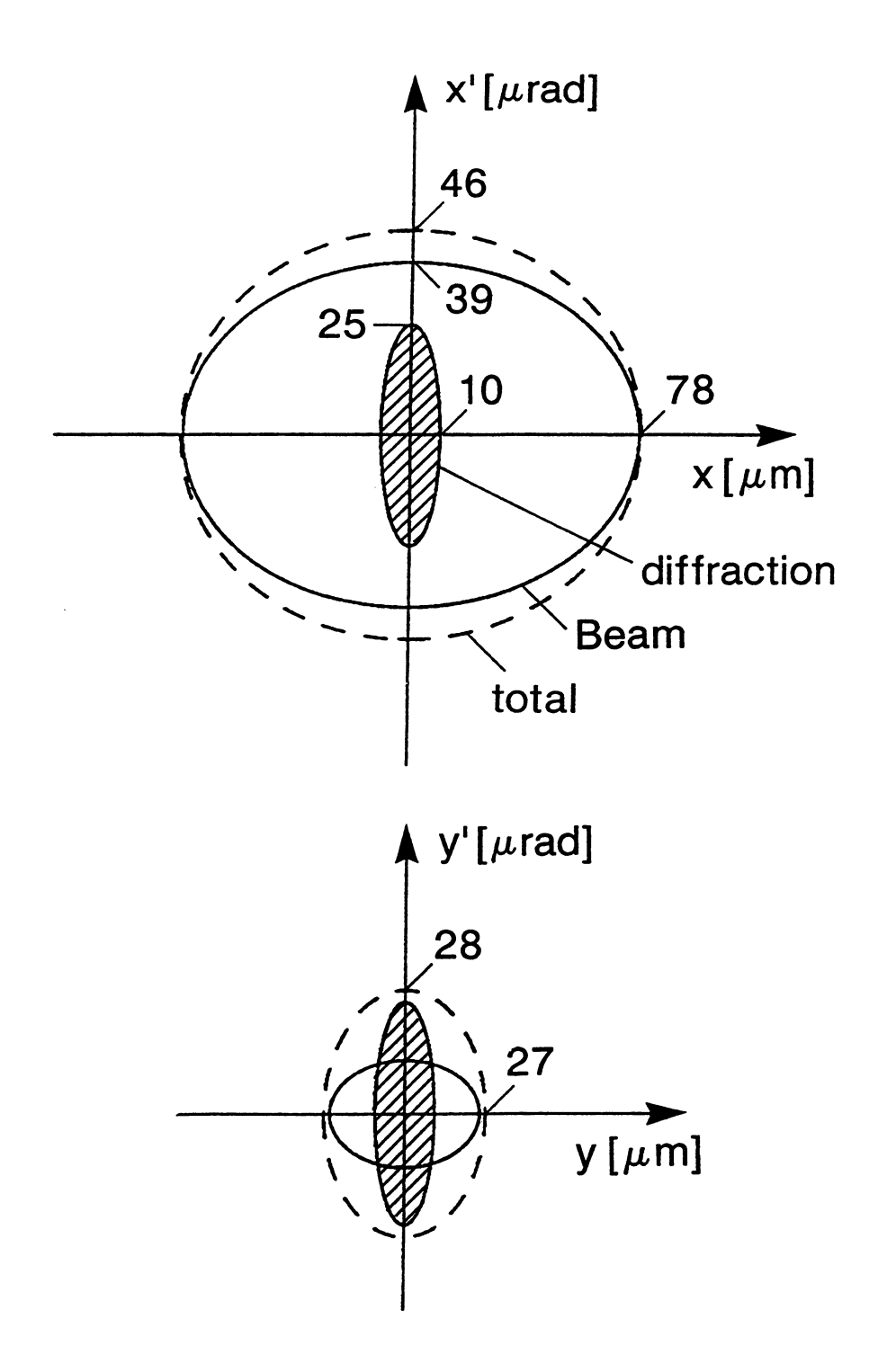
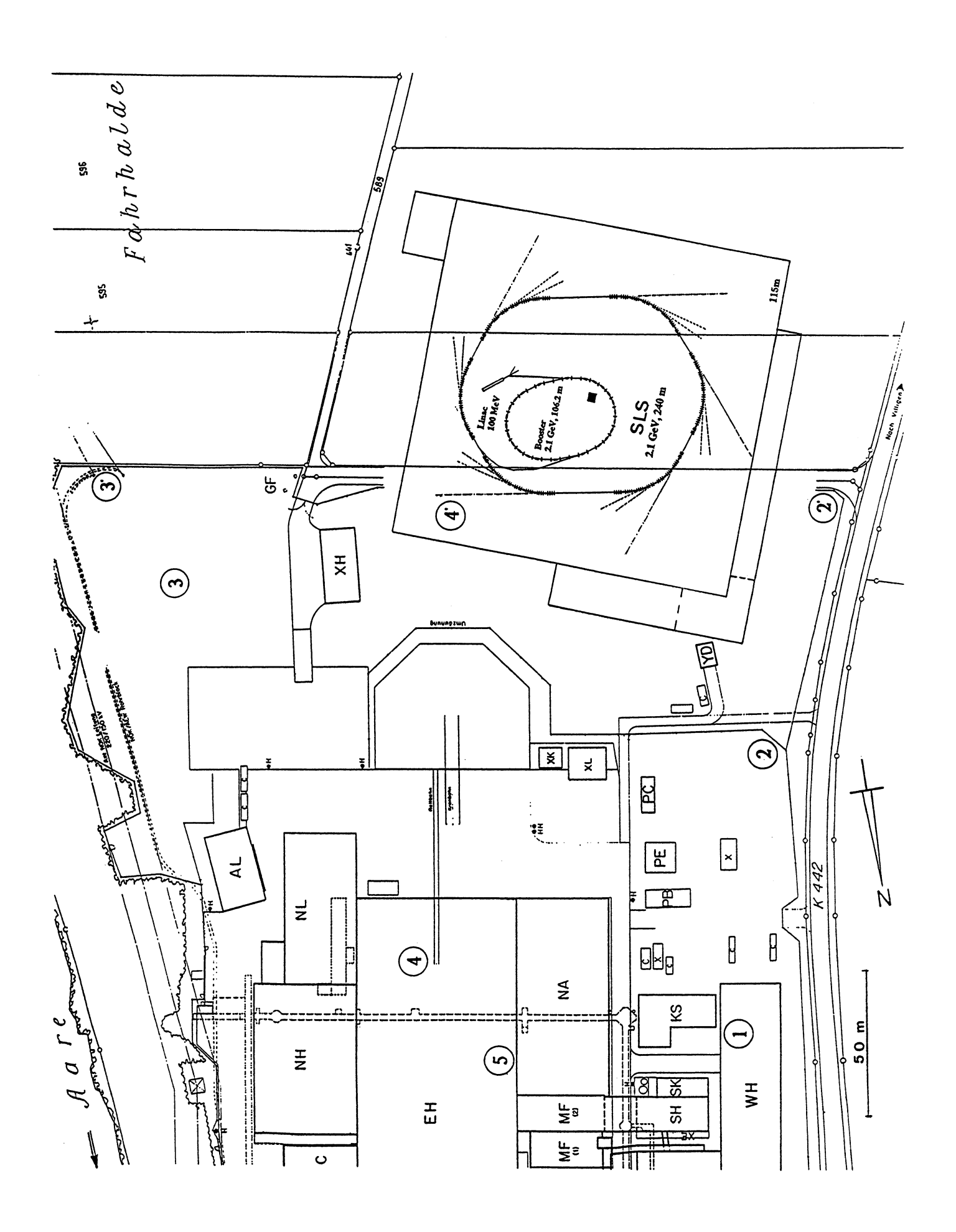


Figure 40: Effective photon source of an SLS-undulator

Shown is the horizontal and vertical phase space at the midpoint of a 5 m long undulator, optimised for a photon energy of about 400 eV. The three different rms-ellipses in each plane represent the diffraction limited source for a single electron, the beam emittance and the total effective photon source



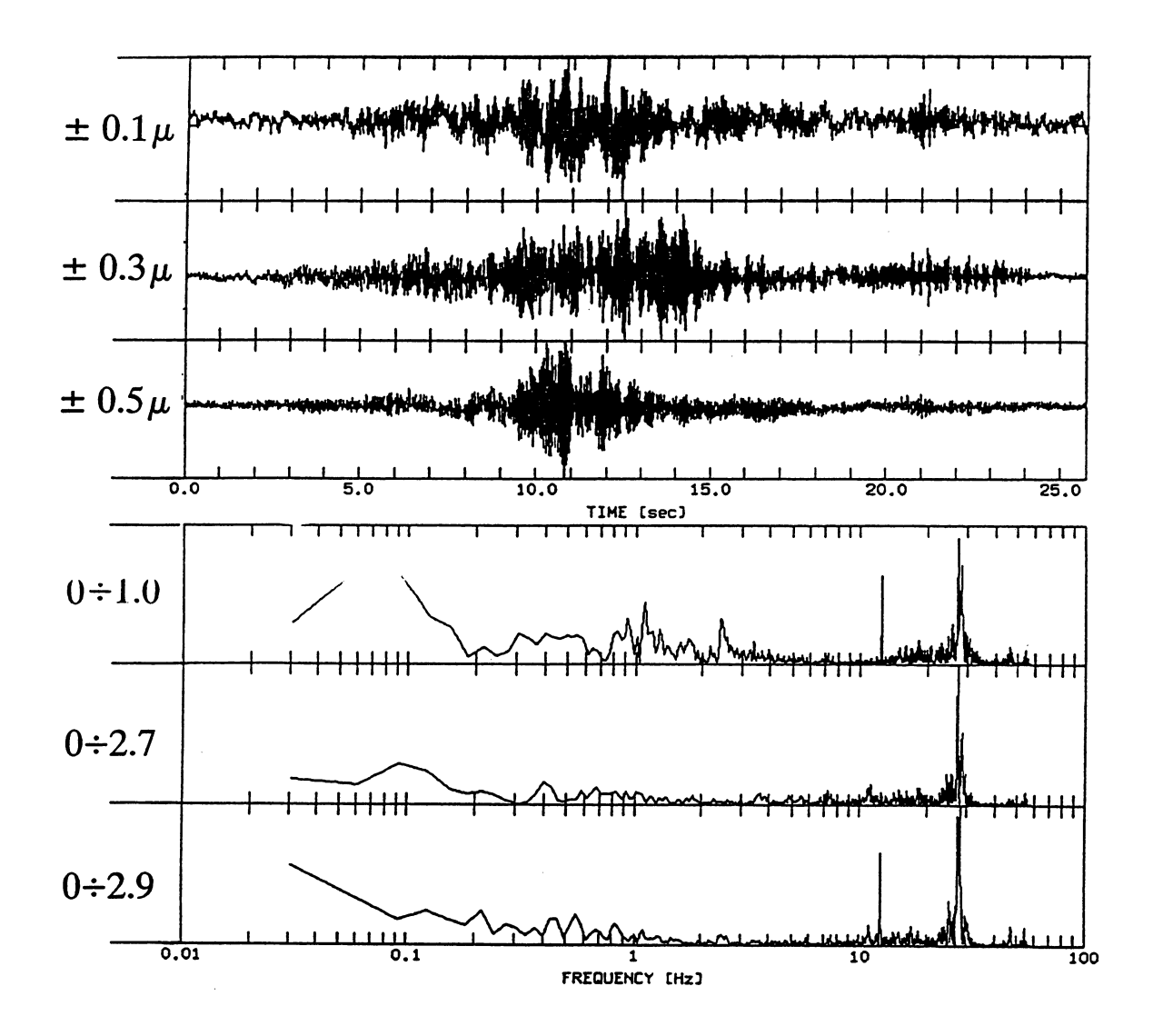


Figure 42: Measured displacements due to traffic

Shown are three orthogonal components (orientation: vertical, north and east) of ground vibrations measured at location 2'. Clearly visible is the response to the passage of a heavy vehicle on the public road situated nearby. The lower three traces show the corresponding frequency spectra in arbitrary units.

\Diamond

Figure 41: Location of Ground Tremor measurements

Shown is the situation of the prospective SLS site within the relevant part of the PSI West Area. The numbered circles correspond to the locations where Ground Tremor measurements were taken using highly sensitive seismometric probes.

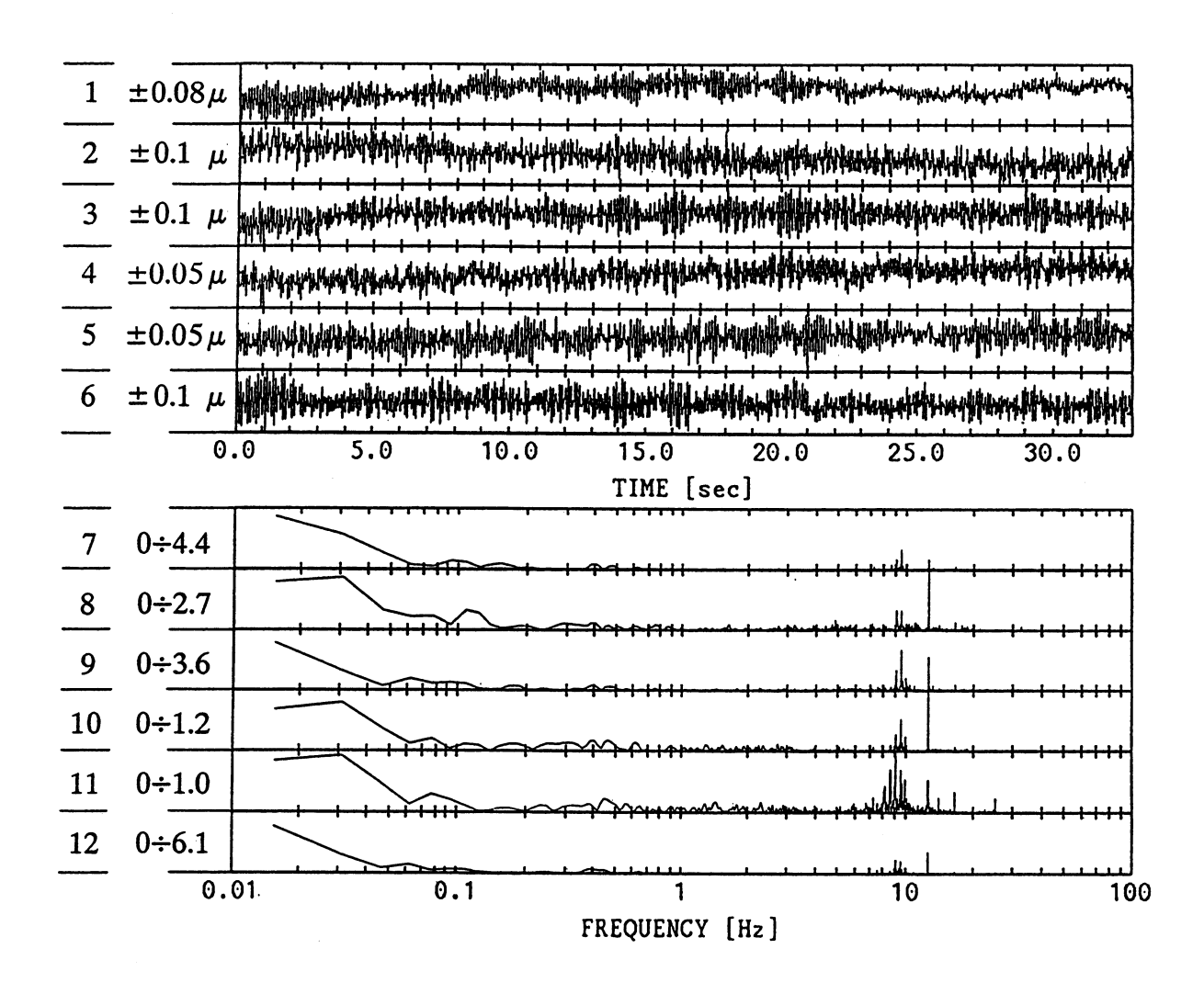


Figure 43: Measured displacements due to Ground Tremor

Traces 1–3 show three orthogonal vibration components measured in location 2' (see figure 41). Traces 4–6 show the same for location 4'. Traces 7–9 (2') and 10–12(4') show the corresponding frequency spectra in arbitrary units.

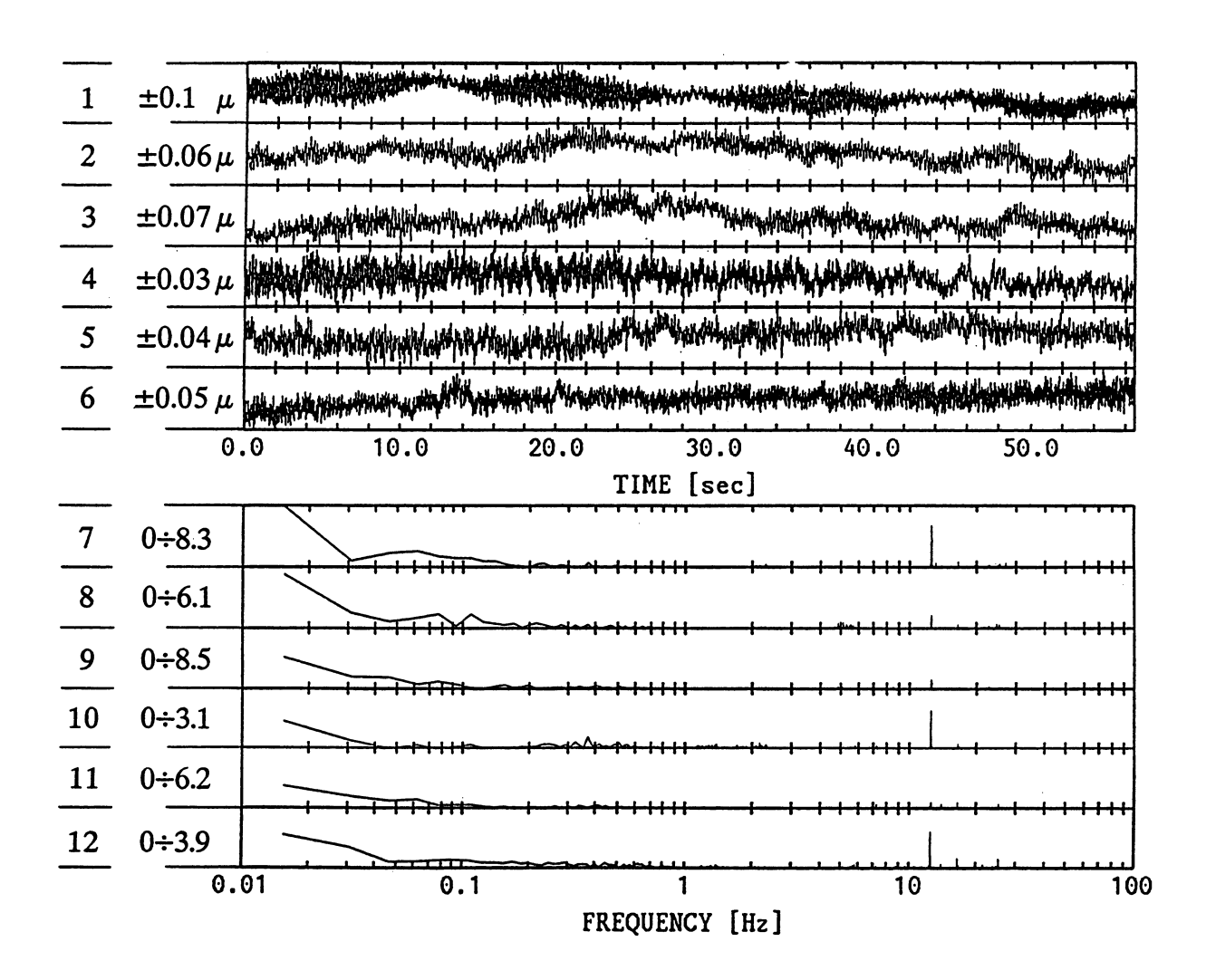


Figure 44: Measured vibrations in the existing experimental hall

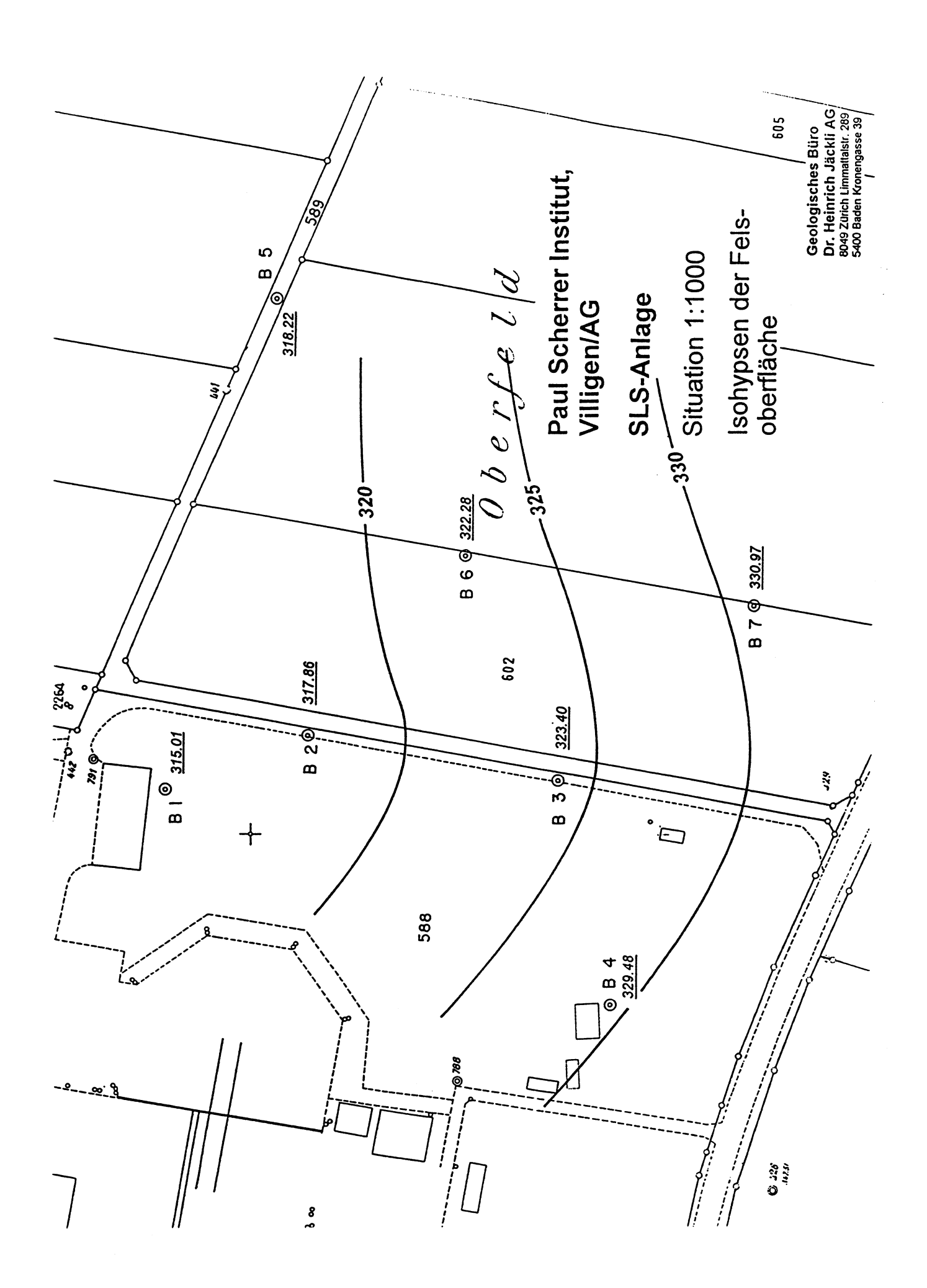
Traces 1–3 and 7–9 show the three orthogonal vibration components and the corresponding frequency spectra in arbitrary units measured at location 5 on the floor of the existing hall (see figure 41). Traces 4–6 and 10–12 show the same for location 2'.

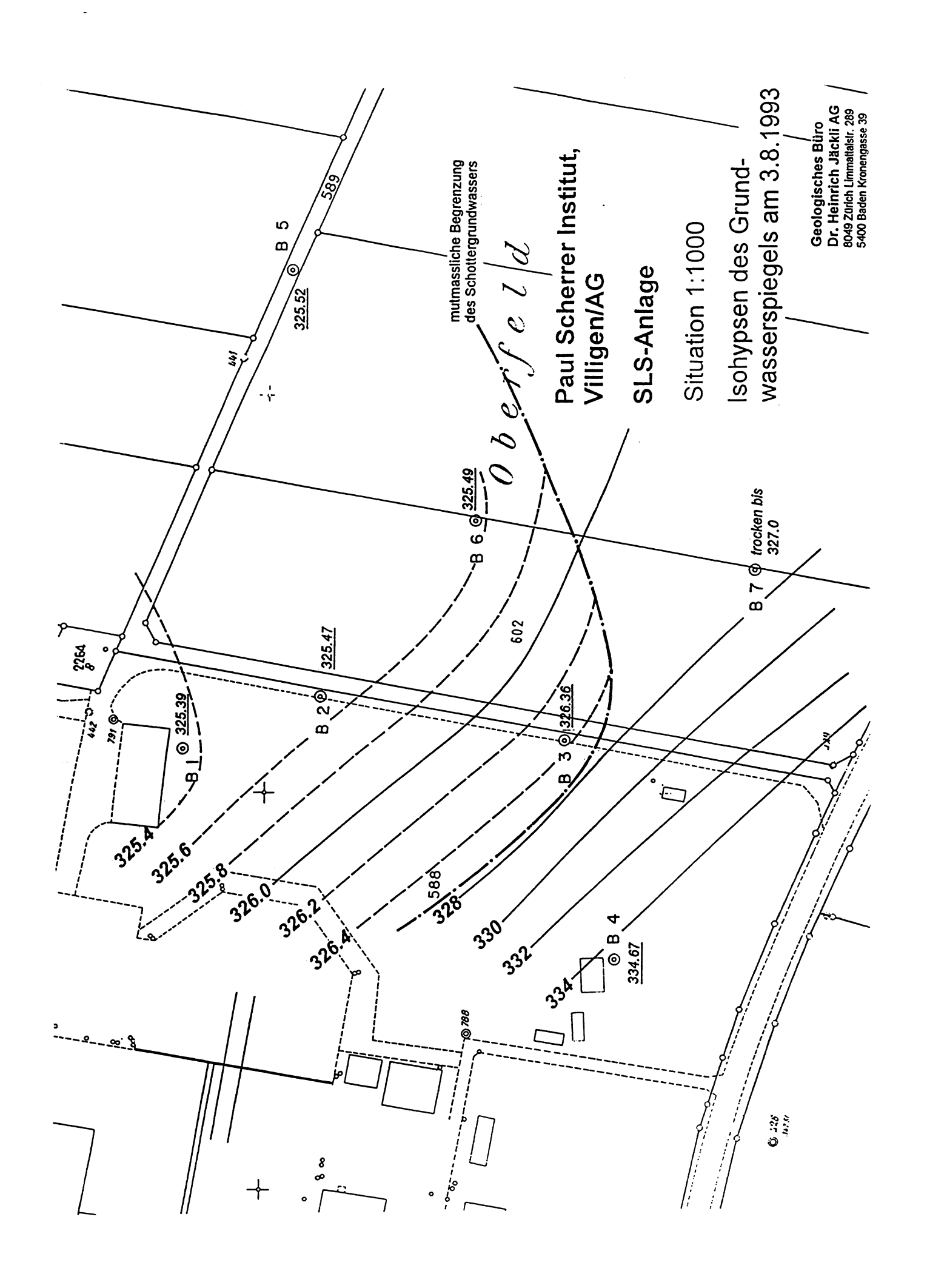
Shown are the contour levels, in m above sea level, of the rock bed at the SLS site. The floor of the experimental hall will be at a level of 347.5 m and thus 15-25 m above the rockbed.

Shown are the contour levels, in m above sea level, of the ground water level at the SLS site. The average distance between the floor of the experimental hall and the ground water is about 20 m.

 \Rightarrow

 $\Rightarrow \Rightarrow$





Comments on the Swiss Light Source by the Machine Advisory Committee (MAC)

The concept of the SLS (Swiss Light Source) is well adapted to the research needs in Switzerland. The ring can operate at a beam energy of 1.5 GeV to provide photons in the VUV (Vacuum Ultra Violet) region with a very low emittance or at a higher energy of about 2.1 GeV to produce x-rays from high field magnets. This wide spectrum is well adapted to the needs of some basic research programs as well as for some applications like nano technology and photo chemistry. The optics of the ring is optimised to provide the photon beams with the required properties and gives the possibility to install advanced devices in long straight sections. With its flexible design the SLS can provide a limited number of specialised beam lines and is complementary to international centers like the ESRF which are more adapted to serve a large community of users with similar requirements.

The general lay-out of the ring is adapted to this task. It has the form of a hexagon with two very long and four intermediate straight sections. The arcs are optically well optimised and compact. As a result the total circumference of 240 m is relatively modest which keeps the cost of the ring and its infra structure within limits. The location of this facility at the PSI laboratory gives the possibility to carry out some investigations with photons and neutrons as well.

The present beam optics is the result of a careful optimisation. The arcs are built up of nearly identical cells. Integrated in the center cell is a short super conducting magnet used for the production of hard photons. The end cells provide the matching to obtain vanishing dispersion and optimised beta functions in the long straight sections. This lattice structure allows a good chromatic correction and results in very impressive optical properties. By varying the strengths of a quadrupole family the emittance can be varied continuously. At a beam energy of 1.5 GeV an emittance as low as 1.4 nm rad. is achieved while the transverse acceptance is still nearly as large as the one given by the physical aperture of the vacuum chamber. These are the best values achieved for any such ring presently under study.

Two straight section with a free length of about 15 m each are included in the ring and their optical effects successfully corrected. They make several interesting developments possible: Very long undulators providing radiation with a spectrum sufficiently narrow for many experiments without the need of monochromators; insertion devices with long periods for low energy photons; combinations of different undulators for radiation with special spectral properties or circular polarisation; an FEL (Free Electron Laser) operating in a continuous mode; bunch rotation schemes to provide very high peak currents with a repetition rate sufficiently small to avoid collective effects like bunch lengthening; a bypass for a pulsed FEL and other applications.

The preliminary design of certain critical machine components have well progressed. The super conducting magnet providing the high energy photons has been calculated in detail. It includes a gradient field which was part of the earlier beam optics. Since this is no longer necessary for the new lattice the magnet is more simple and its field might even be increased. In a study of the vacuum system the gas desorptions rate by the photons and the necessary pumping speed have been calculated. Absorbers placed at strategic locations intercept the radiation. Single turn injection into the storage ring has been foreseen which requires a large peak current and a relatively low emittance for the injected beam. The large acceptance achieved with the present ring optics would also allow a classical injection method with accumulation of many pulses which is less demanding for the injection system. Still, the single turn injection has several advantages. Its high speed is advantageous for operation with very flat beams which might have a short life time due to Touschek scattering. It is well adapted to fill a limited number of bunches without spilling electrons into the neighbouring buckets. This injection does not require a large transverse acceptance and the ring emittance might be reduced further.

The low emittance and high peak current injection system can be realised with a photo cathode RF-gun. To carry out the required development work a test stand should be assembled. This gives the laboratory an opportunity to gain some early experience with electron beams which can be used to test beam position monitors and to measure the impedance of some components under realistic conditions. In a long term the low emittance beams from the linac can be used for FEL work in infrared region which could complement the SLS research program.

The SLS ring represents in its present status a design of a very advanced photon source well adapted to the research needs of the Swiss universities and industry. Thanks to a careful optimisation of the beam optics, very impressive parameters in emittance and acceptance are achieved. The concept of the ring, the development of its optics as well as design of some machine components exhibit much innovation by the study team. It is the most interesting synchrotron radiation source presently considered.

August 1st, 1993

A. Hofmann, CERN (Chairman) G. Mülhaupt, ESRF Grenoble A. Wrulich, ELETTRA Trieste

References

- [1] ALS, Conceptual Design Report, PUB-5172 rev. (1986), Lawrence Berkeley Laboratory, Berkeley, USA.
- [2] Bessy II, Technische Studie 2. Teil, Berlin, Juni 1989.
- [3] ELETTRA, Conceptual Design Report (1989), Sincrotrone Trieste, Italy.
- [4] ESRF Foundation Phase Report, Grenoble Cedex, February 1987.
- [5] APS, Conceptual Design Report, Argonne National Laboratory, Argonne, USA.
- [6] SPring-8 Project, Facility Design 1991, Jaeri-Riken, Japan.
- [7] PLS, Design Report, Pohang Light Source, Pohang Accelerator Laboratory, Pohang, Republic of Korea.
- [8] R. Abela et al., "Plans for the Swiss Light Source (SLS) at PSI", in Proceedings of the 4th International Conference on Synchrotron Radiation Instrumentation, Chester, United Kingdom, July 1991, p. 1606.
 R. Abela et al., "Design considerations for a Swiss Light Source (SLS)", Proceedings of the third EPAC, Berlin, March 1992, p. 486
 PSI, "A Concept for a Swiss Light Source", PSI-PR-92-24, July 1992.
- [9] G. N. Kulipanov et al., "Development of superconducting compact storage rings for technical purposes in the USSR", in Proceedings of the 4th International Conference on Synchrotron Radiation Instrumentation, Chester, United Kingdom, July 1991, pp. 731-736.
- [10] W. Ehrfeld, D. Münchmeyer, "Three-dimensional microfabrication using synchrotron radiation", NIM A 303 (1991), pp. 523-531.
- [11] K. J. Kim, "A synchrotron radiation source with arbitrarily adjustable elliptical polarization", NIM A 219 (1984), p. 425
- [12] A. Streun, "Neue Entwürfe für das SLS-Lattice", SLS-Note 2/93.
- [13] D. Poirier, "Etude des défauts de champ magnetique de Mimas et correction de la chromaticité de Super-Aco", Thesis, Orsay 1984.
- [14] OPTIK, developed by K. Wille and the DELTA-group, Dortmund, and extended at PSI.
- [15] KRAKPOT, written by E. Forest at ALS, Berkeley.

- [16] H. Grote and F. C. Iselin, "The MAD program", CERN/SL/90-13(AP) (Rev. 3), 1993.
- [17] TRACY, written by J. Bengtsson at ALS, Berkeley.
- [18] T. Nakada (ed.), "Feasibility study for a B-meson factory in the CERN ISR tunnel", CERN 90-02, PSI PR-90-08.
- [19] E. Haebel, "Higher order mode suppression in accelerators", Proceedings of the third EPAC, Berlin, March 1992, pp. 307-311.
- [20] A. Massarotti et al., "Further developement of the broad band HOM suppressor at Trieste", Proceedings of the third EPAC, Berlin, March 1992, pp. 1301-1302.
- [21] R. Rimmer et al., "Higher order mode damping studies on the PEP-II B-factory RF-cavity", Proceedings of the third EPAC, Berlin, March 1992, pp. 1289-1291.
- [22] S. Bartalucci et al., "DAΦNE accelerating cavity: R&D", Proceedings of the third EPAC, Berlin, March 1992, pp. 1263-1265.
- [23] J. F. Bridges et al., "High power testing of the prototype accelerating cavity (352 MHz) for the Advanced Photon Source (APS)", Proceedings of the third EPAC, Berlin, March 1992, pp. 1254-1256.
- [24] P. Marchand, "RF-systems for high-luminosity e+ e- circular colliders", Proceedings of the second EPAC, Nice, June 1990, pp. 1088-1090.
- [25] D. Brandt et al., "Further measurements of the impedance of LEP", LEP Commissioning Note 21.
- [26] S. Chattopadhyay (Ed.), "Impedance beyond cutoff", Particle Accelerators, Vol. 25, No. 2–4 (special issue, 1990).
- [27] Fourth advanced ICFA beam dynamics workshop on collective effects in short bunches, KEK Report 90-21, February 1991.
- [28] A. V. Burov and E. A. Perevedentsev, "Coherent synchrotron radiation and its effect on the bunch lengthening", Proceedings of the XVth International Conference on High Energy Accelerators, Hamburg, July 1992, pp. 1112-1114.
- [29] B. Zotter, "BBI a program to compute bunched beam instabilities in high energy particle accelerators and storage rings", CERN Report CERN LEP TH 89-74, December 1989.
- [30] T. Raubenheimer, "The generation and acceleration of low emittance flat beams for future linear colliders", PhD Thesis, SLAC-Report-387, November 1991.

- [31] M. S. Zisman et al., "ZAP user's guide", LBL-21270, December 1986.
- [32] A. Hofmann, Private communication.
- [33] Z. D. Farkas, "SLED: A method of doubling SLAC's energy", International Conference on High-Energy Accelerators, SLAC 1974, p. 576.
- [34] C. Marinucci, "Design study of the SLS-SC-bending magnet with linear gradient", SLS-Note 6/93.
- [35] A. Anghel and G. Vecsey, "The cryogenic design of the SLS bend magnet and cryostat", SLS-Note 5/93.
- [36] N. B. Mistry, "Vacuum Systems for Synchrotron-Light Sources", Conference on Vacuum Design of Advanced and Compact Synchrotron Light Sources, Brookhaven National Laboratory, May 16-18, 1988.
- [37] O. Gröbner et al., "Studies of photon induced gas desorption using synchrotron radiation", Vacuum, Vol.33 (1983) p. 397.
- [38] A. G. Mathewson et al., "Comparision of the synchrotron radiation induced gas desorption in aluminium vacuum chambers after chemical cleaning and argon glow discharge cleaning", J. Vac. Sci. Technol. A5(4) (1987) p. 2512.
- [39] S. Ueada et al., "Photodesorption from stainless steel, aluminium alloy and oxygen free copper test chambers", Vacuum, Vol.41 (1990) p.1928.
- [40] N. B. Mistry, "Vacuum Systems for e+ e- Storage Rings", CERN/US Particle Accelerator School, Spain, October 29–November 4, 1992.
- [41] G. Heidenreich, "Initial considerations for the SLS Vacuum System", SLS-Note 1/93.
- [42] G. Heidenreich, "Photon absorber layout for SLS", SLS-Note 8/93.
- [43] G. Marot, "Design of the ESRF-Absorbers", ESRF internal report, Grenoble, October 1989.
- [44] A. M. Poncet, "Some recent developments at CERN (LEAR)", Cern PS Division internal report, 1986.
- [45] Varian Vacuum Products, product information.

- [46] G. van Doorsen, H. Padmore, W. Joho, "The optimization and comparison of multipole wiggler and bending magnet sources of synchrotron radiation for X-ray experiments", SPIE Conference on Electron Beam Sources of high brightness radiation, San Diego, Conf. Proc. Vol. 2013.
- [47] ALS-handbook, PUB-643 Rev. 2, Lawrence Berkeley Laboratory.
- [48] K. Freudenreich, the L3-Collaboration, "L3 Forward-Backward Muon Detector", L3 Internal Note 1083, 3. Dec. 1991.
- [49] Dr. D. Mayer-Rosa and his collaborators from the Schweizerischer Erdbebendienst of ETHZ are highly acknowledged for preparing, performing and evaluating the measurements.